PONTIFICIA UNIVERSIDAD CATOLICA DE CHILE
SCHOOL OF ENGINEERING

STRUCTURAL SYSTEM IDENTIFICATION, MODEL UPDATING, AND FRAGILITY ANALYSIS OF MASONRY HERITAGE STRUCTURES. THE CASE OF THE METROPOLITAN CATHEDRAL OF SANTIAGO, CHILE.

WILSON RAMIRO TORRES

Thesis submitted to the Office of Graduate Studies in partial fulfillment of the requirements for the Degree of Doctor in Engineering Sciences

Advisors:
JOSÉ LUIS ALMAZÁN
CRISTIÁN SANDOVAL

Santiago de Chile, Agosto, 2018

PONTIFICIA UNIVERSIDAD CATOLICA DE CHILE
SCHOOL OF ENGINEERING

STRUCTURAL SYSTEM IDENTIFICATION, MODEL UPDATING, AND FRAGILITY ANALYSIS OF MASONRY HERITAGE STRUCTURES. THE CASE OF THE METROPOLITAN CATHEDRAL OF SANTIAGO, CHILE.

WILSON RAMIRO TORRES BERNI

Members of the Committee:

JOSÉ LUIZ ALMAZÁN

CRISTIÁN SANDOVAL

FERNANDO CERDA

RUBEN BOROSCHEK

DIEGO LÓPEZ-GARCÍA

FERNANDO PEÑA

JUAN DE DIOS ORTÚZAR

Thesis submitted to the Office of Graduate Studies in partial fulfilment of the requirements for the Degree of Doctor in Engineering Sciences

Santiago, Chile, August 2018

To my family and friends, who have been a great support during this time….

ACKNOWLEDGEMENTS

The author acknowledges:

- *The scholarship for doctorate studies given by SENESCYT (Secretaría Nacional de Educación Superior Ciencia y Tecnología) of Ecuador through a contract number 20120011.*
- *The funds awarded to Researcher Fernando Pérez to investigation of the Metropolitan Cathedral of Santiago de Chile, from the FONDECYT project number 1110481.*
- *To Professor Pablo González of Diego Portales University for the loan of the TROMINO devices for dynamic measuring.*
- *The financial support given by the Vicerrectoría de Investigación (VRI) of the Pontificia Universidad Católica de Chile for the research stage at the Engineering Institute of UNAM, Mexico.*
- *Finally, to "The Legion", group of postgraduate students of 2014 from the Pontificia Universidad Católica de Chile, and the workers group of DICTUC (Dirección de Investigaciones Científicas y Tecnológicas de la Pontificia Universidad Católica de Chile), for the given help in the experimental campaign of the Cathedral.*

TABLE OF CONTENTS

Page

PONTIFICIA UNIVERSIDAD CATÓLICA DE CHILE
ESCUELA DE INGENIERÍA

IDENTIFICACIÓN DEL SISTEMA ESTRUCTURAL, ACTUALIZACIÓN DEL MODELO Y ANÁLISIS DE FRAGILIDAD DE ESTRUCTURAS PATRIMONIALES DE MAMPOSTERÍA. EL CASO DE LA CATEDRAL METROPOLITANA DE SANTIAGO DE CHILE.

Tesis enviada a la Dirección de Investigación y Postgrado en cumplimiento parcial de los requisitos para el grado de Doctor en Ciencias de la Ingeniería.

WILSON RAMIRO TORRES BERNI

RESUMEN

Las edificaciones patrimoniales en los países de América Latina tienen un alto valor arquitectónico. El estudio de estas estructuras sujetas a cargas extremas, particularmente sismos, requiere modelos representativos que permitan simular su condición actual. Esta investigación se focaliza en el análisis de la Catedral Metropolitana de Santiago de Chile. El primer paso para analizar esta estructura es la determinación de las propiedades mecánicas; segundo, la evaluación sísmica de una parte de esta estructura (macroelemento) por medio de un análisis de fragilidad; y finalmente, se propone y valida un modelo simplificado equivalente del macro-elemento construido a partir de barras sujetas a flexocompresión. Todo este proceso permitirá, en una futura investigación, llevar a cabo un análisis de fragilidad de la estructura completa o de una parte de ella con algunos macroelementos trabajando en distintos planos.

Los ensayos no invasivos correspondientes a la teoría de Análisis Modal Operacional (Operational Modal Analysis - OMA) ofrecen alternativas interesantes para actualizar y validar un modelo estructural en este tipo de estructuras. La primera parte de la investigación se concentra en la calibración y proceso de ajuste de un modelo de la Catedral en elementos finitos, basado en las propiedades experimentalmente identificadas tanto mecánicas de los materiales como modales. Se presenta y discute una campaña experimental in situ cuyo objetivo es obtener la respuesta de la estructura a

vibraciones ambientales. En esta campaña se emplearon seis sensores sincronizados de alta sensibilidad, capaces de medir velocidad y aceleración en los 3 ejes ortogonales. Para la identificación se aplicaron los métodos: Descomposición Mejorada en el Dominio de la Frecuencia (Enhanced Frequency Domain Decomposition - EFDD) e Identificación en el Subespacio Estocástico (Stochastic Subspace Identification - SSI). Las consideraciones más importantes en el proceso de actualización del modelo, fueron: el tratamiento de los diferentes tipos de mampostería que conforman la estructura como materiales homogéneos, y el efecto restrictivo de los elementos de borde sobre la estructura de la Catedral causado por estructuras adyacentes. Para definir dichas condiciones de borde y las propiedades iniciales del material se aplicó un proceso preliminar de actualización del modelo. Luego, un grupo de modelos con diferentes valores físicamente posibles de propiedades de materiales, fueron evaluados. La selección del modelo final con las propiedades que mejor se ajustan a la realidad, se basó en el concepto "distancia" entre valores experimentales y analíticos, tomando como base tanto frecuencias naturales como formas modales.

Se realiza el análisis de fragilidad del macroelemento nave típico de la Catedral. El análisis es llevado a cabo mediante el uso del modelo resorte – cuerpo rígido (Rigid Body Spring Model - RSBM), en el cual elementos rígidos planos están conectados uno a otro mediante dos resortes axiales y uno de corte. El modelo bidimensional generado es inicialmente verificado mediante comparación con un modelo tridimensional de elementos finitos previamente calibrado (mediante la Identificación del Sistema de la primera etapa) y generado en el software DIANA. La metodología usada en esta parte corresponde al Análisis Incremental Dinámico (Incremental Dynamic Analysis - IDA) con base en un grupo de 11 registros de sismos reales correspondientes a los 4 sismos mayores que han afectado a la ciudad de Santiago. El análisis llevado a cabo considera desempeño no lineal de la estructura, con base en un índice de daño que cuantifica la degradación de rigidez, y así poder generar las curvas de fragilidad. Como resultado, se

obtuvo la probabilidad de excedencia para diferentes estados de daño basado en una posible aceleración máxima de piso en el sitio.

El tiempo de preparación del modelo y de procesamiento del mismo en el análisis de estructuras complejas como iglesias o castillos es muy grande, por lo tanto su evaluación sísmica no sería posible con recursos normales. Debido a esto es necesario definir modelos simplificados que permitan hacer una aproximación a la evaluación de la estructura para diferentes escenarios sísmicos probables con tiempos de procesamiento adecuados, sin descuidar la confiabilidad que deben tener los resultados. Tomando como base el modelo desarrollado antes con elementos rígidos, se verificó un modelo generado en OpenSees hecho a partir de elementos barra que trabajan a flexocompresión con plasticidad concentrada en los extremos, tanto para análisis estático como dinámico. El patrón de daño encontrado en el modelo de elementos rígidos permitió definir las zonas de plastificación (longitudes de rótula plástica) y las zonas que permanecen elásticas en la estructura. Los resultados obtenidos de esta comparación validan el modelo propuesto. Por lo tanto, para futuras investigaciones de evaluación sísmica de la estructura completa de la Catedral o una parte de ella que contenga varios planos resistentes, solamente sería necesario aumentar la calibración del resto de macro-elementos y ensamblar el modelo espacial de la estructura.

Miembros de la Comisión de Tesis Doctoral:

José Luis Almazán
Cristián Sandoval
Fernando Cerda
Rubén Boroschek
Diego López-García
Fernando Peña
Juan De Dios Ortúzar

Santiago, Agosto, 2018.

PONTIFICIA UNIVERSIDAD CATÓLICA DE CHILE
ESCUELA DE INGENIERÍA

STRUCTURAL SYSTEM IDENTIFICATION, MODEL UPDATING, AND FRAGILITY ANALYSIS OF MASONRY HERITAGE STRUCTURES. THE CASE OF THE METROPOLITAN CATHEDRAL OF SANTIAGO, CHILE.

Thesis submitted to the Office of Research and Graduate Studies in partial fulfillment of the requirements for the Degree of Doctor in Engineering Sciences by

WILSON RAMIRO TORRES

ABSTRACT

Heritage buildings in Latin American countries have a high architectural value. The study of these constructions under extreme loads, particularly earthquakes, requires representative models to simulate their current condition. This research focuses on the analysis of Metropolian Cathedral of Santiago de Chile. The first step to analyze this structure is the determination of the mechanical properties, second, the seismic evaluation of a part of this structure (macroelement) by means of a fragility analysis, and finally, an equivalent simplified model of the macroelement based on beam-columns elements is proposed. All this process will allow carrying out a fragility analysis, of the complete structure or a part of it with many plane resistant macroelements, in a future research.

The noninvasive Operational Modal Analysis (OMA) tests offer interesting possibilities in order to update and validate a structural model of this type of structures. The first part of research focuses on the calibration and model update process of a finite element model of the Cathedral, based on experimentally identified modal and mechanical material properties. An in-situ experimental campaign aimed at obtaining the response to ambient vibrations of the structure is presented and discussed. In this campaign, six high-sensitivity synchronous triaxial sensors where employed, these devices are capable of measure velocity and acceleration. Enhanced Frequency Domain Decomposition

(EFDD) and Stochastic Subspace Identification (SSI), system identification methods were applied. Additionally mechanical tests were performed on the materials of the Cathedral. Several considerations were made in the model updating, the most relevant are: each kind of masonry was considered as homogeneous material with their mortar interface, and the boundary elements restraining effect over Cathedral structure caused by adjacent structures. A preliminary model updating process was applied to define the boundary conditions and initial material properties. Then, a group of models with different material properties were evaluated within a physically possible range. The final model selection was based on the "distance" concept between the experimental and analytical natural frequencies, and mode shapes.

The fragility analysis of the typical naves macro-element of the Cathedral is done. The analysis is carried out by using the Rigid Body Spring Model approach (RBSM), in which rigid elements are connected to each other by means of two axial springs and one shear spring. The 2D model generated is initially verified by comparing modes with a 3D finite element model previously calibrated (System Identification of the first stage) in DIANA software. The methodology used in this part is based on Incremental Dynamic Analysis (IDA) by means of eleven real seismic records corresponding to four major earthquakes that have affected Santiago city. Nonlinear analyses of the macro-element is carried out, and the Fragility curves were built based on a damage index that quantifies the stiffness degradation. As a result, the probability of exceedance for different damage states were obtained based on a possible peak ground acceleration of the site.

The time spent in preparation of model and processing of this for the analysis of complex structures like churches or castles is very large, thus their seismic evaluation wouldn't be possible with normal resources. Due to this, it is important to define simplified models that allow to approach the evaluation of the structure for different probable seismic scenarios with suitable processing times, without neglecting the

reliability of the results. Taking as basis the previously developed model with rigid elements, a model generated in OpenSees made of beam-column elements with concentrated plasticity was verified, for both: static and dynamic analyses. The damage pattern obtained in the model of rigid elements allowed to define the length of plastic hinges and the zones that remain elastic in the structure. The results obtained from this comparison validate the proposed model. Therefore, for future research of the entire structure of Cathedral, or a portion of it that contains several resistant planes, it would only be necessary to increase the calibration of the rest of macro-elements and assemble the spatial model of the structure.

Members of the Doctoral Thesis Committee:

José Luis Almazán
Cristián Sandoval
Fernando Cerda
Rubén Boroschek
Diego López-García
Fernando Peña
Juan De Dios Ortúzar

Santiago, August, 2018.

1. INTRODUCTORY CHAPTER

Studying the structural performance of heritage masonry constructions has become a priority in cities around the world where architectural heritage needs to be preserved. However, this assessment remains a complex task. A major difficulty is knowing the mechanical properties of component materials, the current structural damage, and the degree of interaction between various internal and external elements and systems. Because of these and other difficulties, some general recommendations for structural analysis of historic constructions have been proposed using a multidisciplinary approach (ISCARSAH, 2003a).

Chile is widely recognized as one of the most seismic countries in the world. This is due to its location in the subduction zone between the Nazca plate and the South American plate. There are additional seismic considerations for Santiago, the capital city, since there exist two more seismic sources: an intraplate seismogenic source for medium depth earthquakes, and a crustal seismogenic source for superficial earthquakes (Leyton et al. 2010). An iconic architectural heritage structure of Santiago Chile, is the Metropolitan Cathedral (Figure 1). This historical structure more than 250 years old was chosen as a case study for this research.

The Metropolitan Cathedral of Santiago, Chile, has been affected by environmental factors throughout its history, but mainly by earthquakes occurring on the site (IDIEM 2011). A preliminary research project took place to identify and update the models for the Cathedral (Torres et al. 2016b).

The structural system of the Cathedral consists mainly of stone masonry walls in the bottom and brick masonry in the top of walls. The roof structure involves of wooden trusses in the central and north naves, while the south nave has metal trusses. There are two bell towers that can be distinguished in the main façade (Figure 1). The central nave

is the highest. On the central nave, between the 10-11 and B-C axes, there is the main dome, it is composed of steel beams and brick masonry (Figure 2).

This study will focus in the rigid zone of the Cathedral, i.e. the three longitudinal naves body. The towers, dome and adjacent structures (chapel, tabernacle and sacristy) were represented in a simplified way in the model.

a)

b)

Figure 1. Metropolitan Cathedral of Santiago, Chile: a) Main façade, b) View of the central nave.

A methodological approach to assessing a historic building should incorporate non-destructive or minimally destructive experimental techniques. One example is the well-known vibration analysis technique, used to estimate the structure's natural frequencies and modal shapes. The modal parameters thus obtained can then be used to calibrate numerical models by adjusting their mechanical properties (Binda & Saisi, 2009). Among the non-invasive methods the Operational Modal Analysis (OMA) is the most commonly used (Bayraktar et al. 2008; Elyamani et al. 2016; Ramos et al. 2013). By measuring the response to ambient vibrations and assuming that the input is white noise, the modal properties (frequencies and modal shapes) can be defined based on the system identification process.

a)

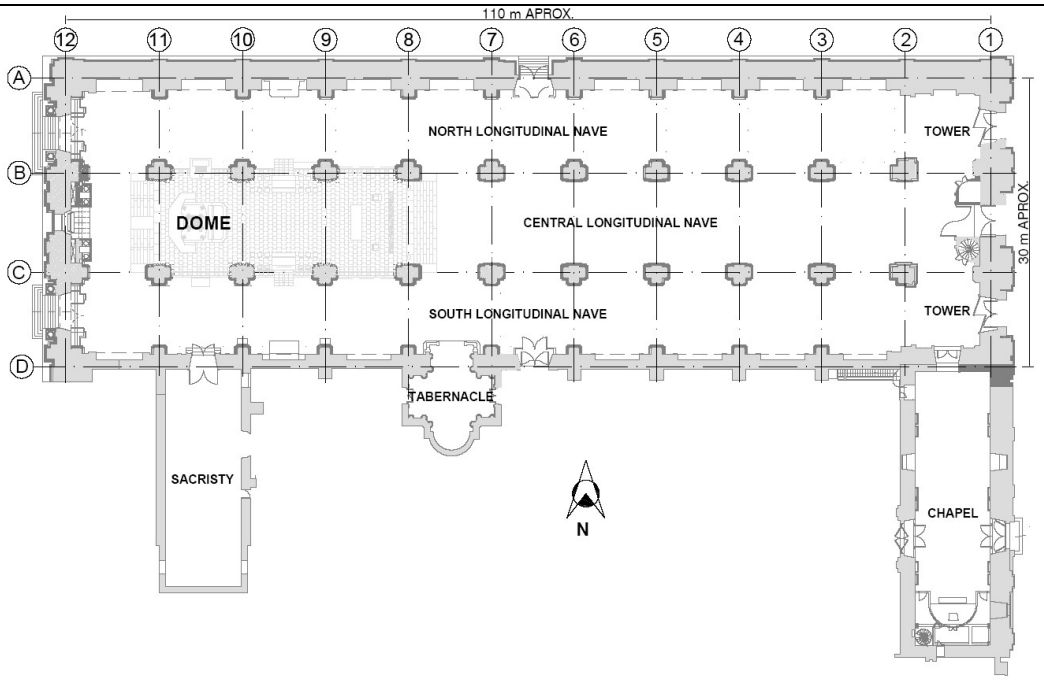

b)

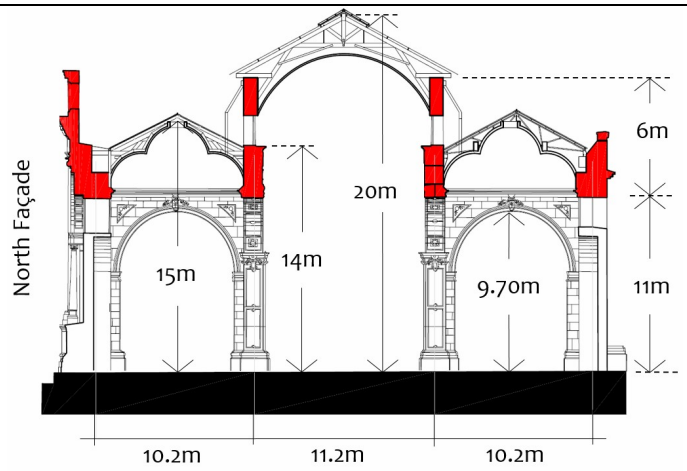

Figure 2. General dimensions of Cathedral: (a) General plan view; (b) Transversal section of a typical nave (brickwork walls in red colour).

Several studies have used OMA methodology with the aim of studying the flexible components of historical constructions, mainly towers (Carpinteri et al. 2005; Gentile et al. 2015). By contrast, defining the modal properties in a historic structure's more rigid zones, like perimeter walls and resistant transverse and longitudinal axes, is a less studied subject. One of the main difficulties relates to the complexity of identifying high-frequency close modes, which are common in structures with uniform stiffness and mass distribution. Additionally, the low response level to ambient excitation and the typical device resolution and precision make their identification a confusing and difficult process (De Stefano & Ceravolo 2007; Doebling et al. 1998).

One additional difficulty in identifying structural systems in this type of structures is that their structural elements do not have purely flexural or torsional modes, but a mixture of the two, unlike what occurs in conventional structures (Caselles et al. 2013). Therefore, the measuring devices need to be distributed in the structure, to capture all these special movements. Another common difficulty relates to the highly nonlinear response, which is due to the friction interaction between units at low deformation levels; this introduces anomalies, which can be confused with structure modes, i.e. they generate spurious

vibration modes that can cause interpretation problems in the identification process (De Stefano & Ceravolo 2007).

In similar previously developed cases, preliminary analytical models were developed, from which an optimal location for the response measuring devices was defined (Masciotta et al. 2016) based on the modes to be identified. Although this analysis is a good initial guide for defining the location of measuring points, the final location will depend on the structure's accessibility and operational conditions for measuring its response to environmental vibration.

Within the identification process, there is a list of previous research in which a frequency domain method (Frequency Domain Decomposition - FDD) is contrasted with a time domain method (Stochastic Subspace Identification - SSI), as making a comparison is important for highly uncertain problems, in order to generate consistent results (Foti et al. 2012; Lourenço et al. 2007; Ramos et al. 2010). However, there is other research into heritage structure, in which the FDD method alone is enough to identify the structure's mechanical properties (Aras et al. 2011; Gentile & Saisi 2007; Lorenzoni et al. 2013). One of the final aims of some similar studies (Aguilar et al. 2015; Gentile et al. 2015; Ramos et al. 2013) is to determine the structures' modal properties using the OMA methodology and subsequently update the model with multivariable optimization techniques (Douglas & Reid 1982).

With the structure's mechanical properties defined by means of System Identification and Model Updating processes, the next step in the study of Cathedral is the seismic analysis to different possible intensities. About this, a brief state of the art is described below.

Typically, ancient masonry churches are massive structures that, in general, were built without provisions for earthquake resistance. Due to this, complex and varied failure

mechanisms are usually observed in this type of constructions after an earthquake. However, several and different post-earthquake surveys have shown that damage observed in masonry churches can be grouped in accordance with their different architectonic elements, named macro-elements (Doglioni et al. 1994; Petrini et al. 1999, Lagomarsino & Podesta 2004; Cattari & Lagomarsino 2012; Da Porto et al. 2012). A macro-element corresponds to a portion of the structure generally related to an architectural part of the whole (facade, nave, apse, transept, dome, bell tower, etc.), and whose seismic response can be analysed independently from the rest of the structure (Irizarry et al. 2003; Lagomarsino & Cattari, 2015). Therefore, the subdivision of the complete structure of a church into macro-elements is a way to face their seismic assessment.

Several researchers have investigated the structural behavior of historic masonry churches in terms of their macro-elements (Lourenco et al. 2012; Roca et al. 2013; Diaferio & Foti 2017, among others). In this type of studies, different analysis methods according to the level of accuracy and simplicity desired have been employed. However, complex non-linear analyses, which demand a high computational cost, are commonly used. Therefore, it is desirable to explore more simplified analytical processes to achieve shorter processing times for this type of evaluations. On the other hand, another key aspect related to the study of ancient churches made of unreinforced masonry is the low tensile strength of the material. This fact produces a highly nonlinear behaviour in the structure. The modelling of this material in structures such as churches, castles, bridges, aqueducts, etc. remains a challenge although nowadays, powerful computational tools are available. One of these strategies is the Rigid Body Spring Model (RBSM) (Casolo 2004, 2009; Casolo & Peña 2007), which has certain advantages since it was specifically designed to undertake the non-linear dynamic analysis of this type of structures. Based on RBSM, Peña and Casolo (2012) have developed a specific numerical tool, RIGID software, which has been successfully applied to the analysis of existing masonry

structures such as castles (Casolo & Sanjust 2009), towers (Casolo et al. 2013), and churches (Casolo & Sanjust 2009; Peña & García 2016).

Recently, Lagomarsino and Cattari (2015) have proposed an exhaustive and detailed procedure to assess cultural heritage masonry structures. In this proposal, a performance-based assessment is promoted, where the performance levels are related to damage states (Grünthal 2009) and levels of performance. Additionally, the study of Lagomarsino and Cattari (2015) suggests that the seismic assessment of heritage masonry structures can be carried out by two methods. The first method is based on nonlinear static (pushover) analysis combined with the capacity spectrum method, while the second one involves nonlinear dynamic analysis based on an adequate number of appropriate records and scaled to develop an incremental dynamic analysis (Vamvatsikos & Cornell 2002).

As is well known, fragility curves show the probability of exceeding a damage state of a structure, or a portion of it, as a function of a seismic intensity given by force, acceleration, deformation, or any other engineering demand parameter (EDP) (Porter et al. 2007). In addition, as already mentioned, the damage state can be quantified based on some damage measure (DM) in the structure. A damage index frequently used in fragility studies is the maximum inter-storey drift (e.g. Mandal et al. 2016) while, for the case of masonry structures, Asteris et al. (2014) have recently proposed a DM based on the percentage of the damaged area of the structure relatively to the total area of the structure. For the specific case of heritage masonry structures, Casarin (2006) introduced as response parameter the structural stiffness where the ratio between the base shear and the displacement of a given control point is the base to assess the damage in the structure. This latter index, understood as a stiffness index, has not been previously used as a damage measure for fragility analysis of masonry structures, and therefore, has been adopted in the present research.

Several fragility studies on masonry structures have confirmed the importance of performing analyses for a range of seismic intensities according to the location of the building (Abo-el-ezz et al. 2013; Negulescu et al. 2014; Rota et al. 2010; Simoes et al. 2015). In addition, it is well known that a vulnerability analysis requires the estimation of the damage level of structure or macro-element under study when is subjected to earthquakes of different intensities. In these studies, the seismic damage can be described through a qualitative way (Augusti et al. 2001; Lagomarsino & Podesta 2004; Oliveira 2003) or by means of a quantitative measure (Asteris et al. 2014; Mandal et al. 2016). In any case, it should be noted that there are several methodologies to carry out fragility analyses, each of one depends on the degree of accuracy desired (Lagomarsino 2006; Mandal et al. 2013).

The fragility analysis of the nave macro-element will be the focus in the seismic evaluation of the Cathedral, based on RBSM methodology. The fragility curves will give us information about the probability of exceedance for different damage states based on possible peak ground accelerations on the site.

The contribution of the RBSM methodology in the study of the Cathedral's macro-element fragility analysis is important, but is not enough to address the seismic evaluation of the entire Cathedral, or part of it using a three-dimensional model with various resistant planes (macro-elements). As mentioned before, while the models generated with this tool must be plane, there is no restriction regarding the geometry that can be obtained e.g. in the architecture of the churches: arches, flying buttresses, abutments, etc. Based on this, there are many cases in which certain macro-elements of heritage churches or castles have been modeled with the RIGID software, and the results show good agreement with the current state of those structures (Casolo & Sanjust, 2009; Peña & García, 2016; Torres et al. 2017).

The study of unreinforced masonry structures can be done through various methodologies and tools developed for this purpose (Roca, Cervera, Gariup, & Pela, 2010). Among them, nonlinear approaches based on Finite Element Method (FEM) are widely used in the seismic assessment of masonry constructions (e.g. Mallardo et al. 2008; Peña et al. 2010; Sandoval et al. 2017; among others). Generally, in this type of modelling strategy, the masonry is treated as a fictitious homogeneous continuum while the structure can be described by means of 2D or 3D finite elements. The use of this type of models in the seismic assessment of large structural members or full masonry structures often requires high computational effort because of the structure geometry generation and the complexity of model resolution.

Masonry structures can also be analyzed by means of others numerical strategies, such as the Equivalent Frame Method (EFM) (Lagomarsino, Penna, Galasco, & Cattari, 2013). The structures studied using this method correspond to buildings where the following conditions must be satisfied: (i) the openings (doors and windows) of the walls must be regularly distributed, and based on this, the decomposition of resistant planes and facades in piers and spandrels is possible (Clementi, Gazzani, Poiani, & Lenci, 2016); (ii) the horizontal displacement is coupled at the floor levels by the presence of horizontal diaphragms (Lagomarsino et al., 2013); and (iii) mass is concentrated at the story levels (Magenes, 2000). The EFM method, which essentially discretizes the masonry elements by means of column-beam elements, has been employed in several investigations with interesting results (Addessi, Mastrandrea, & Sacco, 2014; Belmouden & Lestuzzi, 2009; Chen, Moon, & Yi, 2008; Magenes & Della Fontana, 1998; Roca, Molins, & Marí, 2005). However, due to the aforementioned conditions of use, masonry structures with irregular geometry, without intermediate floors where mass could be concentrated, and roofs without the adequate stiffness to unify the displacements of the wall tops, often they cannot be modeled with this type of approach.

The models based on bar-type elements have less degrees of freedom compared with the FEM models with 2D or 3D elements. For this reason, this modelling way constitutes a valuable solution to the problem of processing times. Additionally, there are several analysis programs —such as OpenSees (McKenna, 2014), SAP2000 (Computers and Structures, 2009), or Perform-3D (Computers and Structures, 2016)— that have very interesting tools for evaluating structures subjected to seismic loading considering bar-type elements with nonlinear constitutive laws.

Based on the facts described regarding EFM method and the model developed in RBSM as a reference model, there is a need to develop a simplified method that allows for optimization of time in the generation of structure geometry and reduction of processing times for finite element models, without neglecting the precision and reliability that the results must achieve. The aforementioned characteristics, which should be fulfilled by buildings in the EFM, do not correspond to the reality of churches. Thus, a new Nonlinear Framed Model (NLFM) will be proposed to solve, with appropriate reliability, the problems related to the optimization of resources in the modelling of these heritage structures.

To address the seismic evaluation of the entire Cathedral, or part of it, using a three-dimensional model, the research being developed would thus follow a path that it is important to describe. First, an experimental campaign was carried out, in which mechanical properties were defined for the model by identifying its modal properties (Torres et al. 2017). Second, the definition of the macro-elements of the Cathedral, and the fragility analysis for one of these components was carried out (Torres et al. 2017). Third, the generation of a new model is proposed, which is composed of axial-bending bars with masses concentrated in singular points of the model. This third stage corresponds with the third article of the research. Finally, as a future research, a three-dimensional model with several resistant planes could be generated, this simplified

model will help to carry out a complete fragility analysis of the Cathedral, taking into account seismic behavior in the two main directions of the building.

1.1 Objectives, Hypothesis and Methodology.

The research will be developed based on the following hypothesis:

- Accurate system identification of natural frequencies in narrow bandwidths can be achieved by increasing resolution in the frequency domain and the combined use of several identification methods based on the measurement of structure's response to ambient excitation, based on OMA methods.
- The fragility curves of the complete structure can be obtained from: pushover analysis proportional to the mass, and the generation of simplified nonlinear models

The background detailed in before section shows the importance of develop many subjects with the following objectives:

1. Estimate the values of mechanical properties for the materials of the Cathedral, based on a System Identification process, and update these properties in an analytical model.
2. Obtain the fragility curve of an important part of the structure. This is the nave macro-element. This analysis is carried out by means an incremental dynamic analysis (IDA).
3. Define a simplified framed model equivalent to a developed model in the second part. The elements used in this model are beam – column bars.

The first objective is reached by means of an experimental campaign where many devices were located in special points of the structure. These devices record the response of the structure to ambient vibrations. Then, this information is processed by means a System Identification software and the mechanical properties are defined. The process of Model Updating is solved by a multivariable optimization process. At the end of this

first part, there is a model with updated mechanical properties. This process is in Paper I: OPERATIONAL MODAL ANALYSIS AND FE MODEL UPDATING OF THE METROPOLITAN CATHEDRAL OF SANTIAGO, CHILE.

The second objective is managed as follows: Cathedral is divided in many components, which are called macro-elements. One of these is the nave macro-element, the most recurrent of the whole structure. Taking as basis the RBSM (Rigid Body Spring Model) a model of the nave macro-element is developed in the RIGID software. This model is solved for 11 records, scaled to 15 intensities by means of spectral matching methology. All of these cases give the base information to define the fragility curves. This process is in Paper II: FRAGILITY ANALYSIS OF THE NAVE MACRO-ELEMENT OF THE CATHEDRAL OF SANTIAGO, CHILE.

Finally the simplified model is developed by means of OpenSees software. In this model the rigid zones and length of plastic hinges are defined by the pattern damage generated in the model of rigid elements of the previous part. The verification of the model is carried out by comparison between the model with rigid elements and the model with bars, based on static and dynamic analyses. This process is in Paper III: SEISMIC ASSESSMENT OF A MASONRY MACRO-ELEMENT THROUGH A NONLINEAR FRAMED MODEL. A CASE STUDY.

The methodology to aim the objectives and the results of each mentioned article are described in the following sections.

1.2. System identification of the Metropolitan Cathedral of Santiago de Chile.

An experimental campaign was designed and implemented to estimate the modal properties of the Cathedral. This campaign consists of measuring the response of the structure to ambient vibrations at selected points. To select these points, areas were first

selected where the fundamental modes of a preliminary numerical model possessed higher amplitudes, and then the most easily accessible points were chosen. Six Trominos devices (MICROMED, 2012), which measure accelerations and velocity in 3 orthogonal directions, were used during the campaign. Twenty-two set-ups were defined to cover the entire structure. A set-up is an array of instruments where the structure response is recorded for at least 20 minutes.

The obtained signals were processed in ARTEMIS software (Structural Vibration Solutions A / S, 2015). This software has among others two different OMA methods that were used in this research: Enhanced Frequency Domain Decomposition - EFDD (Brincker et al., 2001) and Stochastic Subspace Identification - SSI (Van Overschee & De Moor, 1996). The EFDD method was applied using a manual peak-picking process on the singular value curves. On the other hand, the SSI method was applied based on Crystal Clear algorithm (Goursat et al., 2010) and stabilization diagrams for the visualization of results. The potential EFDD frequencies were first selected by peak peaking process to evaluate the experimental mode validities, the frequency selection was then confirmed by SSI method. The linear independence of these experimental modes was verified from the calculus of Modal Assurance Criterion (MAC) (Allemang & Brown, 1982) between them. The defined experimental modes can be seen on Table 1. For all experimental mode pairs observed in Table 1, the frequencies defined according to EFDD are very close to SSI frequencies. The differences between frequencies are because the frequency values identified correspond to a band and not to precise values, given the non-linearity in the behavior of the structure.

First proposed mechanical properties of materials for analytical model were determined experimentally, for stone masonry (Oliveira, 2002), and in the case of brick masonry based in previous research of another heritage structure contemporaneously built (Valledor et al. 2015). It is important to note that the top of the north façade of Cathedral is reinforced with metal anchors; then there is a third material, called reinforced brick

masonry, whose modulus is initially assumed to be at the same brick masonry value. Table 2 summarizes the initial values for calibration parameters.

Table 1. Experimental frequencies.

	EFDD method	SSI method
Experimental mode	Frequency (Hz)	Frequency (Hz)
1	1.81	1.74
2	1.96	1.93
3	2.03	2.06
4	2.38	2.38
5	2.55	2.56
6	2.76	2.79
7	2.86	2.86
8	2.95	2.93
9	3.18	3.20

Table 2. Initial calibration parameter values.

Calibration parameter	Initial value
Young's modulus of stone masonry E_{sm} (MPa).	1,390
Young's modulus of brick masonry E_{bm} (MPa).	1,780
Young's modulus of the reinforced masonry E_{rm} (MPa).	1,780
Lateral stiffness factor from Chapel	1.00
Lateral stiffness factor from Sacristy	1.00
Lateral stiffness factor from Tabernacle	1.00

The model updating is developed using a two-stage optimization problem. The first adjustment of mechanical properties and boundary conditions, given by adjacent structures, is based on minimizing the error function between experimental and analytical frequencies. A second stage of model updating process is carried out, based on

minimizing the difference between frequency and MAC values, when varying the Young's moduli of the three main materials within physically ranges.

The analytical model to model updating process is generated in DIANA software (TNO DIANA, 2015). This model considers only the rigid zones of the Cathedral. In such a way that the flexible components (towers and dome) and adjacent structures (chapel, tabernacle and sacristy) were considered in the model but in a simplified way.

The first stage of model updating process was made by comparing the frequencies obtained experimentally (Table 1) with those calculated by the FE model, based on the initial parameter values (Table 3). The match between modes for model updating is based on the visual qualitative assessment of the mode shapes and quantification of the MAC between experimental mode shapes and those obtained from the numerical model (Table 4). Based on Table 4, the four first numerical modes were not considered, because they are related to towers movement, and the experimental model cannot reproduce this, because the response of the structure was not recorded in this flexible zones.

The method proposed by Douglas & Reid, (1982) was initially applied in this study for updating model. This process is based on: first, the definition of approximating function expressing the numerical frequency based on a quadratic function of the calibration parameters, second, the error is defined as difference between the analytical frequency and the experimental frequency; third, all error functions are concentrated in a single expression, and so the problem becomes a multi-variable (each of one of calibration parameters) optimization problem with a single objective (total error). Finally, after this function error minimization process, the calibration parameters were obtained (Table 5).

Table 3. Numerical frequencies (initial calibration parameters).

Numerical mode	Frequency (Hz)	Mass participation based on FE model (%)	Mode description
1	1.38	0.48	Bending of south tower.
2	1.39	0.15	Bending of north tower.
3	1.41	0.61	Bending of south tower.
4	1.43	0.43	Bending of north tower.
5	1.90	27.48	Transverse bending of longitudinal walls.
6	2.02	0.27	Transverse bending of south longitudinal walls.
7	2.19	1.73	Transverse bending of longitudinal walls and bending dome.
8	2.27	0.11	Bending dome.
9	2.32	1.55	Transverse bending of longitudinal walls and bending dome.
10	2.40	0.53	Transverse bending of south longitudinal walls.
11	2.54	5.44	Bending dome.
12	2.56	0.02	Transverse bending of longitudinal walls.
13	2.59	0.63	Transverse bending of longitudinal walls.
14	2.83	2.24	Transverse bending of longitudinal walls.
15	2.97	0.22	Transverse bending of longitudinal walls.

Table 4. Couples experimental and numerical (obtained with initial parameters) frequencies according to their similarity in modal shape and MAC.

Experimental Mode number	Experimental frequency (Hz)	Numerical Mode number	Numerical frequency (Hz)	MAC
2	1.96	5	1.90	0.85
4	2.38	7	2.19	0.61
8	2.95	14	2.83	0.55
9	3.18	15	2.97	0.69

Table 5. Frequency optimized values of calibration parameters with model updating based on function error minimization.

Calibration parameter	Frequency optimized value
Young's modulus of stone masonry E_{sm} (MPa).	1560
Young's modulus of brick masonry E_{bm} (MPa).	1700
Young's modulus of the reinforced masonry E_{rm} (MPa).	1870
Lateral stiffness factor from Chapel	3.265
Lateral stiffness factor from Sacristy	3.526
Lateral stiffness factor from Tabernacle	3.063

The second stage of model updating was based on large number of models, generated in a grid search, in which the Young's modulus of materials vary within a defined range. The lateral stiffness factors do not change and the frequency optimized values were fixed.

A wider range of variation for the calibration parameters values was allowed (between 50% and approx. 150%. of central values). The step increases in each parameter range were 10% but, when close to the central values, the increase was 5%. The total number of models generated with the described increments is 910. The change of the calibration parameters is given by a multidimensional matrix where all possible combinations are given. The order of variation of the calibration parameters starting with the variation of Young's modulus of the reinforced masonry, then the variation of Young's modulus of brick masonry, and finally the variation of Young's modulus of the stone masonry. The models for which Young's modulus of reinforced masonry was lower than for brick masonry were not included.

The model updating process was done by comparing the modal parameters obtained experimentally with those calculated by FE model perturbation. The distance between models was calculated using expression (Eq. 1).

$$d = \sum_{i=1}^{M} w_{i,MAC}\left[w_f \frac{\left| f_i - fex_i \right|}{fex_i} + w_\phi \left[1 - MAC(\phi_i, \phi ex_i) \right] \right] \quad (1)$$

where: f_i represents the analytical frequency, fex_i is the experimental frequency, ϕ_i represents the vector of the analytical modal shape, ϕex_i is the vector of experimental modal shape, $w_{i,MAC}$ is the weighting factor based on the MAC between the analytical modal shape and experimental one, w_f is the weighting factor of frequency summation term and w_ϕ is the weighting factor of modal shape summation term; the last two weighting factors add up to unity. In all these terms, i subscript means the mode number that is being evaluated.

The expression (1) proposes that the frequency and modal shape have different weighting factors based on the confidence that exists in their experimental determination (Friswell & Mottershead, 1995). This expression relates all modes that participate in the model updating, distinguishing the different participation for frequency term against modal shape term, and additionally the different participation of each mode.

Several different weighting factors w_f and w_ϕ were tested to evaluate their effect on model selection. From these tries, when the factor w_f assumes a value of 0.90 the model updating process is refined to get calibration parameters more adjusted.

A new variation range for the calibration parameters was therefore defined for the new area of interest, where the steps of variation were 3%. The additional number of models generated for this last step is 147. For this new group of models, the error between experimental and analytical frequencies, and the MAC variation between the analytical and experimental modal shapes are analyzed directly. The errors have been calculated based on frequencies and modal shapes obtained in analytical model with the calibration parameters of the first stage (Table 5), these reference values are in Table 6.

Table 6. Reference values for frequencies and modal shapes.

	Mode 1	Mode 2	Mode 3	Mode 4
Experimental frequencies (Hz)	1.96	2.38	2.95	3.18
Analytical frequencies for frequency optimized values (Hz)	2.00	2.28	2.97	3.11
Percentage errors betweeen frecuencies	2.0%	4.2%	0.8%	2.4%
MAC	0.85	0.64	0.59	0.74

For defining the final ranges of calibration parameters, the graphs of error frequency and MAC variation were constructed for this second group of models (Figure 3). The analytical model is appropriate when the frequency error is below the segmented lines; and in the case of MAC, the analytical model is appropriate when the MAC values are above the segmented lines. Therefore, adequate ranges of calibration parameters are shown in Table 7.

Information more detailed about this part is in the Chapter 2 of this document (Paper 1).

1.3. Fragility Analysis of naves macroelement of the Cathedral.

The fragility analysis of a complex structure like the Cathedral requires simple computational models but sufficiently validated. As already commented, the subdivision of the complete structure of a church into macro-elements is a way to face this task. Figure 4 shows the portion of the whole model corresponding to the nave macro-element. Such macro-element has been considered as the most representative for the purpose of investigating the seismic fragility of the Cathedral.

The Young's modulus of the materials were obtained from the first part of this research, but there are many other properties that require been defined for nonlinear analysis of

the structure. The compressive strength of brick masonry was defined based on a contemporary structure that is located close to Cathedral: Palacio Pereira building (Valledor et al. 2015). The compression strength of stone masonry was based on the expression E= α fc, with α=200 (Tomazevic, 1999). Moreover, all tensile strengths were assumed as 10% of compression strength (Angelillo, Lourenco, & Milani, 2014; Meli, 1998). The cohesion was assumed as the same value of tensile strength (García & Meli, 2009). The residual tensile strength was assumed as the half of tensile strength based on the fracture energy and the ductility index (Angelillo et al., 2014). Table 8 summarizes all mechanical properties required for nonlinear analyses.

a)

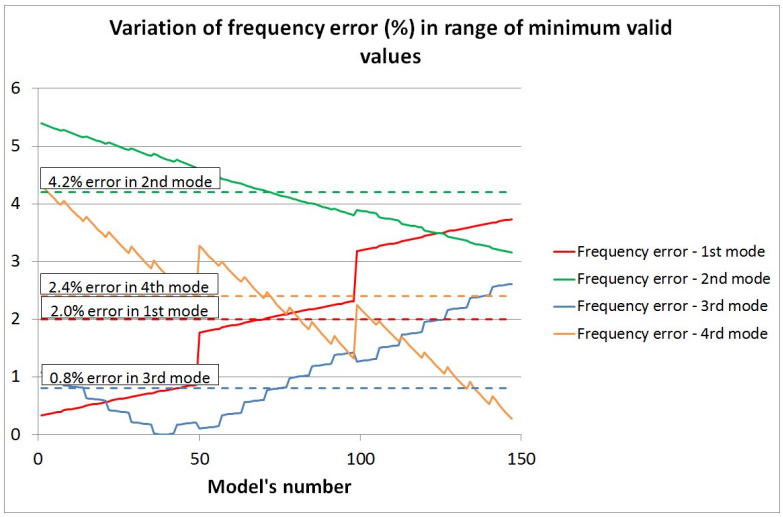

b)

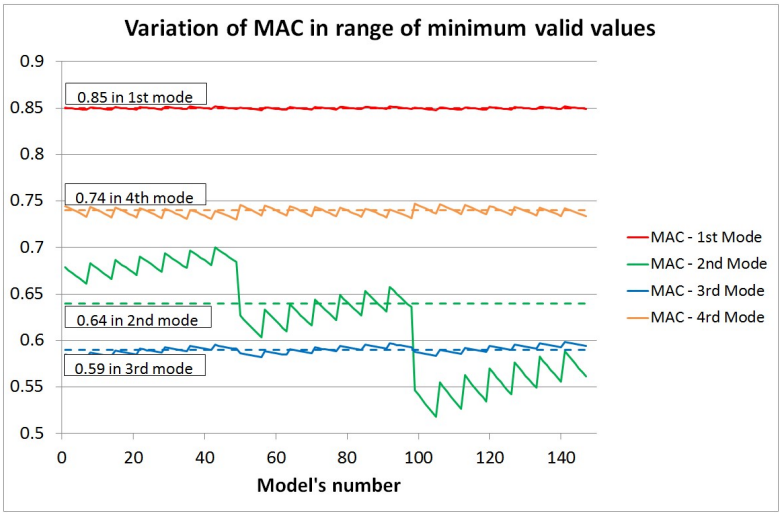

Figure 3. Results of the second stage of model updating a) Frequency error for each mode. b) MAC for each mode.

Table 7. Valid ranges of calibration parameters.

Calibration parameter	Min. value	Max. value
Young's modulus of stone masonry E_{sm} (MPa).	1510	1550
Young's modulus of brick masonry E_{bm} (MPa).	1540	1850
Young's modulus of the reinforced masonry E_{rm} (MPa).	1780	2140

The macro-element also includes materials that do not correspond to masonry, such as the roof structure of the north and south naves, the vault of the central nave and the steel shoring of the highest part of the central walls. The structural components before mentioned were modelled as linear-elastic, since the damage survey reports only damage in the masonry.

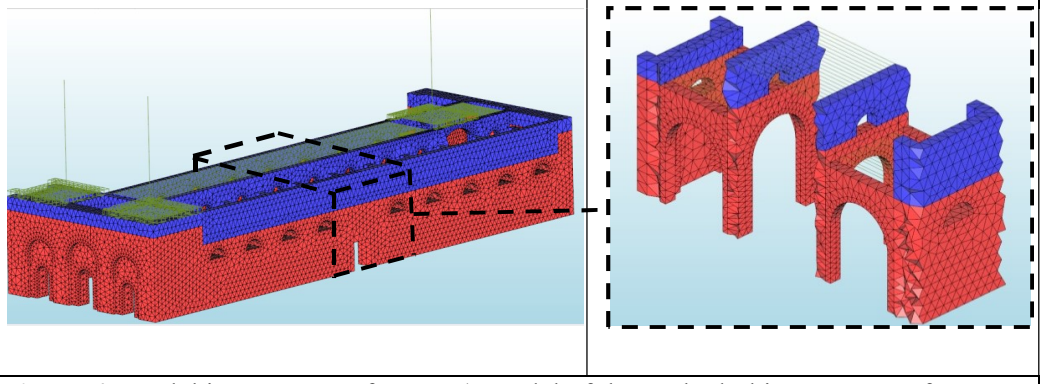

Figure 4. Model in DIANA software. a) Model of the Cathedral in DIANA software, b) FE model of the nave macro-element.

Table 8. Mechanical properties required for non-linear analysis of the macro-element.

	Stone masonry	Brick masonry	Reinforced masonry
Compressive strength (MPa)	7.80	3.25	3.58
Tensile strength (MPa)	0.78	0.33	0.36
Residual Tensile strength (MPa)	0.39	0.18	0.22
Cohesion (MPa)	0.78	0.33	0.36
Friction angle (degrees)	30	35	35

For this study, the RBSM approach (Casolo 2004, 2009; Casolo & Peña 2007) was selected as a simple method to analyse the nave macro-element. This is a simplified numerical method for masonry structures, which models the masonry as a set of rigid elements connected to each other through springs concentring the nonlinear behaviour. Each interface of the elements has incorporated three non-linear springs, i.e. two axial ones located near the edges of the interface and one central shear spring. The RBSM model is considered as in-plane model.

The nave macro-element has been modelled using the software package RIGID (Peña & Casolo, 2012). The model is composed of 386 undeformable elements, i.e. there are 1158 dof in this model, a very small number compared with approximately 60,000 dof of the DIANA equivalent model. There are many sections in the macro-element, each one of those has a specific thickness because the model represents a three-dimensional part of the whole structure in a two-dimensional model. The base interfaces are fixed as they represent the support of the ground to the structure. Figure 5 shows the model of the macro-element.

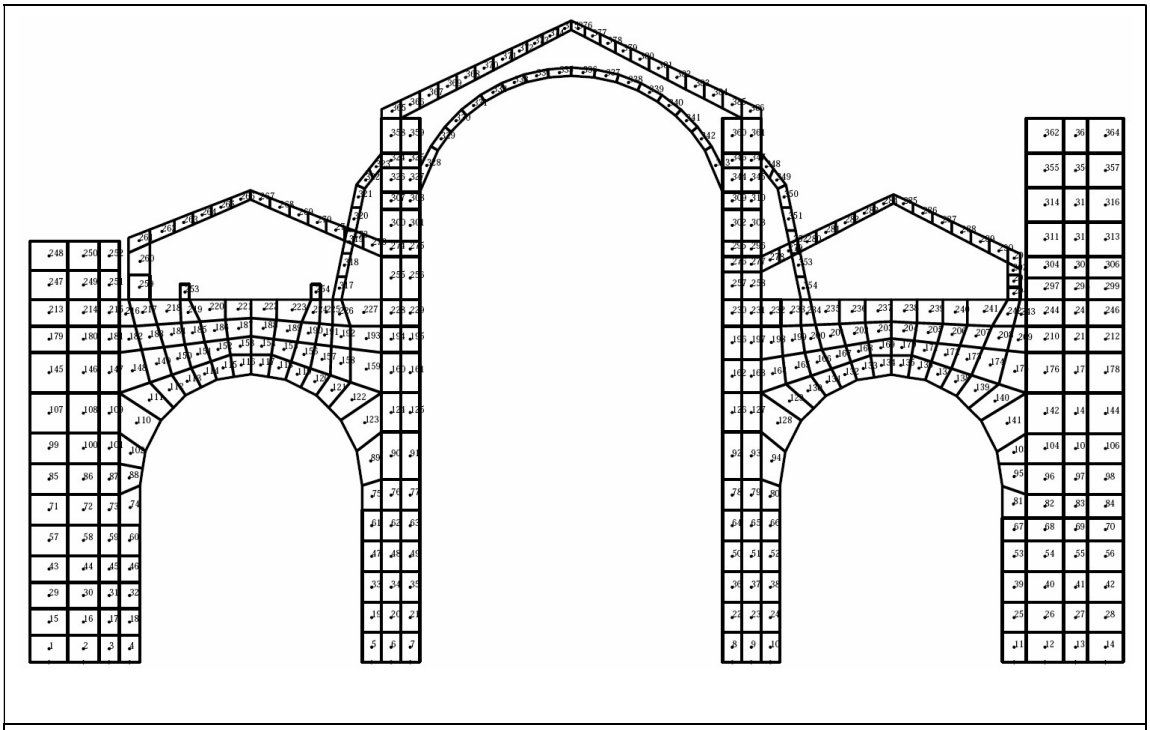

Figure 5. Macro-element model generated in RIGID software package.

Based on research by Irizarry et al. (2003) and by Lagomarsino & Cattari (2015), the dynamic behavior of a macro-element is very similar irrespective of whether analyzed separately or as part of a complete structure. This is because the macro-element shows a sufficiently autonomous seismic response in respect to the rest of the structure. From comparison between the individual macro-element and complete model of Cathedral,

the MAC values and the errors between the natural frequencies are shown in Table 9. Based on the values displayed in this table, the behavior of an isolated macro-element is equivalent to the corresponding portion in the full model.

Once validated, the RIGID model of the nave macro-element is used to study it under different seismic intensities. Eleven real seismic records were selected for the fragility analysis based on giving a greater statistical confiability to the mean response of structures (Haselton et al., 2014). This recommendation comes from comparison between Chapter 16 of proposed ASCE/SEI 7-16 standard and the existing one (ASCE, 2010). These events have been important in the recent history of seismic instrumentation in Santiago de Chile. Fifteen response spectrum-matching were generated using the 11 real records as a seed ground motions (Clough & Penzien, 2003). It is important to generate these synthetic accelerograms because the real records define an objective spectrum different to the spectrum of Chile earthquake standard; therefore, it is important to scale the record in the frequency domain. The variation of sesimic intensities was based on the design earthquake of the Chilean seismic code (INN 2009) (475 years of return period) and the hazard curve of Santiago de Chile (Fischer et al., 2002).

Table 9. Comparison of two modes of the respective portion of the full model with model of the nave macro-element.

	First similar mode	Second similar mode
Frequency of complete model (Hz)	2.00	2.28
Frequency of isolated nave macro-element model (Hz)	2.01	2.14
Error between frequencies based on frequency of complete model (%)	0.50	6.14
MAC	0.84	0.77

Eleven real seismic records were selected for the fragility analysis based on giving a greater statistical confiability to the mean response of structures (Haselton et al., 2014).

This recommendation comes from comparison between Chapter 16 of proposed ASCE/SEI 7-16 standard and the existing one (ASCE, 2010). These events have been important in the recent history of seismic instrumentation in Santiago de Chile. Fifteen response spectrum-matching were generated using the 11 real records as a seed ground motions (Clough & Penzien, 2003). It is important to generate these synthetic accelerograms because the real records define an objective spectrum different to the spectrum of Chile earthquake standard; therefore, it is important to scale the record in the frequency domain. The variation of seismic intensities was based on the design earthquake of the Chilean seismic code (INN 2009) (475 years of return period) and the hazard curve of Santiago de Chile (Fischer et al., 2002).

Based on related research on fragility analysis performed on masonry and concrete structures, four levels of performance are defined using as damage parameter the drift of the structure (Lagomarsino & Giovinazzi, 2006). For the case under study, the macro-element of the naves does not correspond to a regular body of masonry as it also contains two bodies of arches with roof systems of wood or metal, which are connected by a wooden roof and vault. Therefore, the damage parameter proposed in this study is the damage index based on stiffness degradation, which is defined as the ratio between the base shear and the displacement of a control point (Casarin, 2006).

All the damage levels of the structure based on stiffness degradation were established based on the two extremes of performance of Lagomarsino & Giovinazzi (2006), and intermediates were determined by comparison of the stiffness degradation index with the drifts given in the same reference. This comparison was carried out based on two static non-linear (pushover) analyses proportional to the mass (Caselles et al., 2011), one in the positive direction and the other in the negative direction. Despite the structure is not symmetrical, the relation between drift and stiffness degradation presents the same result in this second damage parameter. Performance levels according to

Lagomarsino & Giovinazzi (2006) and the stiffness degradation index are shown in Table 10.

Table 10. Relation of damage parameters for each performance level (d_Y = yielding displacement and d_U = ultimate displacement)

Performance level	Drift based on Lagomarsino & Giovinazzi (2006)	Stiffness index i_k (%)
1. No damage	$0.70*d_Y$	90
2. Damage limitation	$1.5*d_Y$	70
3. Significant damage	$0.5*(d_Y+d_U)$	35
4. Near collapse	d_U	20

The performance levels defined in Table 10 generates five performance damage states: Slight damage state for a stiffness degradation index more than 90%, Moderate damage state if the stiffness degradation index between 70 and 90%, Heavy damage state for a stiffness degradation value between 35 and 70%, Very heavy damage state for a stiffness degradation value between 20 and 35%, and Collapse damage state for stiffness degradation values less than 20%.

The values of base shear and displacement of the control point were obtained from numerical models for each accelerogram, with this information, the number of cycles was determined. A cycle is defined as the portion of information with a positive slope between the extreme values, i.e. the changes in base shear and displacement of the extreme values are either positive or negative, and the stiffness index is calculated from the extreme points of each cycle. Finally, to facilitate the interpretation and to improve the visualization of results, the stiffness index value was processed by a moving average with a window of 8 values of width.

As an example, in Figure 6 graphs depict the stiffness degradation index versus the number of cycles for some of the seismic intensities (2%, 5%, 10%, 30%, 60% and 90% probability of exceedance in 50 years) of the Maule (2010) earthquake at the Santiago Centro station (one of the eleven records). As the seismic intensity increases, the residual stiffness degradation index decreases. The continuous curve is an approximation of the segmented curve based on the least square method.

For the definition of fragility curve, the engineering parameter adopted was the Peak Ground Acceleration (PGA). This parameter was calculated using the average of the PGA of synthetically generated records for each intensity. The distribution of the conditional probability of failure was assessed by numbering the cases where the remaining stiffness degradation index was located within each of the ranges given before (slight damage, moderate damage, heavy damage, very heavy damage and collapse damage).

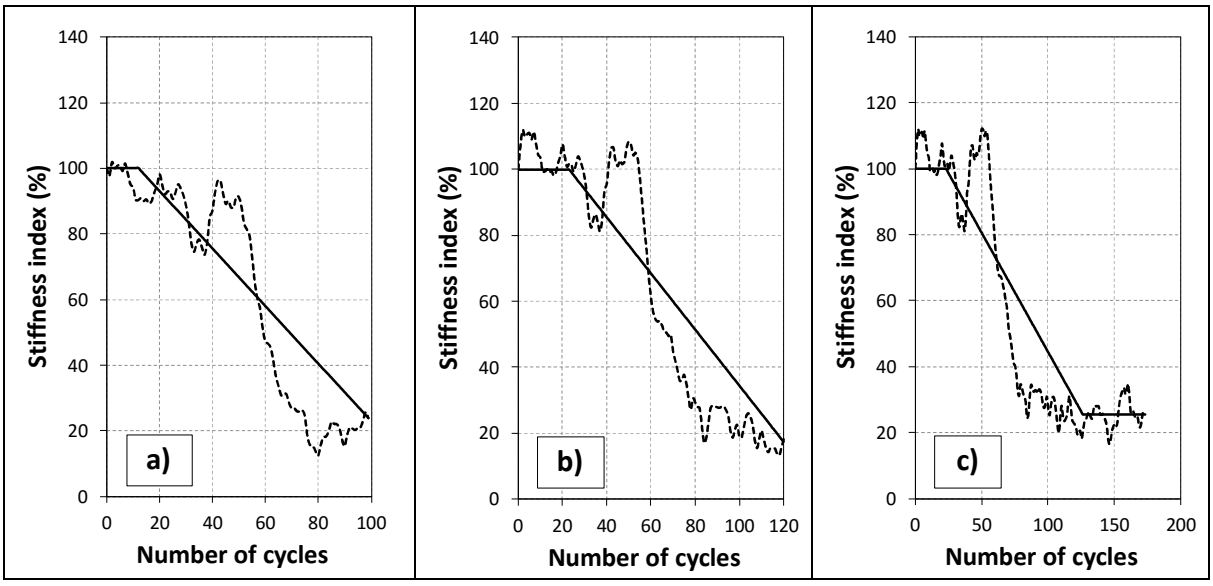

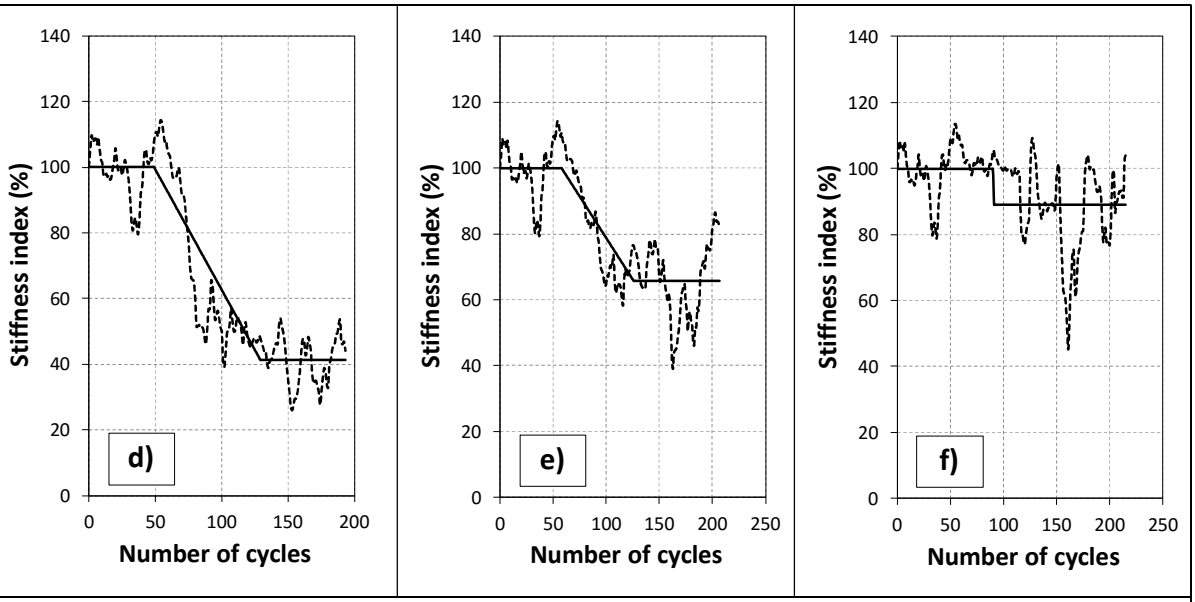

Figure 6. Evolution of stiffness degradation for the 2010 Maule earthquake (Santiago Centro station) with some dependent intensities of the probability of exceedance in 50 years: a) 2%; b) 5%; c) 10%; d) 30%; e) 60%; f) 90%.

The collapse mechanism defined based on pushover analysis is given by the development of plastic hinges on the arches and in the base of the columns. In a previous research (Torres et al. 2017), one of the damage found in the structure (many arches of northern longitudinal nave) given by its seismic history shows the coherence between the finding of this study and the current state of the Cathedral (Figure 7).

The fragility curves for the four damage states can be seen in Figure 8.

More detailed information about this part is in the Chapter 3 of this document (Paper 2).

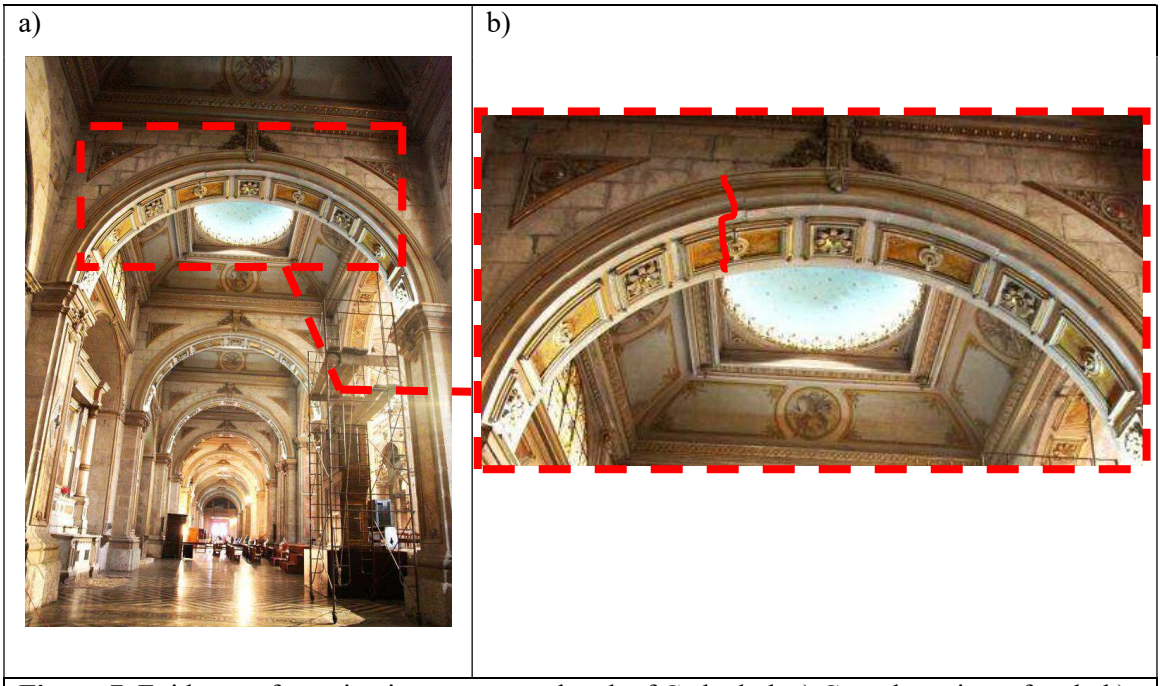

Figure 7. Evidence of opening in a transversal arch of Cathedral. a) Complete view of arch, b) Zooming the cracking of the arch.

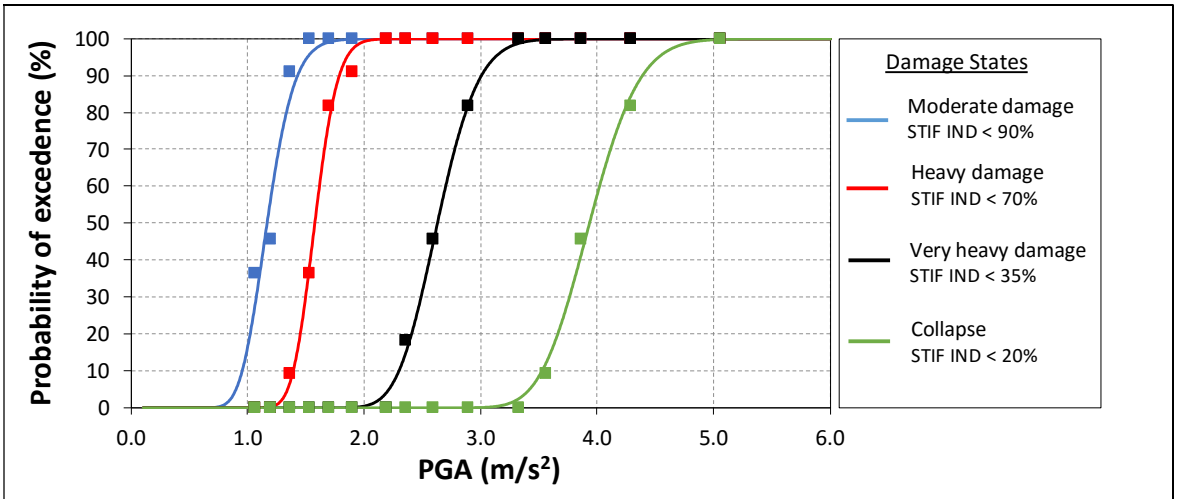

Figure 8. Fragility curves for Nave macro-element.

1.4. Framed simplified model of nave macro-element of the Cathedral.

Despite the previous model built in RIGID (RBSM model) is suitable for seismic analysis, it is limited to a plane analysis; therefore, it is necessary the generation of the NLFM model. The proposed model must be equivalent to the first one.

One of the results that can be obtained from the RBSM model is the damage pattern after the dynamic analysis has been carried out. This damage pattern shows the areas yielded in the model (Figure 9).

The methodology to built and validate the proposed NLFM model has two steps. The first step is to propose an initial geometry based on interpreting the damage pattern obtained of the RBSM model (Figure 9), i.e. recognizing the zones that remain essentially elastic without damage and the zones where the plasticity should be concentrated. The second step is the verification of the model by means of static and dynamic analyses.

Geometry of the model (size and shape) play an important role in any structure, and further in heritage buildings. Various beam shape options were studied in the trial and error process. The last of these was the arch-shaped beam with rigid zones at the ends, length of potential hinges, and variable section height. This shape allows to the NLFM model to have a geometry and bending behavior similar to the RBSM model.

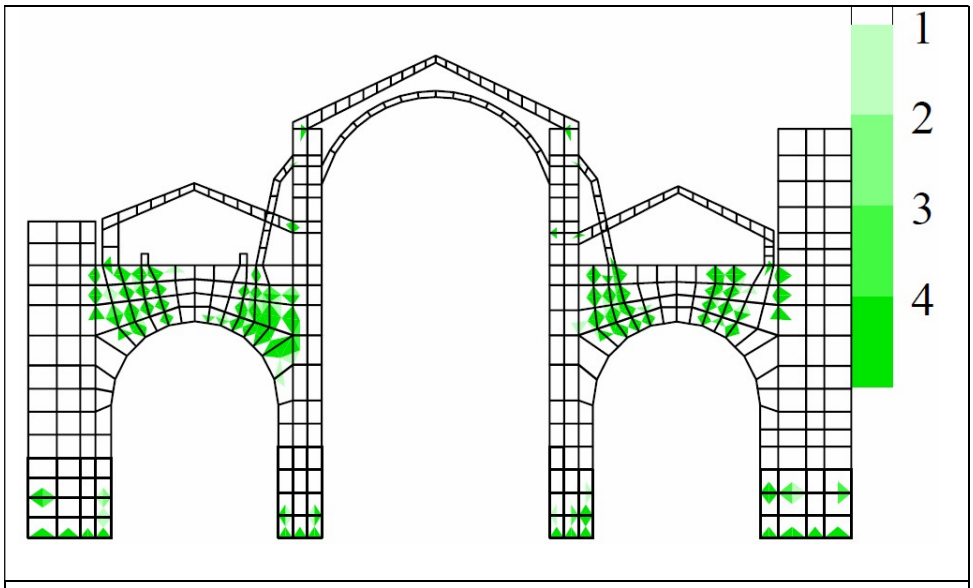

Figure 9. Damage pattern of the nave macro-element for a cyclic pushover, obtained from RBSM model by means RIGID software (Torres et al. 2017).

The NLFM model was generated by means of Opensees software (McKenna, 2014). Each of the bars for columns and beams in the arches is a *BeamwithHinges* element of Opensees software (Mazzoni et al. 2007). This element has a plastic hinge length at its ends (the length of yielding is defined by the user) and its intermediate zone remains elastic. Figure 10a shows the location of plastic hinges in the base of columns and in the portions of beams L1 and L2. The location of rigid zones should additionally be noted; i.e. the connection zone between piers and arches that are without damage, according to Figure 9. Aditionally, Figure 10b shows the distribution of all kind of masonry materials in the macro-element.

a)

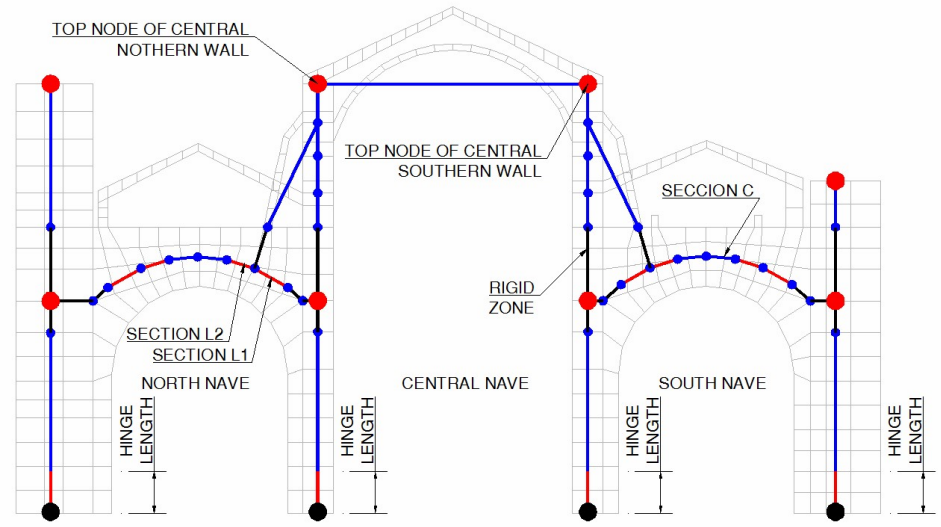

b)

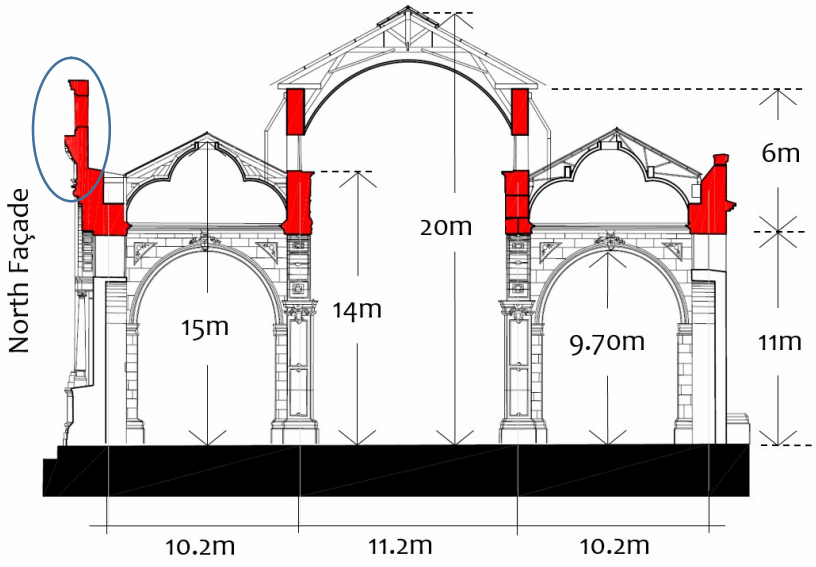

Figure 10. Opensees model of the nave macro-element: a) Location of hinges (red lines), rigid zones (black lines), zones that remains elastic (blue lines), structure nodes (blue filled circles), mass nodes (red filed circles), and fixed nodes (black filled circles), b) Materials that make up the nave macro-element: stone masonry at the base of structure, brickwork walls in red colour, and the highlighted top zone of north façade is made of reinforced brickwork, as was seen in the previous chapter (Torres et al. 2017).

After several alternatives to define the geometry of the arches in the structure, it was decided that straight sections of beams that define arch shape in the Cathedral's south and north naves would be used (Figure 10a). The section of the beams is not unique, as it changes based on the height of sections generated when defining a barycentric axis with respect to the top and bottom borders of the north and south arches (Figure 11). As previously mentioned, sections L1 and L2 are plastic hinge zones, and section C of the arch remains elastic in the analysis.

An important factor to be taken into account in the comparison between the models is the difference between the lateral load pattern for the RBSM and the proposed NLFM. In the first model, lateral force is applied by low frequency acceleration in the base (quasi-static force), and thus the apparent force present is related to a distributed force over the entire length of the vertical elements. By the contrast, in the NFLM model the force is concentrated at certain nodes of the structure (Figure 10a).

This difference was previously studied by Biggs (1964), who proposed an equivalent model for a single degree of freedom for a simple frame, and detected that certain equivalences could be established between the real model (with distributed mass) and that of a single degree of freedom (lumped mass).

To exemplify this issue, a vertical bar model fully restricted at the bottom end and subject to a uniformly distributed load in its length was taken as basis. This model was compared with the same bar, subject to a concentrated load of the free end node. If there is a condition in which the displacement in the free node is the same for both models, a relationship can be obtained between the reactions in the restricted node of the models (Figure 12). The adjustment factor between the two models is 8/3 = 2.67. The displacement of the free node is taken as basis since it provides an idea of the element's deterioration within a non-linear analysis.

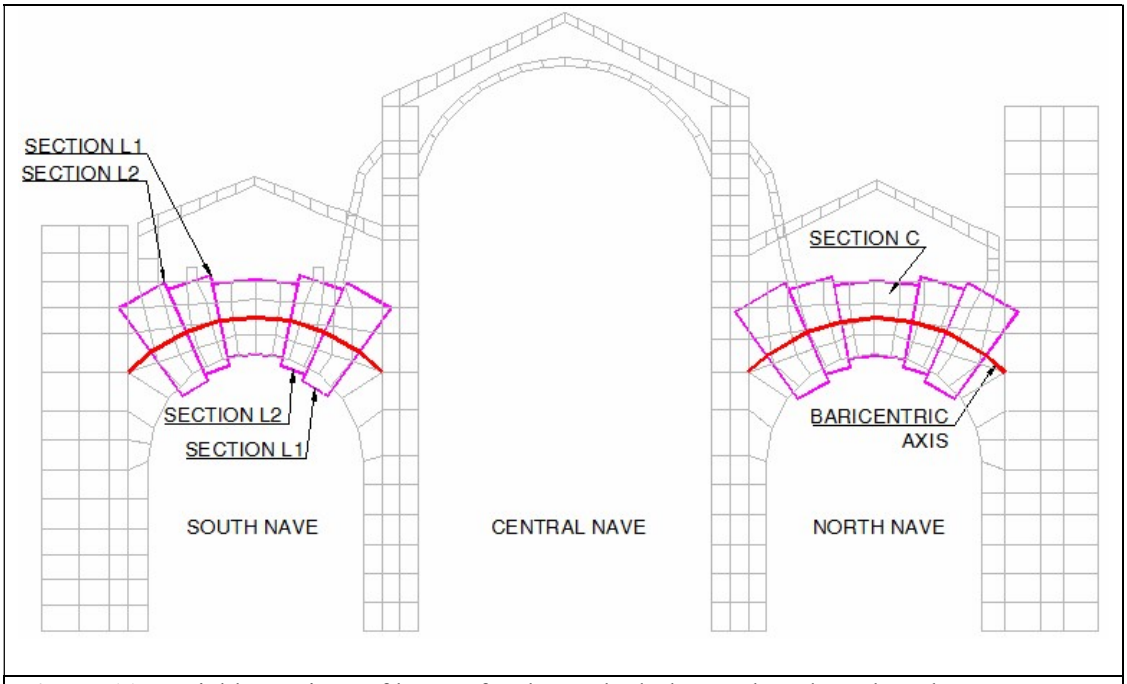

Figure 11. Variable sections of beams for the Cathedral's north and south arches.

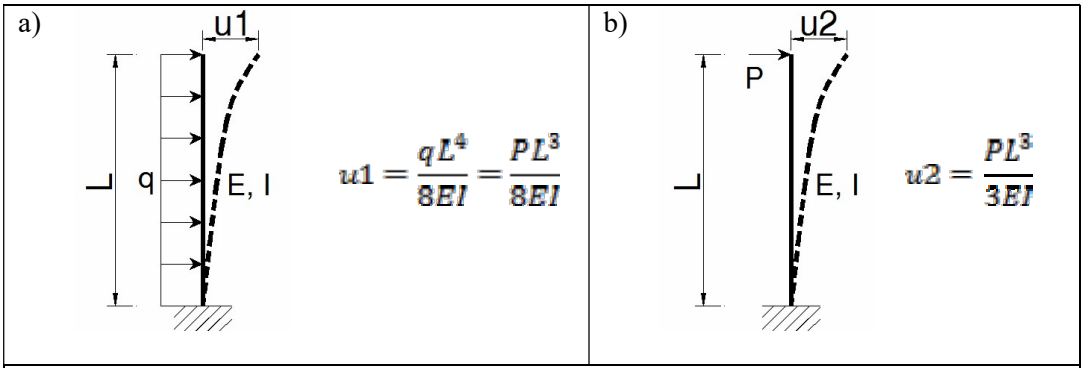

Figure 12. Comparison between models of cantilever column: a) Wilth uniform distributed load, and b) With concentrated load.

Likewise, the RIGID model with distributed load should have an adjustment factor for comparison with the NLFM model. Unlike in the previous case, this factor is not easy to determine because there are many particularities in the macro-element model, such as the beam's stiffness compared with the stiffness of the piers, the non-uniform

distribution of the load (based on mass distribution), etc. It is thus known that there is an adjustment factor, but its value cannot be easily determined.

The monotonic pushover analysis of the macro-element was generated based on the series of displacements of the control point obtained from the RIGID model of Torres et al. (2017). Two nodes were selected as control points: the top node of the southern center wall and the top node of the northern center wall (Figure 10a). The first control point is for the pushover from left to right, and the second for the pushover from right to left. These cases were analyzed as such because of the structure's non-symmetry.

In this comparison it can be seen that there are differences between the frequencies of the models for the two modes; this is precisely due to the mass difference considered, since there is an amount of mass concentrated in the support nodes.

Because the analysis of the RBSM model corresponds with a cyclic pushover (pseudo-static analysis), and the analysis of NLFM model is a monotonic pushover with a return to cero of the displacement in the control point, the response of the second model should be the envelope of the first. Therefore, if an adjustment factor is defined for the NLFM model to relate the two responses, it could be seen that the two models have a very close correspondence in shape and amplitude (Figure 13). The behavior and successive loss of stiffness can thus be shown to be logical between the two models. It should be noted that this adjustment factor ought to be validated in future analyses of other structural macro-elements.

Given that the process to calibrate static properties based on stiffness was developed in the previous section, it is now necessary to confirm that the dynamic behavior, fundamentally dependent on damping and mass, is similar between the two models. The critical damping ratio (for the Rayleigh case) assumed for this type of structures is 6%

(Meli, 1998) based only on the structure's mass (Casolo & Pena, 2004). The damping value was the same in both models.

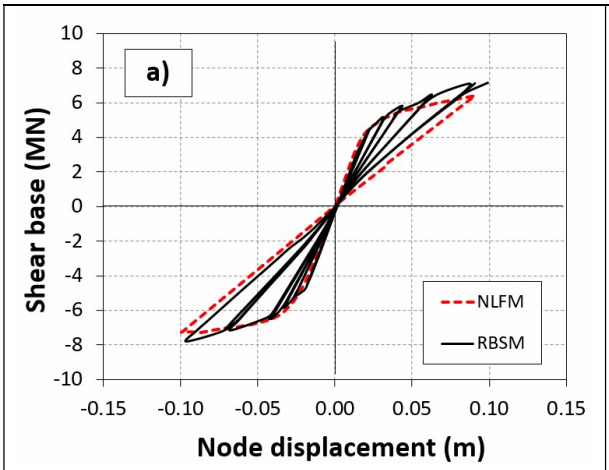

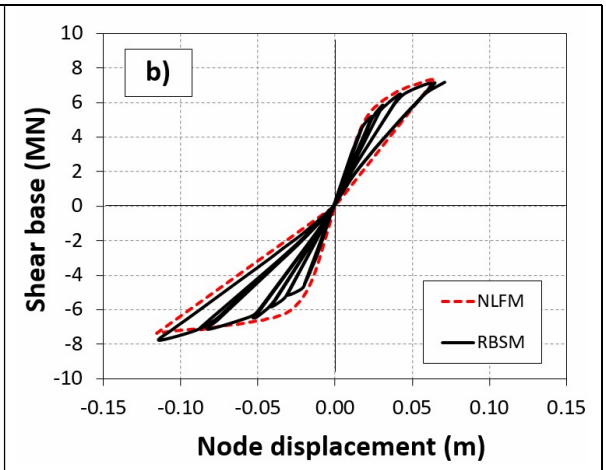

Figure 13. Comparison between the static responses of the RIGID model and bars model with adjustment factor: a) for the top node of the southern central wall, and b) for the top node of the northern central wall.

Considering that one of the proposed model's basic assumptions is to define lumped masses at the points of intersection with the rest of the possible transversal elements (for the case of three dimensional model in future research), the proposed mass distribution can be seen in Figure 10a. The mass of each vertical element is divided equally between its two extreme nodes; additionally, the mass of the arches is concentrated in the node that they reach in the columns. Based on this assumption of mass distribution, the first and second natural frequencies obtained from the NLFM model by means of the Opensees software were calculated and compared with those calculated from the RBSM model using the RIGID software (Table 11).

For the dynamic verification, the fragility analysis carried out in the nave macro-element by means of the RIGID software in the previous section (Torres et al. 2017) is

taken as basis. The stiffness index is also assumed as a measure of damage in this section.

Table 11. Comparison between the natural frequencies of the RBSM model and the NLFM model.

Mode	RIGID model frequency (Hz)	OpenSees model frequency (Hz)	Difference based on RIGID model frequency (%)
1	2.01	2.33	16%
2	2.14	2.38	11%

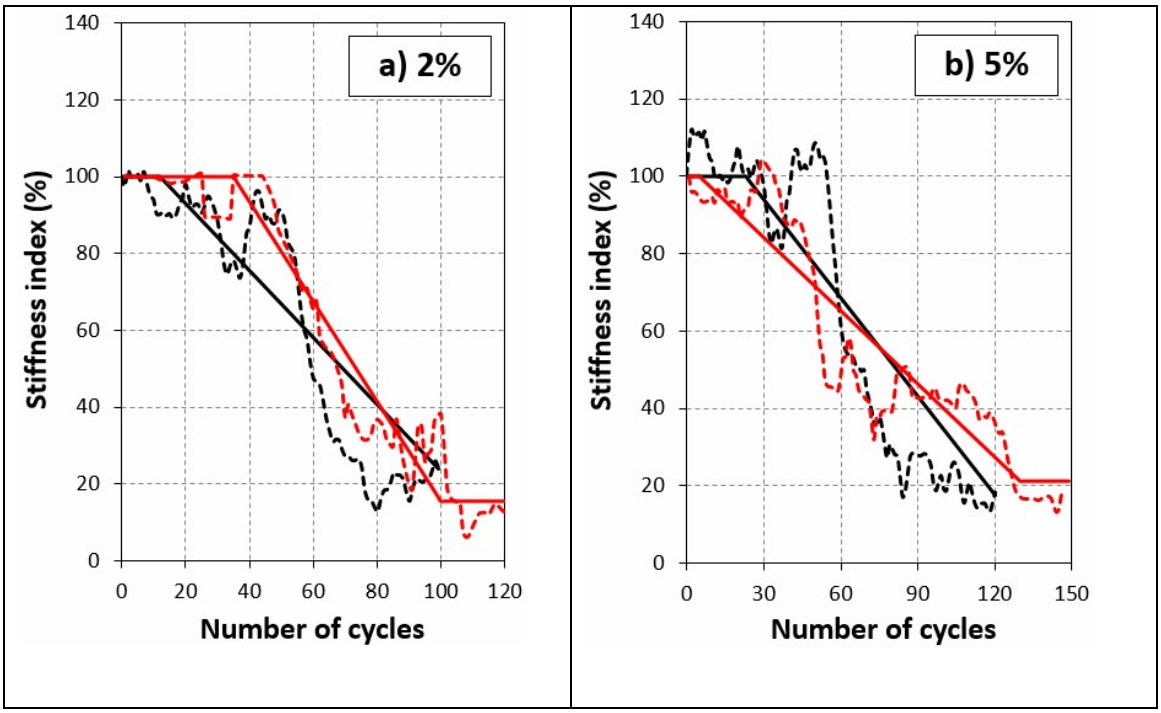

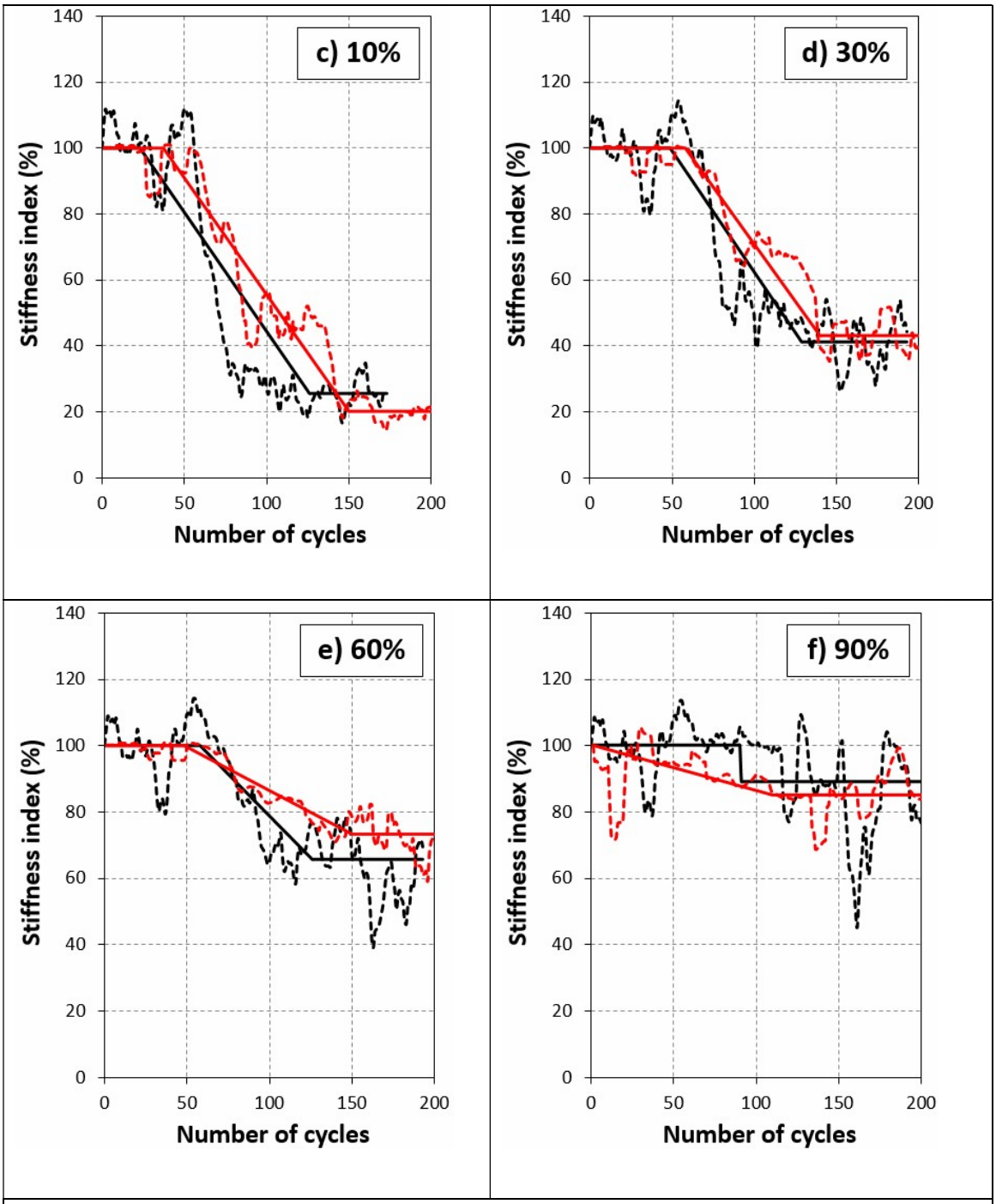

Figure 14. Comparison between the dynamic responses of the RBSM model and the NLFM model, for different seismic intensities based on exceedance probability in 50 years. In black the response obtained from RBSM model, and in red the response obtained from NLFM model.

The model was tested based on 6 scaled seismic intensities (varying the exceedance probability of an event over a time period of 50 years) according to spectral matching methodology (Clough & Penzien, 2003), from a seed record of the 2010 Maule earthquake (Santiago Centro Station). The performance of both structure models can be seen in the graphs shown in Figure 14.

The Figure 14 graphs have two types of lines: the dashed line represents the evolution of a stiffness index processed by a mobile media with a window of 8 width values, and the continues line is an approximation of the segmented line based on the least square method. With the behavior graphs showing the loss of stiffness for each of the seismic intensities, it can be seen that the final results are very similar for the two models.

Information more detailed about this part is in the Chapter 4 of this document (Paper 3).

2. OPERATIONAL MODAL ANALYSIS AND FE MODEL UPDATING OF THE METROPOLITAN CATHEDRAL OF SANTIAGO, CHILE.

Wilson Torres[a], José Luis Almazán[a], Cristián Sandoval[a,b], Rubén Boroschek[c]

[a] *Department of Structural and Geotechnical Engineering, Pontificia Universidad Católica de Chile, Vicuña Mackenna 4860, Santiago de Chile, Chile.*

[b] *School of Architecture, Pontificia Universidad Católica de Chile, Casilla 306, Correo 22. Santiago de Chile, Chile.*

[c] *Department of Civil Engineering, University of Chile, Beauchef 850, Santiago de Chile, Chile.*

Nomenclature and abbreviations:

a_i, b_i, c_i: Quadratic function constants for ith frequency.

d: Distance between experimental and numerical model.

E: Young's module.

$E_{30\text{-}60\%}$: Young's module, experimentally determined in the monotonic compression test, in the range 30% to 60% of the maximum strength.

E_{bm}: Young's modulus of brick masonry.

E_{rm}: Young's modulus of reinforced brick masonry.

E_{sm}: Young's modulus of stone masonry.

fc: Compressive strength.

fex_i: ith frequency obtained from experimental model

f_i: ith frequency obtained from numerical model

Im(*): Imaginary part of the complex mode.

J: Minimizing function in the model update process.

Re(*): Real part of the complex mode.

w_i: ith weighting factor for each ith frequency .

w_f: Weighting factor for frequency term.

$w_{i,MAC}$: ith weighting factor based on the MAC between experimental modal shape and numerical one.

w_φ: Weighting factor for modal shape term.

x_j: jth calibration parameter for the model updating process.

ε_i: Error between experimental and numerical frequency.

φex_C: Experimental complex mode.

φex_R: Equivalent real mode to the experimental complex mode.

φex_i: ith experimental modal shape.

φi: ith numerical modal shape.

$()^T$: Transposed matrix.

$()^{-1}$: Inverse matrix.

CTE10: Quadratic tetrahedral element of 10 nodes.

DD: Damage in dome.

DLW: Damage in central longitudinal wall.

DTA: Damage in transverse arch.

EFDD: Enhanced Frequency Domain Decomposition.

FDD: Frequency Domain Decomposition.

FMAC: Frequency scaled MAC.

GPS: Global Positioning System.

MAC: Modal Assurance Criterion.

OMA: Operational Modal Analysis.

SA: Setup located on base of arches.

SSI: Stochastic Subspace Identification.

ST: Setup located on top of walls.

SW: Setup located on base of windows.

UTC: Coordinated Universal Time.

2.1. INTRODUCTION

Studying the structural performance of heritage masonry constructions has become a priority in cities around the world where architectural heritage needs to be preserved. However, this assessment remains a complex task. A major difficulty is knowing the mechanical properties of component materials, the current structural damage, and the degree of interaction between various internal and external elements and systems. Because of these and other difficulties, some general recommendations for structural analysis of historic constructions have been proposed using a multidisciplinary approach (ISCARSAH, 2003).

Powerful computational tools are currently available for assessing the structural behavior of historic masonry construction. A summary of the different available strategies can be found in Roca et al. (2010). Analytical models of these structures can be from detailed models, like micro-modelling (Lourenço, 1996) or simplified models

that consider the masonry as a continuous isotropic material (Page, 1978). In the latter modelling type, the yield surface for compression is given by the Hill criterion and the yield surface for traction by the Rankine criterion (Feenstrat & De Borsts, 1996). This approach is more manageable, because it has adequate computational effort, fewer parameters and a mathematically simpler representation (Roca, Cervera, Gariup, & Pelà, 2010).

A methodological approach to assessing a historic building should incorporate non-destructive or minimally destructive experimental techniques. One example is the well-known vibration analysis technique, used to estimate the structure's natural frequencies and modal shapes. The modal parameters thus obtained can then be used to calibrate numerical models by adjusting their mechanical properties (Binda & Saisi, 2009). Among the non-invasive methods the Operational Modal Analysis (OMA) is the most commonly used (Bayraktar et al., 2008; Elyamani et al., 2016; Ramos et al., 2013). By measuring the response to ambient vibrations and assuming that the input is white noise, the modal properties can be defined based on the system identification process. There are some complications involved in using OMA methodology, including: signal noise from the very long cables (Foti et al., 2012), the difficulty of detecting modal shapes for very close modes, definition of adequate system order (in case of parametric identification method), and detection of spurious modes generated by signal noise (Masjedian & Keshmiri, 2009).

Several studies have used OMA methodology with the aim of studying the components of historical constructions, mainly towers, vaults, domes and arches (Carpinteri et al., 2005; Gentile et al., 2015). By contrast, defining the modal properties in a historic structure's more rigid zones, like perimeter walls and resistant transverse and longitudinal axes, is a less studied subject. One of the main difficulties relates to the complexity of identifying high-frequency close modes, which are common in structures with uniform stiffness and mass distribution. Additionally, the low- response level to ambient excitation and the typical device resolution and precision make their

identification a confusing and difficult process (De Stefano & Ceravolo 2007; Doebling et al., 1998).

One additional difficulty in identifying structural systems in this type of structures is that their structural elements do not have purely flexural or torsional modes, but a mixture of the two, unlike what occurs in conventional structures (Caselles et al., 2013). Therefore, the measuring devices need to be distributed in the structure, to capture all these special movements. Another common difficulty relates to the highly nonlinear response, which is due to the friction interaction between units at low deformation levels; this introduces anomalies, which can be confused with structure modes, i.e. they generate spurious vibration modes that can cause interpretation problems in the identification process (De Stefano & Ceravolo 2007).

In similar previously developed cases, preliminary analytical models were developed, from which an optimal location for the response measuring devices was defined (Masciotta et al., 2016) based on the modes to be identified. Although this analysis is a good initial guide for defining the location of measuring points, the final location will depend on the structure's accessibility and operational conditions for measuring its response to environmental vibration.

Within the identification process, there is a list of previous research in which a frequency domain method (FDD) is contrasted with a time domain method (SSI), as making a comparison is important for highly uncertain problems, in order to generate consistent results (Foti et al., 2012; P.B. Lourenço et al., 2007; L. F. Ramos et al., 2010). However, there is other research into heritage structure, in which the FDD method alone is enough to identify the structure's mechanical properties (Aras et al., 2011; C. Gentile & Saisi, 2007; Lorenzoni et al., 2013). One of the final aims of some similar studies (Aguilar et al., 2015; Gentile et al., 2015; Ramos et al., 2013) is to determine the structures' modal properties using the OMA methodology and

subsequently update the model with multivariable optimization techniques (Douglas & Reid, 1982). These techniques minimize error function, where the calibration parameters (model variables that can vary within a range) comply with user-given constraints. This error function is given by the difference of the natural frequencies and the structure's modal shapes, between the experimental and analytical model (Cabboi et al., 2013).

Chile is widely recognized as one of the most seismic countries in the world. This is due to its location in the subduction zone between the Nazca plate and the South American plate. There are additional seismic considerations for Santiago, the capital city, since there exist two more seismic sources: an intraplate seismogenic source for medium depth earthquakes, and a crustal seismogenic source for superficial earthquakes (Leyton et al., 2010). An iconic architectural heritage structure of Santiago Chile, is the Metropolitan Cathedral. This historical structure more than 250 years old was chosen as a case study for this research.

The Metropolitan Cathedral of Santiago, Chile, has been affected by environmental factors throughout its history, but mainly by earthquakes occurring on the site (IDIEM, 2011). A preliminary research project took place to identify and update the models for the Cathedral (Torres et al. 2016). In this research, a mathematical optimization technique was used by minimizing an error function (Douglas & Reid, 1982) in the model updating process, using only the modal frequency.

The methodology used in this article is as follows: i) Develop an analytical model of the main Cathedral structure, ii) An experimental campaign where the response is recorded by synchronized velocity meters at selected points in the structure, iii) Processing the signals obtained in the experimental campaign, iv) Modal identification of the structural system, v) Compression tests on rock samples from the structure, vi) Initial adjustment of mechanical properties by solving an optimization problem using only modal

frequency, vii) Develop a grid search with models with different mechanical properties. After this introductory section, the article is organized as follows: ii) Overview of the Cathedral; iii) Analysis of ambient vibrations (OMA); iv) FE models and Model Updating; v) Brief discussion and suggestions; and vi) Conclusions.

2.2. THE METROPOLITAN CATHEDRAL OF SANTIAGO

2.2.1. General Description

The Metropolitan Cathedral of Santiago is probably the most important historical structure in Chile's capital city. It is east-west oriented and is located in the northern center of the city. Its construction dates back to 1746 and its architectural style is neoclassical. It has a length of 110 m and a width of 30 m, with three longitudinal naves (Figure 1).

The structural system consists mainly of stone masonry walls up to a height of 11 m and then brick masonry walls to a height of 17 m. The roof structure consists of wooden trusses in the center and north naves, while the south nave has metal trusses. Two bell towers of 45 m height can be distinguished in the main façade (Figure 2a). These structures are composed of steel columns at the corners, covered by brick masonry. The central nave is the highest (Figure 2b), with a ridge height of 20 m, while the lateral naves are 15 m high. On the central nave, between the 10-11 and B-C axes (Figure 1), there is the main 50 m high dome. The dome base is composed of steel beams, which support the brick masonry walls creating its outline. On top of this dome, there is a three-dimensional lattice structure supporting the roof.

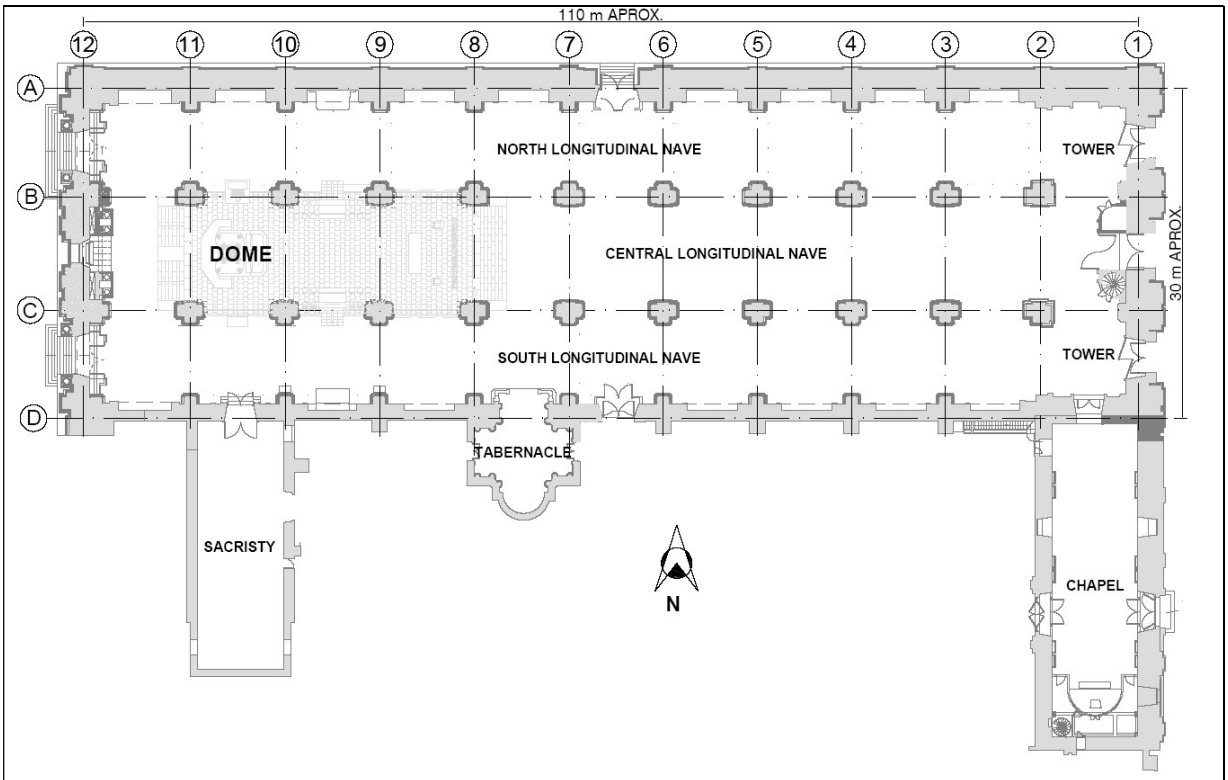

Figure 1. General plan view of the Metropolitan Cathedral of Santiago, Chile.

a)

b)

Figure 2. Metropolitan Cathedral of Santiago, Chile: a) Main façade, b) View of the central nave.

2.2.2. History of construction

Before the Cathedral that exists today, the original structure had a south-north orientation. This structure was planned and built between 1544 and 1570 (Prado & Barrientos, 2011). Several earthquakes have hit the Cathedral over its history, and in 1769 was almost completely destroyed by fire. In 1746, years before its complete destruction, the Bishop at the time decided to build a new cathedral, which is the basis of the present building. The construction of the new Cathedral began in 1748; the two Cathedrals coexisted in the same place up to 1769, with the old structure oriented perpendicularly to the new one.

Based on experience with the first structure, it was concluded that the new Cathedral should have buttresses to provide more lateral resistance; stone blocks, instead of adobe, were determined to be the base material of the new structure. Construction proceeded from the western toward the eastern facade, but after the death of the chief architect, a new builder took charge of the project in 1770. In 1830, the first stage of the construction ended, without towers or the dome. Construction of the chapel started in 1846, later stopped and then resumed in 1858. Additionally, the first tower was built, but it did not correspond to any existing tower in the current Cathedral.

Subsequently, two earthquakes occurred in Santiago, one in 1851 and another in 1874. Severe damage was generated by the first one in most of central nave arches; only the first and tenth arches from the western facade have no damage. The damage was repaired in 1854. The 1874 earthquake affected the 3 main arches of the eastern facade. The Bishop ordered the remodeling of the Cathedral in 1897, which included two towers on the main facade, the dome above the altar, the roof, the removal of intermediate pilasters supporting the choir, and other architectural remodeling. The tower was demolished in 1898, and the rest of the works were completed by 1906 (IDIEM, 2011).

The Metropolitan Cathedral of Santiago was declared a National Historic Monument in 1951, and another major remodeling took place on the cathedral, specifically the archbishop's crypt in 2006. Thanks to this work, many stones could be obtained that have the same quality as the walls, because they were extracted from the structure base.

2.2.3. Historical seismic behavior and the current state

The main cause of the Cathedral's damage is the numerous earthquakes that have affected the structure over its lifetime. The March 3rd, 1985 earthquake (Mw 8.0 - Valparaiso) affected both the Cathedral structure and cladding. This led to a repair process of the most significant structural damage, which began in 1999 (Pérez et al., 2009). Serious but eventually recoverable damages were observed in the Cathedral after the 2010 Maule earthquake.

After the February 27, 2010 earthquake (Mw 8.8 - Maule), the following Cathedral damage was identified as part of this study (DD – Damage in dome, DLW – Damage in longitudinal wall, DTA – Damage in transverse arches):

- DD1: Cracking at the dome base and reinforcing buttress head (Figure 3).
- DD2: Shear cracks in brick masonry walls that make up the dome (Figure 4).
- DLW1: Vertical cracks at the junction of central longitudinal walls on the western façade (Figure 5).
- DLW2: Vertical cracks at the junction of central longitudinal walls with transversal axis 2 wall (Figure 6).
- DLW3: Punching cracks in all the pillar heads that support the brick masonry portion in the central longitudinal walls (Figure 7).
- DLW4: Slippage between the upper brick masonry and stone masonry of the longitudinal walls of the nave, axes B and C (Figure 8).
- DLW5: Cracks in the upper window of B axis between axes 11 and 12 (Figure 9).
- DTA1: Cracks in the internal transversal arches, some axes (Figure 10).

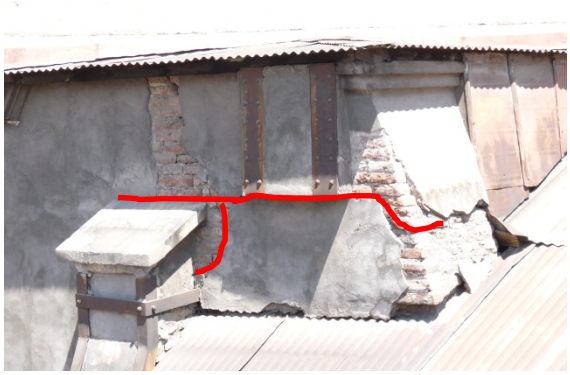

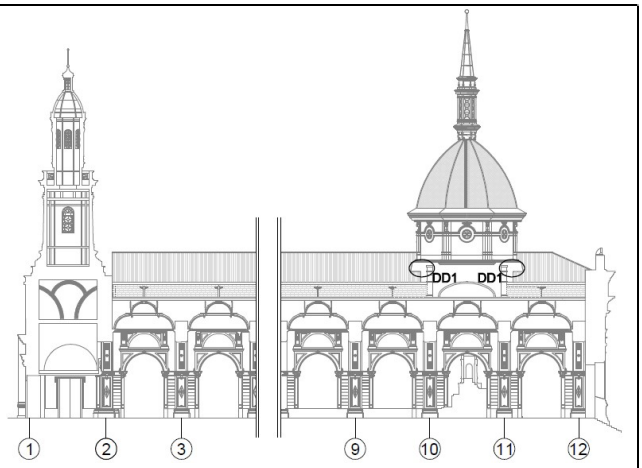

Figure 3. Cracking at the base of the dome.

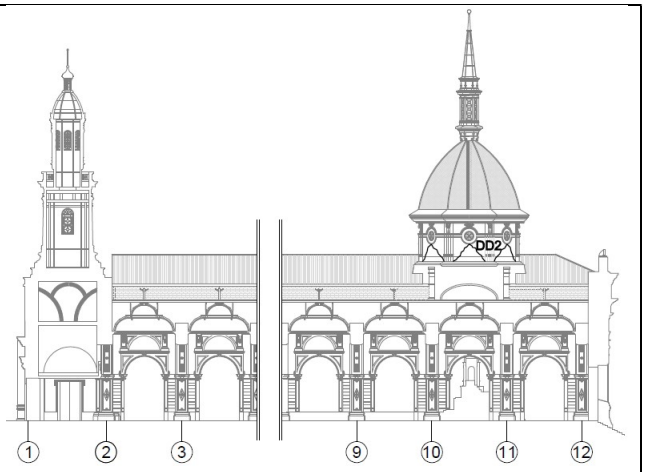

Figure 4. Cracking at the dome.

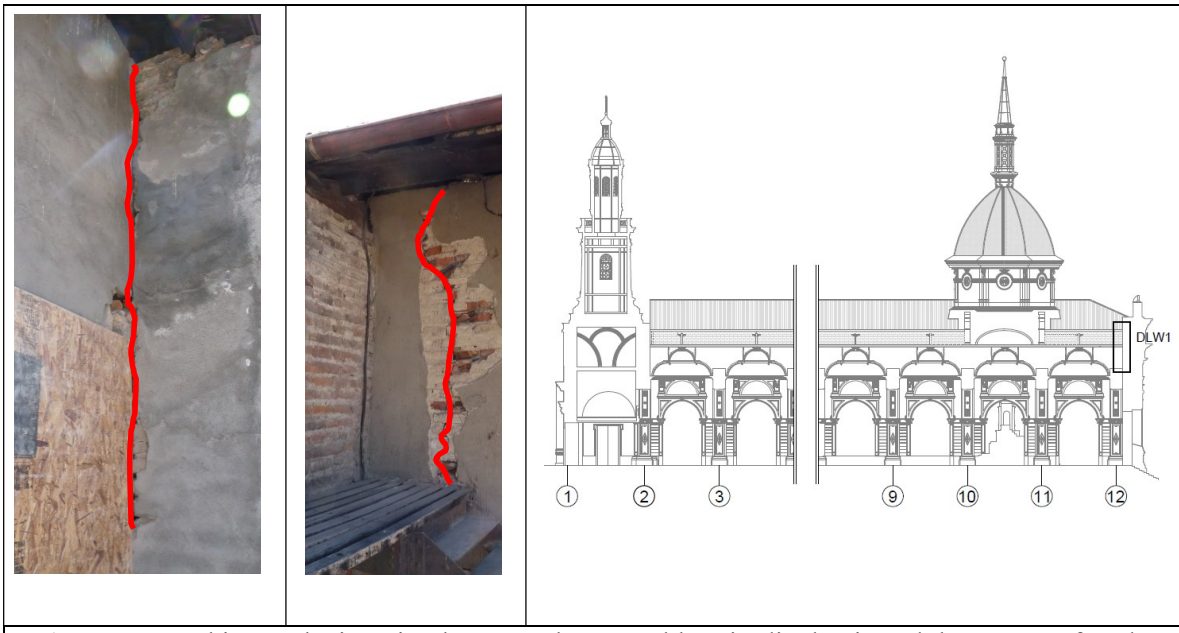

Figure 5. Cracking at the junction between the central longitudinal axis and the western facade.

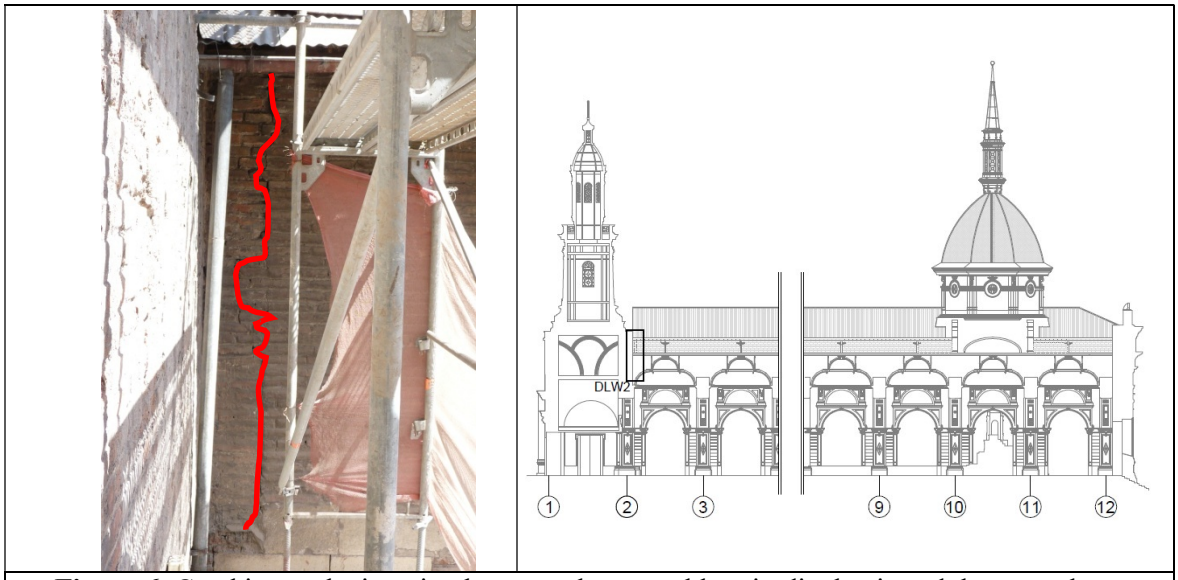

Figure 6. Cracking at the junction between the central longitudinal axis and the tower base.

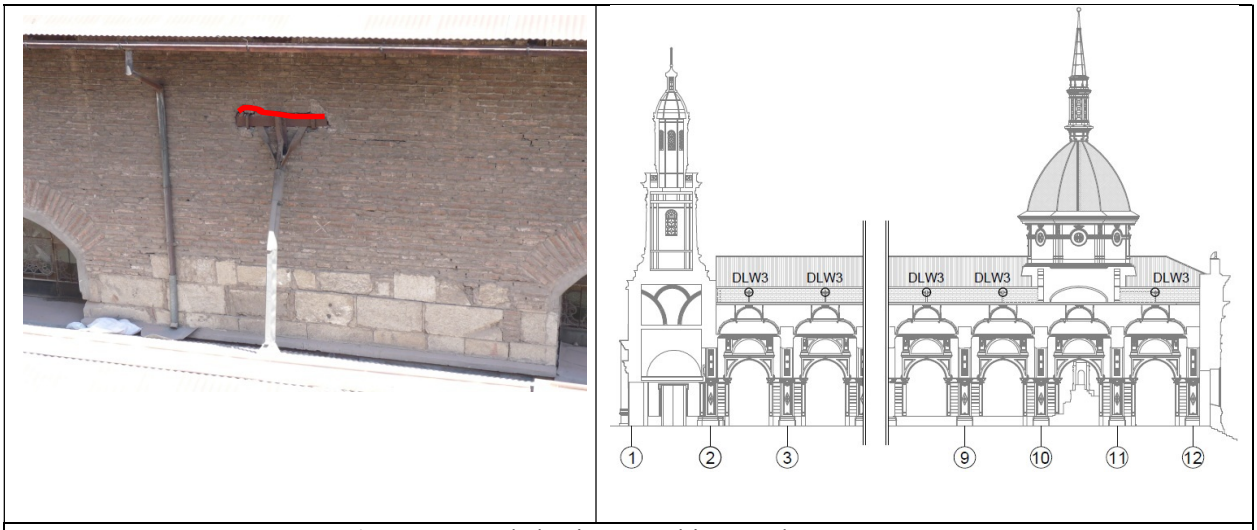

Figure 7. Steel shoring punching on the masonry.

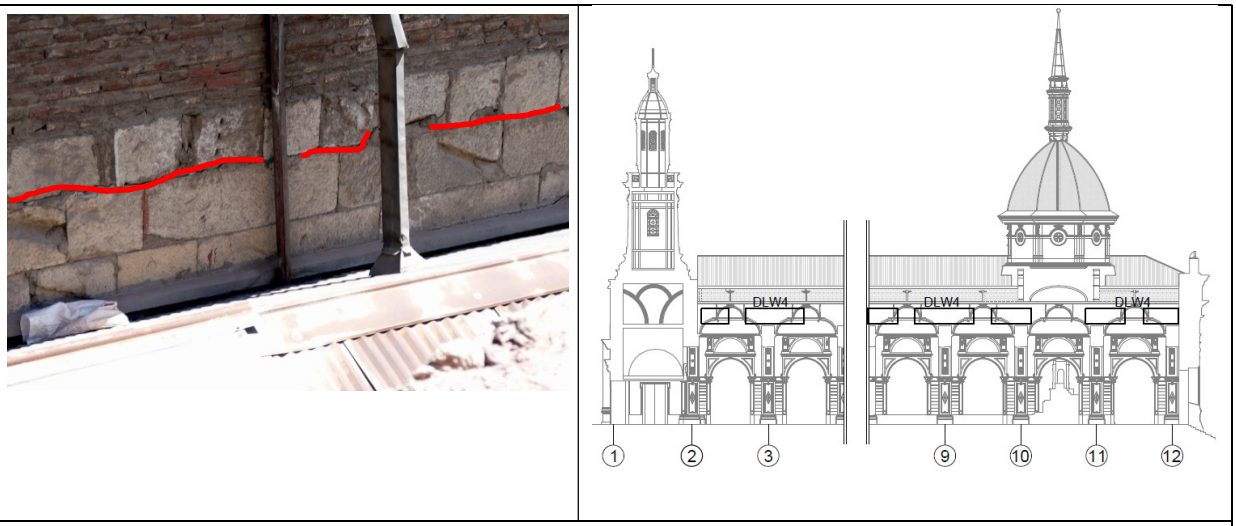

Figure 8. Cracking at the junction of brick masonry and stone masonry.

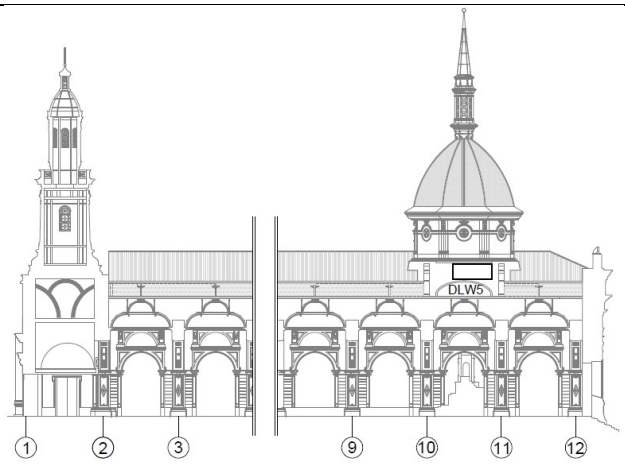

Figure 9. Window of B axis between axes 11 and 12.

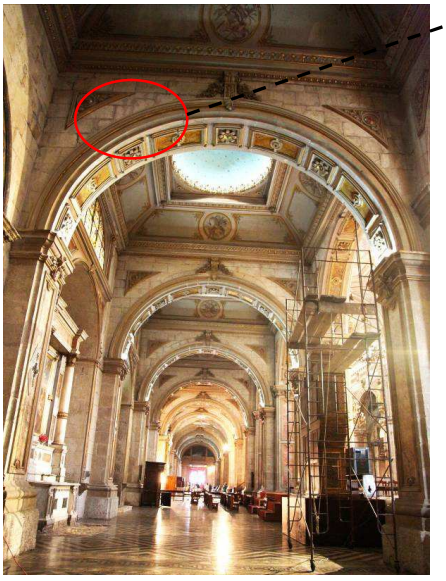

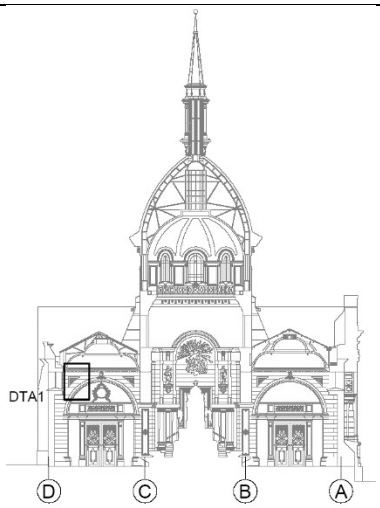

Figure 10. Cracks in the internal transversal arches.

The Metropolitan Cathedral of Santiago de Chile's current damage status does not compromise its overall stability, but could affect the local stability of certain elements in a potential seismic event (IDIEM, 2011). On the other hand, due to the massive structure, all these fissures detected in the structure most probably do not work against the low intensity of the ambient vibration. Therefore, even though it is important to define the current damage in the structure, the numerical model of the structure is considered as continuous, as will be mentioned later in the model assumptions.

2.3. AMBIENT VIBRATION ANALYSIS

An experimental campaign was designed and implemented to estimate the modal properties of the Metropolitan Cathedral of Santiago Chile. A description of the campaign and its main results are presented in this section.

2.3.1. Experimental campaign

The experimental campaign consists of measuring the response of the structure to ambient vibrations at selected points. To select these points, areas were first selected where the fundamental modes of a preliminary numerical model possessed higher amplitudes, and then the most easily accessible points were chosen.

Six Trominos devices (MICROMED, 2012), which measure accelerations and velocity in 3 orthogonal directions, were used during the experimental campaign. The sensor clock was adjusted using UTC time, obtained from a GPS device. This time set-up allows for equipment and signal synchronization. Structure vibration was recorded by measuring velocity, due to its larger signal-to-noise ratio.

Twenty-two set-ups were defined to cover the entire structure; locations are shown in Figure 11. A set-up is an array of instruments where the structure response is recorded for at least 20 minutes; this is consistent with an empirical rule given by Rodriguez (2004), where the measurement duration is recommended to be at least 2000 times the natural period of interest, e.g. if this structure begins with a natural frequency of approximately 2 Hz, the measurement duration should be at least 17 minutes. Two

reference instruments, always located at the same position, were used in all set-ups (called REF 1 and REF 2 in Figure 11). A sampling rate of 128 Hz was used. It is important to note that the instruments were located at different heights, as can be seen in Figures 12 and 13. To facilitate interpretation of its location a description was defined as follows:

SA: Bases of the arches in the north and south longitudinal naves. This was the location of the reference instruments (C6 and B7 axes).

ST: Top of south and north longitudinal walls.

SW: Window bases of the central longitudinal walls (B and C axes).

Reinforcements were being installed in the Cathedral during the measurements, so some areas were inaccessible. This affected the measurements in the main facade towers and the dome located above the altar. Another inaccessible area was the inside western wall. Figure 14 shows the sensor location in the experimental model defined by the ARTEMIS identification software (Structural Vibration Solutions, 2015) of the main Cathedral structure.

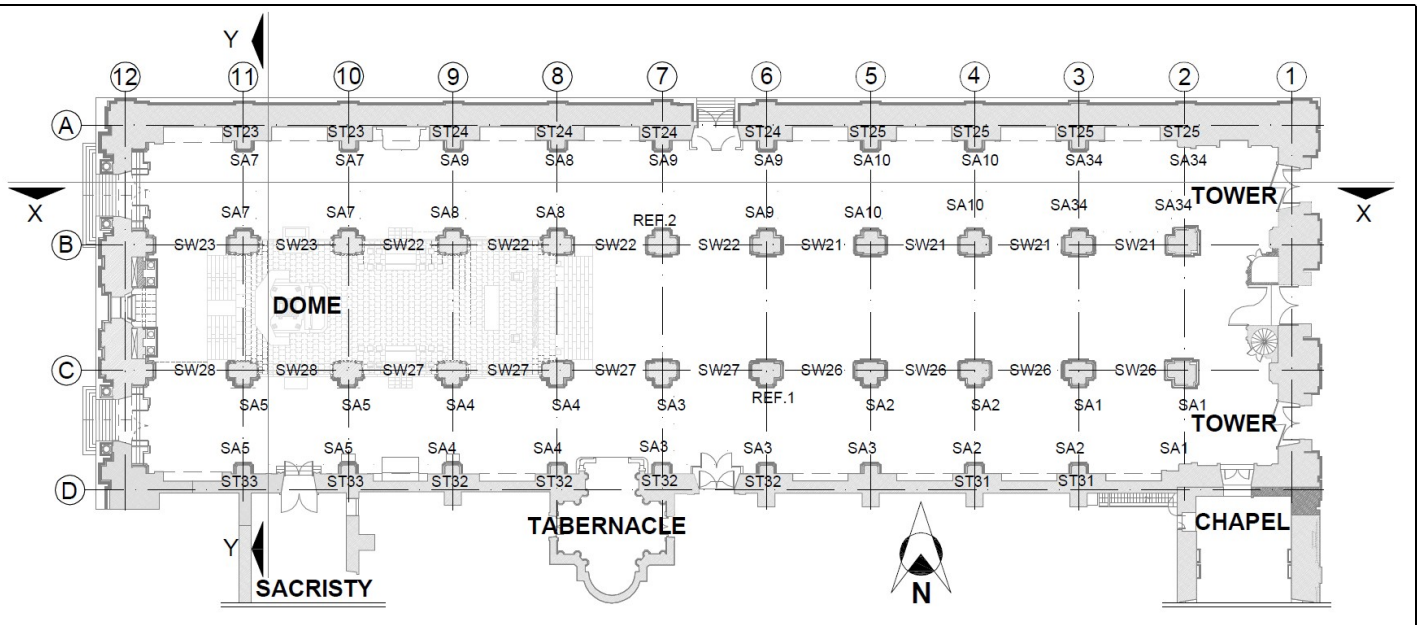

Figure 11. Location of setups defined in the experimental campaign.

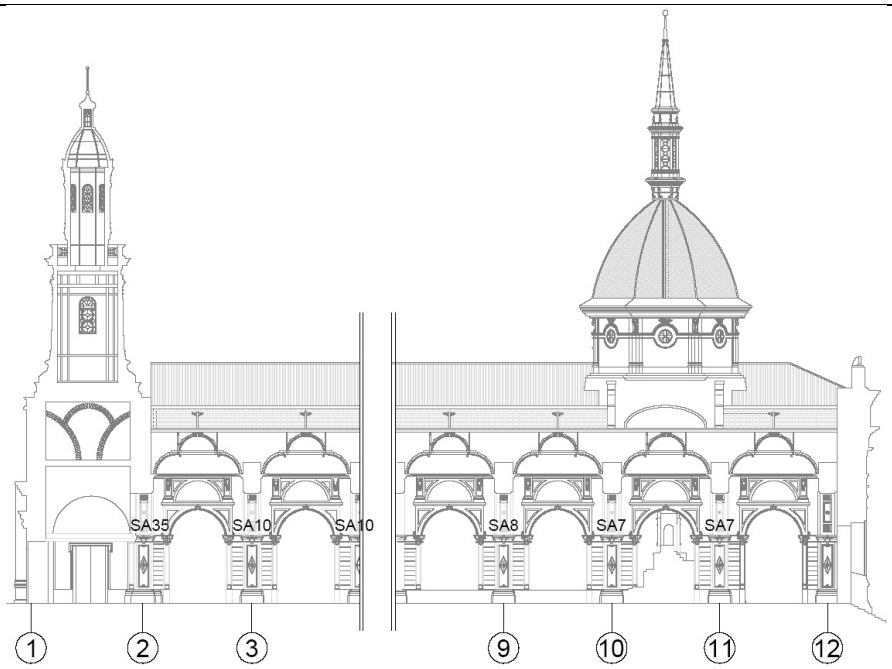

Figure 12. Section X-X according to plan in Figure 11, with location of set-ups.

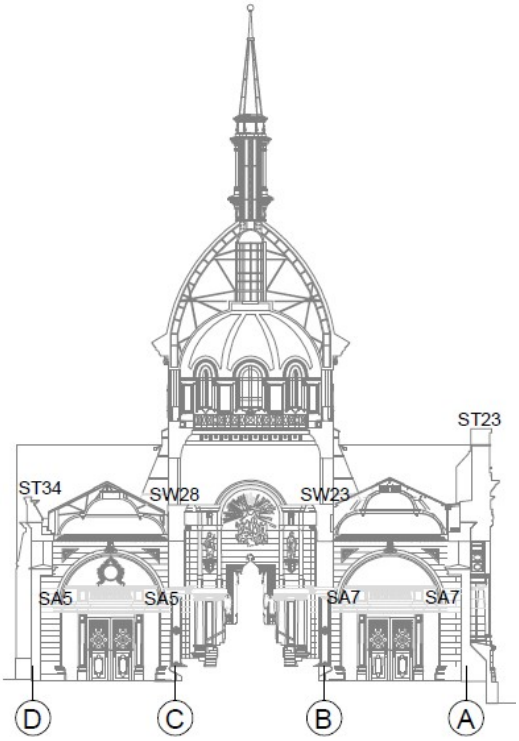

Figure 13. Section Y-Y according to plan in Figure 11, with location of set-ups.

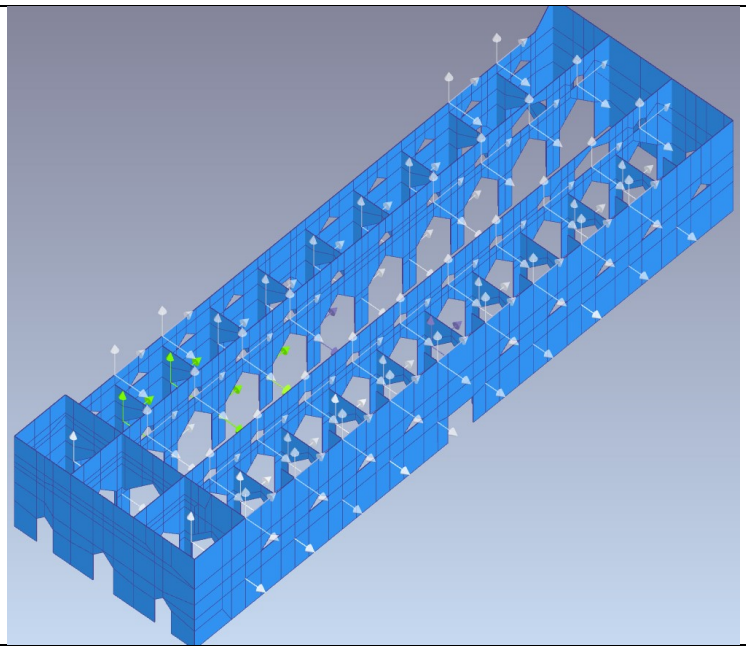

Figure 14. Artemis model of the Cathedral with localization of sensors.

2.3.2. Signals processing and system identification

Figure 15a shows the measured velocity records at the reference position (see Figure 11 – position REF2). Note that the amplitude of the recorded movement is very low (about 4.0E - 5 m/s), which is a characteristic response to ambient vibration in rigid structures. Additionally, Figure 15b shows the Fourier spectrum for the corresponding signals. This indicates that the recorded structure signals include detectable predominant frequencies in their response.

The signal conditioning consisted of a two-step process: an initial series de-trending, then low-pass filtering with cutoff 8 Hz frequencies, and finally a decimation process in a band between 0 and 8 Hz. This whole process generated signals for further processing the structural system identification.

Two different OMA methods were used in this research: EFDD (Brincker et al., 2001) and SSI (Van Overschee & De Moor, 1996). As the name implies, the first method is an improved version of the FDD method (Frequency Domain Decomposition) (Brincker et al., 2000). These improvements consist mainly of determining frequencies and damping

by the correlation function, and determining the mode shape by the weighted sum of the singular vector decomposition. The EFDD method was applied using a manual peak-picking process on the singular value curves. On the other hand, the SSI method was applied based on Crystal Clear algorithm (Goursat et al., 2010) and stabilization diagrams for the visualization of results.

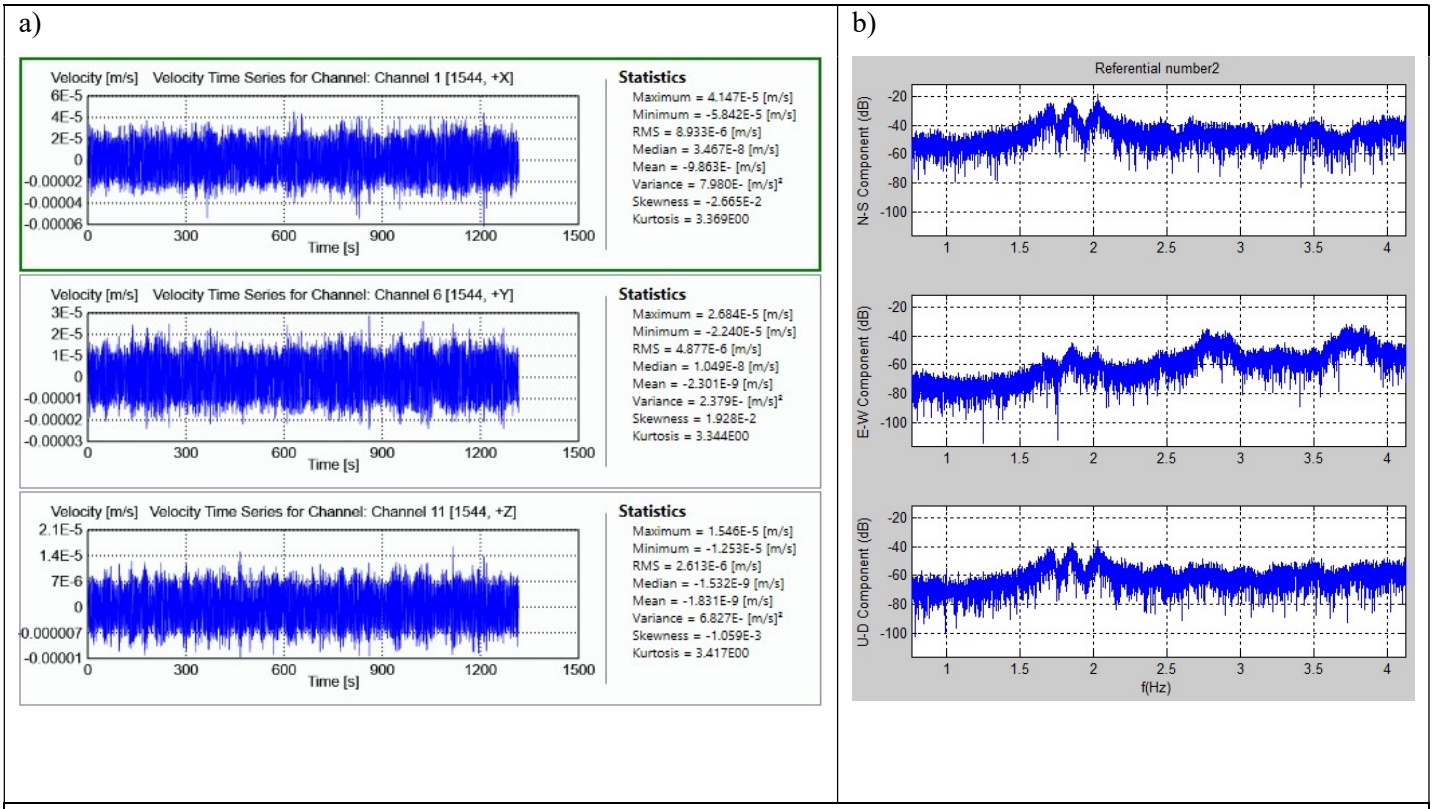

Figure 15. Velocity signals of a second reference point in setup 1 a) Time series. b) Fourier spectrum of the time series.

Figure 16 shows the singular values of the spectral densities for two cases: Fig. 16a is the average singular value for all setups, and Fig. 16b is the singular values graph of setup #10 that shows the peaks not clearly visible in Fig 16a. The potential EFDD frequencies were first selected by peak peaking process to evaluate the experimental mode validities, the frequency selection was then confirmed by SSI method. Figure 17 shows the stabilization diagrams for two setups (13 and 8), in which the frequencies obtained confirm the modes obtained from the EFDD method. Finally, the linear

independence of these experimental modes was verified from the calculus of Modal Assurance Criterion (MAC) (Allemang & Brown, 1982) between them.

a)

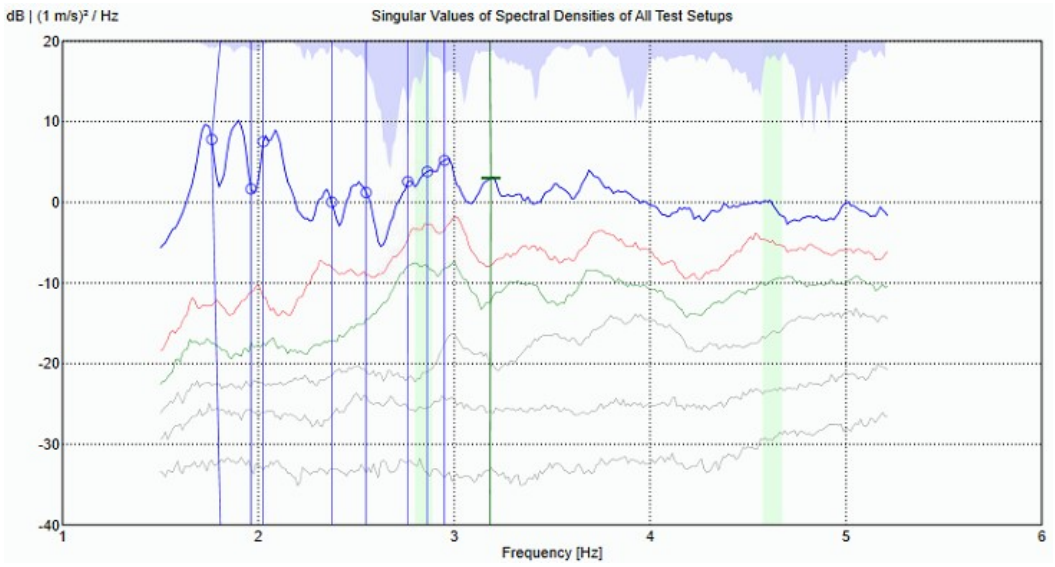

b)

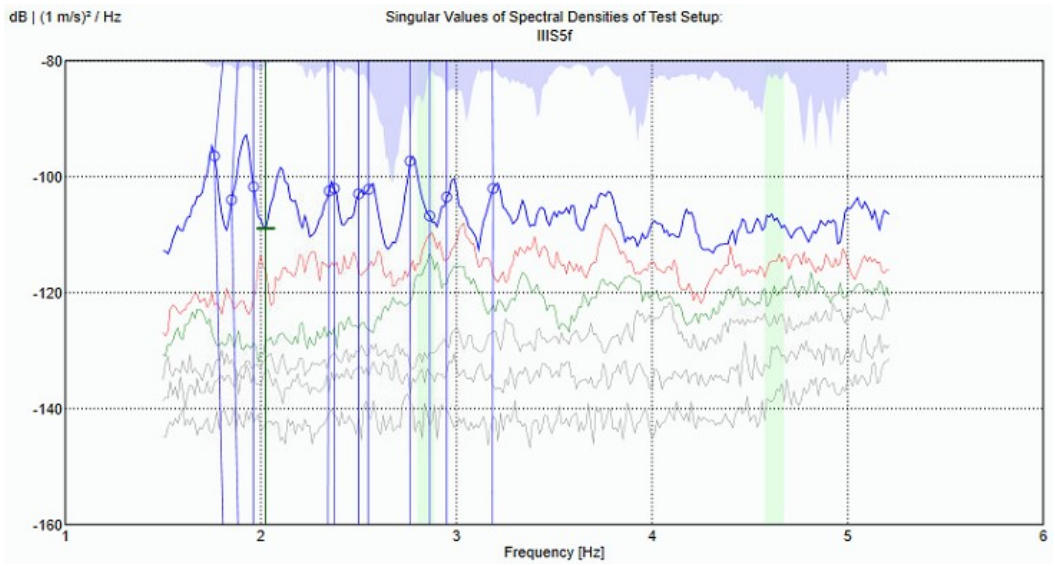

Figure 16. Singular values of the spectral densities marking natural frequencies by manual peak peaking process in: a) Average of singular values of Spectral Densities for all test setups. b) Singular values of Spectral Densities for test setup 10.

Figure 18 shows the MAC between experimental modes. The final experimental modes used in the model updating process will be based on a visual comparison between experimental and analytical mode shapes, and their MAC calculation.

a)

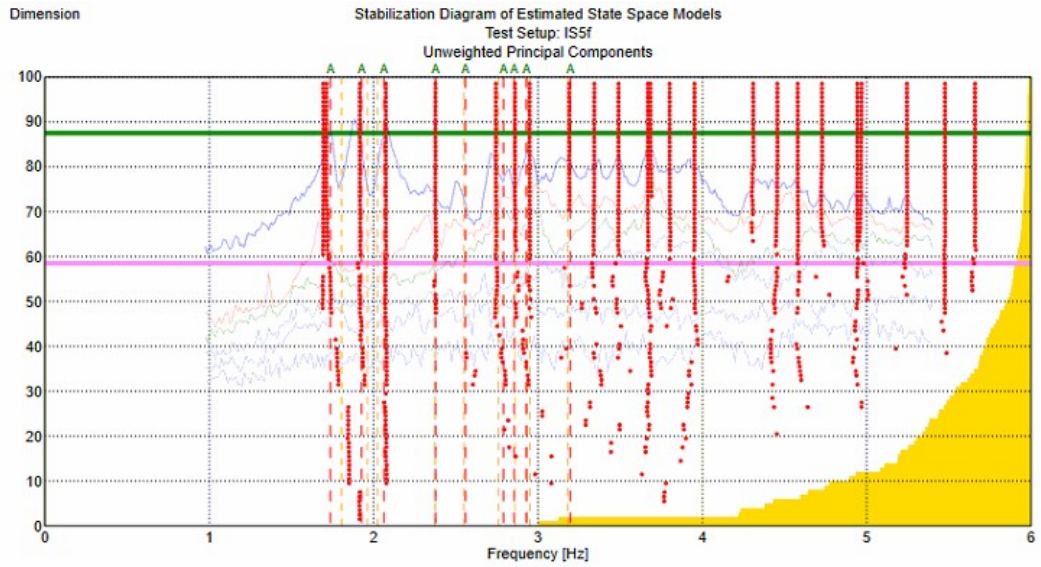

b)

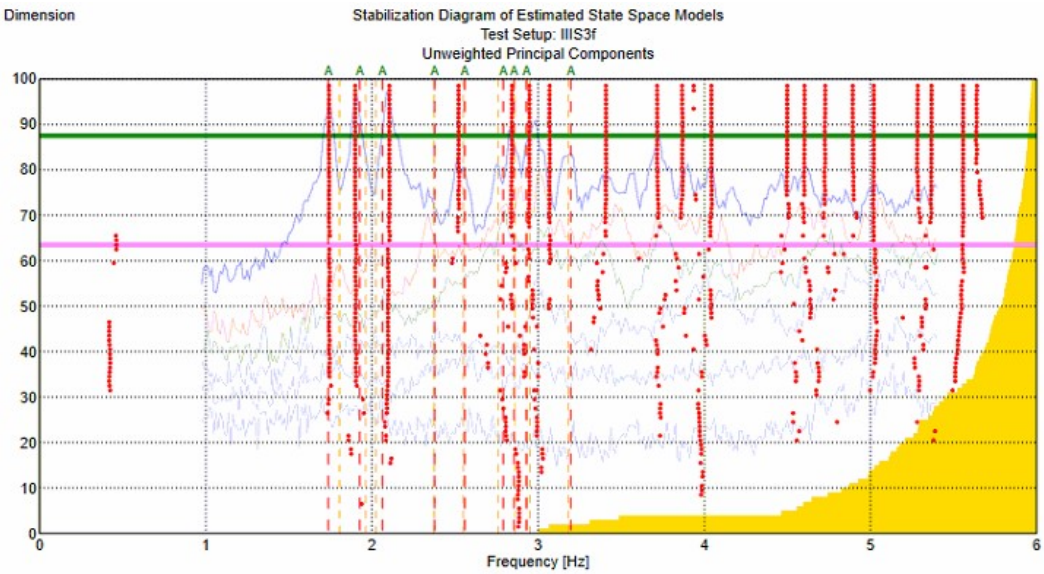

Figure 17. Stabilization diagrams to define stable modes for two particular setups: a) Setup 13, b) Setup 8.

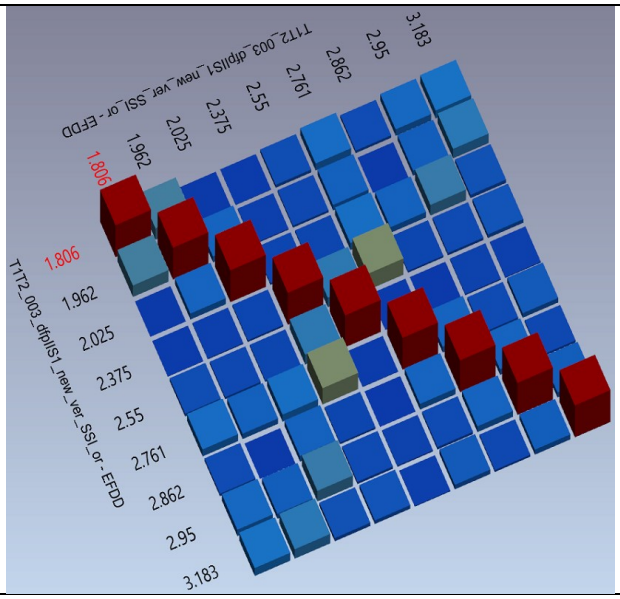

Figure 18. MAC between experimental modes.

Therefore, the defined experimental modes, based on the identification methods, can be seen on Table 1. For all experimental mode pairs observed in Table 1, the frequencies defined according to EFDD are very close to SSI frequencies. The differences between frequencies are because the frequency values identified correspond to a band and not to precise values, given the non-linearity in the behaviour of the structure.

2.3.3. Determination of mechanical properties of materials.

Following the procedure proposed by Oliveira (2002), 3-cylinders, 12 cm high and 5 cm in diameter were extracted from an intact rock block used in the structure. The samples were subjected to monotonic compression testing; the results are shown in Table 2. Additionally, a value of 2400 kg/m^3 was experimentally determined for the stone density.

According to Table 2, the average value of Young's modulus obtained in the 30% to 60% range of maximum strength was 13,900 MPa, and the average compressive

strength value was 111 MPa. These values can be associated with a high quality limestone (Meli, 1998).

Table 1. Experimental frequencies.

	EFDD method	SSI method
Experimental mode	Frequency (Hz)	Frequency (Hz)
1	1.81	1.74
2	1.96	1.93
3	2.03	2.06
4	2.38	2.38
5	2.55	2.56
6	2.76	2.79
7	2.86	2.86
8	2.95	2.93
9	3.18	3.20

The elasticity modulus required for the computational model should consider the entire wall behavior of this material, as well as joints. The investigations of Oliveira (2002) and Lourenço (1996) show that the Young's modulus for cores obtained from stone is much higher than from block and mortar wall. This is not surprising: in the field of rock mechanics, an intact rock modulus is well known to be up to 10 times greater than the cracked solid modulus (Goodman, 1989). So, the joints between blocks were assumed to behave like cracks in a (pseudo) rock mass, and an initial Young's modulus of stone masonry was adopted to the order of one tenth of the value obtained in the intact specimen test, i.e. 1,390 MPa. The assumed value of Young's modulus is consistent with that of roughhewed stone masonry suggested by Italian Code for Constructions (NTC08, 2008), where the Young’s modulus is between 1,020 and 1,440 MPa.

Table 2. Results of Young's modulus and compressive strength obtained from monotonic compression testing of stone cylinders.

Specimen	$E_{30\%-60\%}$ (MPa)	Fc (MPa)
P1	13400	115
P2	11000	111
P3	17200	109
Average values	13900	111
Coef. of Variation	0.23	0.03

In the case of brick masonry located on top of the stone masonry, it was not possible to obtain representative material for a compressive test. Therefore, an experimental value obtained by Valledor et al. (2015) from another heritage building located close to the Cathedral and contemporaneously built, coinciding with the finishing of the walls in height and the growth of the Cathedral central nave at the end of the 19th century, is used as the first proposed value. Consequently, an initial value of the Young's modulus of 1,780 MPa and a density of 1800 kg/m^3 were defined for brick masonry. It should be note that the assumed Young's modulus is within the range of reference values (1,200 – 1,800 MPa) for brickwork suggested by the above-mentioned building code (Italian Code for Constructions NTC08, 2008). The top of the north façade of Cathedral is reinforced with metal anchors; which is why there is a third material, called reinforced brick masonry, whose modulus is initially assumed to be at the same brick masonry value. Table 3 summarizes the initial values for calibration parameters.

As mentioned above, once the structure's modal properties were identified, the Finite Element (FE) model was updated by adjusting the mechanical properties of materials making up the structure.

Table 3. Initial calibration parameter values.

Calibration parameter	Initial value
Young's modulus of stone masonry E_{sm} (MPa).	1,390
Young's modulus of brick masonry E_{bm} (MPa).	1,780
Young's modulus of the reinforced masonry E_{rm} (MPa).	1,780
Lateral stiffness factor from Chapel	1.00
Lateral stiffness factor from Sacristy	1.00
Lateral stiffness factor from Tabernacle	1.00

2.4. FINITE ELEMENT ANALYSIS AND MODEL UPDATING

This section first describes the finite element model, then the mechanical properties are defined using a two-stage optimization problem. The first adjustment of mechanical properties and boundary conditions, given by adjacent structures, was based on minimizing the error function between experimental and analytical frequencies. A second stage of model updating process was carried out, based on minimizing the difference between frequency and MAC values, when varying the Young's moduli of the three main materials within physically ranges. So, the research will compare the results obtained by the two stages of model updating.

Some assumptions are made as a basis for the model. Firstly, the structure's behavior is considered as continuous, without discontinuities in the wall intersections. Secondly, the structure's flexible components (towers and dome) have been represented as simple elements, because the rigid part of the structure is the focus. Thirdly, the adjacent structures (sacristy, tabernacle and chapel) that interact with the principal Cathedral structure can be represented as elastic elements, to simplify the principal Cathedral structure. Finally, mechanical material properties of the structure can be characterized as representative values for the whole structure, disregarding the high variability of these properties in different structural zones.

2.4.1. Model description.

Given the model's complexity and size, the mesh had been previously generated with GID software (CIMNE, 2014). The structure's computer model was analyzed using the DIANA software (TNO DIANA, 2015).

The finite element model includes detailed modeling of the structure's rigid area and simplified modeling of the towers and dome, using concentrated masses connected by frame elements with flexo-compression capacity. Additionally, the effect of the adjacent structures (chapel, tabernacle and sacristy, as seen on Figure 1) is represented by elastic elements that generate lateral interaction with the structure. This way of representing the adjacent structures is used because each one was built at different times (IDIEM, 2011; Pérez et al., 2009). This leads to the conclusion that if the model included all adjacent structures, additional parameters and uncertainty would increase, which in turn would increase the difficulty of optimization. The soil type in the area is high quality gravel (Valenzuela, 1978), and so the base nodes are considered to be fully restricted.

The model is built mainly with quadratic tetrahedral elements of 10 nodes (CTE10) with 3 degrees of freedom (translational) per node. The quadratic property of the elements contributes greatly to convergence in obtaining the natural frequencies model. The complete model has 271,106 nodes, 5,195 of which are fully restricted at the base. Therefore, there are 797,733 degrees of freedom. There are 153,992 CTE10 elements, 3,038 frame elements to represent flexible zones of the structure; and 450 axial rods to simulate roof structures at the head of walls. Thus, there are 157,480 elements in the entire model. Figure 19 shows the generated FE model for the Cathedral.

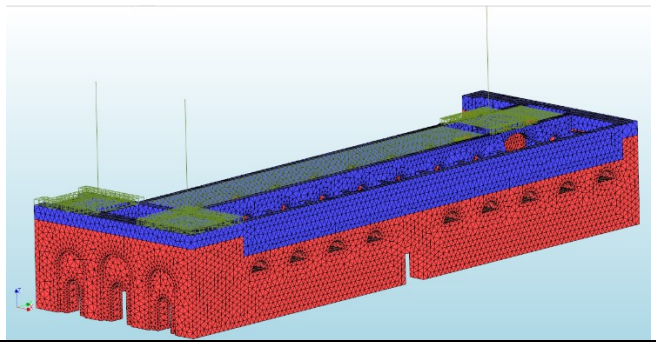

Figure 19. FE model of the Cathedral

2.4.2. First adjustment of mechanical properties.

The first stage of model updating process was made by comparing the frequencies obtained experimentally (Table 1) with those calculated by the FE model, based on the initial parameter values (Table 4). The match between modes for model updating is based on the visual qualitative assessment of the mode shapes (see Figure 20) and quantification of the MAC between experimental mode shapes and those obtained from the numerical model (Table 5).

Given that the MAC will be used for comparing the analytical and experimental modes, the experimental modes require transformation to real values to compare them with the analytical ones. This transformation is important, because energy dissipation in a real structure cannot be represented by only viscous (proportional) damping, and therefore complex experimental modes are identified (Friswell & Mottershead, 1995). This is related to the presence of cracks in the structure and therefore the influence of these in the damping of the structure. The complexity of the experimental modes is then related to the presence of these cracks and gives us an idea of the current damage of the structure. The comparison between these modes and the analytical modes was performed using the numerical transformation (Eq. 1) purposed by (Niedbal, 1984):

$$\phi ex_R = \mathrm{Re}\left(\phi ex_C\right) + \mathrm{Im}\left(\phi ex_C\right)\left(\mathrm{Re}\left(\phi ex_C\right)^T \mathrm{Re}\left(\phi ex_C\right)\right)^{-1} \mathrm{Re}\left(\phi ex_C\right)^T \mathrm{Im}\left(\phi ex_C\right) \quad (1)$$

where Re (*) and Im (*) are the real and imaginary parts of the complex mode, respectively; φex_C and φex_R are the experimental complex mode (obtained directly from the identification process) and the equivalent real mode, respectively. The lower limit value of MAC that was considered to be valid for this "modal equivalence" was 0.50. Some other studies (e.g. Ramos et al., 2013) have started with MAC equal to 0.4 as the lower limit value.

Table 4. Numerical frequencies (initial calibration parameters).

Numerical mode	Frequency (Hz)	Mass participation based on FE model (%)	Mode description
1	1.38	0.48	Bending of south tower.
2	1.39	0.15	Bending of north tower.
3	1.41	0.61	Bending of south tower.
4	1.43	0.43	Bending of north tower.
5	1.90	27.48	Transverse bending of longitudinal walls.
6	2.02	0.27	Transverse bending of south longitudinal walls.
7	2.19	1.73	Transverse bending of longitudinal walls and bending dome.
8	2.27	0.11	Bending dome.
9	2.32	1.55	Transverse bending of longitudinal walls and bending dome.
10	2.40	0.53	Transverse bending of south longitudinal walls.
11	2.54	5.44	Bending dome.
12	2.56	0.02	Transverse bending of longitudinal walls.
13	2.59	0.63	Transverse bending of longitudinal walls.
14	2.83	2.24	Transverse bending of longitudinal walls.
15	2.97	0.22	Transverse bending of longitudinal walls.

Table 5. Couples experimental and numerical (obtained with initial parameters) frequencies according to their similarity in modal shape and MAC.

Experimental Mode number	Experimental frequency (Hz)	Numerical Mode number	Numerical frequency (Hz)	MAC
2	1.96	5	1.90	0.85
4	2.38	7	2.19	0.61
8	2.95	14	2.83	0.55
9	3.18	15	2.97	0.69

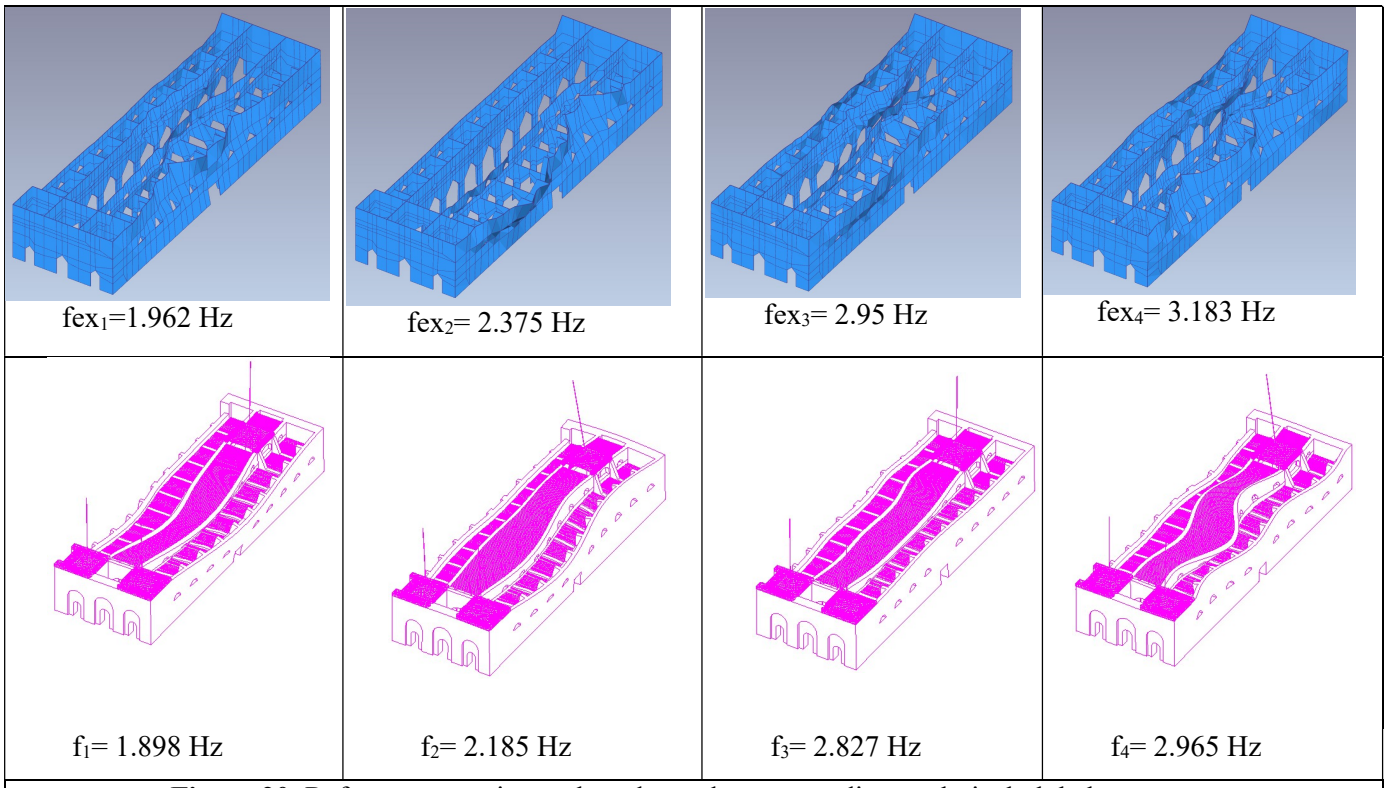

Figure 20. Reference experimental modes and corresponding analytical global ones.

Based on Table 4, the four first numerical modes were not considered, because they are related to towers movement, and the experimental model cannot reproduce this. It can be clearly seen in Tables 4 and 5 that 3 of the 4 selected modes have relatively large participation mass percentages. Note that in this type of structure, values accumulated

from mass participation can only be achieved with many more modes than for conventional structures. Additionally, there are two important modes (modes 9 and 11) that have not been taken into account because these are related to dome movement.

As seen in Table 3, the calibration parameters considered for the model update were: (1) the Young's modulus of stone masonry; (2) the Young's modulus of brick masonry; (3) the Young's modulus of the reinforced masonry; (4) the lateral stiffness factor in the chapel support area; (5) the lateral stiffness factor in the tabernacle support area; and (6) the lateral stiffness factor in the sacristy support area. These three last calibration parameters are dimensionless, because they are factors that multiply a vertical distribution of elastic supports in the zones where the principal structure is adjacent to before mentioned external structures. The vertical distribution of elastic supports has the following mean values per square meter: 472 MN/m for chapel, 2040 MN/m for tabernacle and 307 MN/m for sacristy. The initial values for these factors take unity values to begin the model updating. These calibration parameters have high uncertainty and influence in the model, so it is important to define their values in the model updating process. There are many other important calibration parameters that can participate in the model updating, like material mass, but their uncertainty is relatively low, as its identification was done in laboratory.

Various techniques have been proposed for updating models (Friswell & Mottershead, 1995; Kim & Park, 2004). The method proposed by Douglas & Reid, (1982) was initially applied in this study.

The modal updating begins by defining an approximating function expressing the numerical frequency based on a quadratic function of the calibration parameters (Eq. 2).

$$f_i = a_i x_j^2 + b_i x_j + c_i \tag{2}$$

where f_i represents the numerical frequency; a_i, b_i and c_i the quadratic function constants for each frequency, where i is the vibration mode; and x_j are the calibration parameters of the model, in this case j=1..6. Then the error is defined as:

$$\varepsilon_i = f_i - fex_i \tag{3}$$

where fex_i is the corresponding experimental frequency.

This problem can now be treated as a multi-objective multivariable optimization problem, where each of the errors would be minimized. To simplify the problem, all error functions are concentrated in a single expression, and so the problem becomes a multi-variable optimization problem with a single objective, i.e. to optimize the function (Eq. 4):

$$J = \sum w_i \varepsilon_i^2 \tag{4}$$

where w_i are the weights for each error, depending on the mode being evaluated. This weighting factor depends on the uncertainty associated with the experimental measurement, and the uncertainty associated with the numerical model (Friswell & Mottershead, 1995). Therefore, the expressions 2, 3 and 4 define the process for obtaining the error function that subsequently will be minimized in the first stage of model updating. The optimization process was performed based on the Karush-Kuhn-Tucker method using MATLAB Optimization (Mathworks, 2015).

As the dependence of the frequency on the parameters was assumed to be quadratic (Douglas & Reid, 1982), 3 points needed to be defined on each parameter variation. The structure's natural frequencies were calculated when taking the minimum, maximum and nominal value for material parameters. The parameters were modified one at a time.

The nominal values for the parameters in the optimization process were: Young's modulus of stone masonry (E_{sm}) 1390 MPa (range of variation was from -15% to 40%),

Young's modulus of brick masonry (E_{bm}) 1690 MPa (range of variation was from -25% to 5%), Young's modulus of the reinforced masonry (E_{rm}) 1870 MPa (range of variation was from -5% to 25%). Since the contributed stiffness from adjacent structures does not have a single representative value, as they vary in height, the calculated value was multiplied by a factor of 1.00 and its variation was made based on this factor (range of variation was from -40% to 500%). After this function error minimization process, the calibration parameters were obtained (Table 6). These values are called frequency optimized values from now on.

Table 6. Frequency optimized values of calibration parameters with model updating based on function error minimization.

Calibration parameter	Frequency optimized value
Young's modulus of stone masonry E_{sm} (MPa).	1560
Young's modulus of brick masonry E_{bm} (MPa).	1700
Young's modulus of the reinforced masonry E_{rm} (MPa).	1870
Lateral stiffness factor from Chapel	3.265
Lateral stiffness factor from Sacristy	3.526
Lateral stiffness factor from Tabernacle	3.063

2.4.3. Definition of Models based on changing mechanical properties.

The second stage of model updating was based on large number of models, generated in a grid search, in which the Young's modulus of materials vary within a defined range. The lateral stiffness factors do not change and the frequency optimized values were fixed.

A wider range of variation for the calibration parameters values was allowed (between 50% and approx. 150%. of central values). Table 7 summarizes the central values (obtained from frequency optimization), minimum and maximum values for each parameter. The step increases in each parameter range were 10% but, when close to the

central values, the increase was 5%. The total number of models generated with the described increments is 910.

Table 7. Range of calibration parameters (910 models).

Calibration parameter	Min. value	Central value	Max. value
Young's modulus of stone masonry E_{sm} (MPa).	780	1560	2330
Young's modulus of brick masonry E_{bm} (MPa).	850	1700	2550
Young's modulus of the reinforced masonry E_{rm} (MPa).	940	1870	2810

The change of the calibration parameters is given by a multidimensional matrix where all possible combinations are given. The order of variation of the calibration parameters for exposition of the results in the next section is in cascade, starting with the variation of Young's modulus of the reinforced masonry, then the variation of Young's modulus of brick masonry, and finally the variation of Young's modulus of the stone masonry. The models for which Young's modulus of reinforced masonry was lower than for brick masonry were not included.

2.4.4. Model updating

The model updating process was done by comparing the modal parameters obtained experimentally with those calculated by FE model perturbation. The distance between models was calculated using expression (Eq. 5).

$$d = \sum_{i=1}^{M} w_{i,MAC}\left[w_f \frac{\left| f_i - fex_i \right|}{fex_i} + w_\phi \left[1 - MAC(\phi_i, \phi ex_i) \right] \right] \quad (5)$$

where: f_i represents the numerical frequency, fex_i is the experimental frequency, ϕ_i represents the vector of the analytical modal shape, ϕex_i is the vector of experimental modal shape, $w_{i,MAC}$ is the weighting factor based on the MAC between the analytical modal shape and experimental one, w_f is the weighting factor of frequency summation term and w_ϕ is the weighting factor of modal shape summation term; the last two

weighting factors add up to unity. In all these terms, i subscript means mode that is being evaluated.

The expression (5) proposes that the frequency and modal shape have different weighting factors based on the confidence that exists in their experimental determination (Friswell & Mottershead, 1995). This expression relates all modes that participate in the model updating, distinguishing the different participation for frequency term against modal shape term, and additionally the different participation of each mode.

The value of the distance between the experimental model and each of the analytical models is plotted in Figure 21. This figure shows a clear trend towards a minimum value in models with a Young's modulus of stone masonry between 1320 and 1630 MPa (model's number 300 to 500). In addition, the location of the model with nominal initial properties, and the model with frequency optimized values are shown. Even though the overall trend in Figure 21a defines the existence of an optimum range of properties, focussing in on the area of interest (Figure 21b) it shows that there is no unique representative minimum, from a practical point of view, since the trend of the curve is always monotonic when varying the Young's modulus of reinforced masonry.

Several different weighting factors w_f and w_ϕ were tested to evaluate their effect on model selection, Figure 22. This figure indicates that for the area of interest, located between the models with a Young's modulus of stone masonry between 1400 and 1720 MPa (model's number 350 and 600) approximately, the frequency participation is not similar to the weighting factors entered. It is noted that for the case where the two terms weigh the same (each 50%), the frequency term has a 10% of participation in the distance value and correspondingly the modal shape term would present a 90% of participation within the area of interest. For the case in which the weighting factor in the frequency term is 0.70, its participation reaches approximately 20% of the distance. For the case in which the weighting factor of the frequency term is 0.90, its participation is

50% of the distance. Finally, just when it has a weighting factor of 0.95 of the frequency term, its participation is about 65% of the distance. It is only in the latter case when the recommendation in the literature is fulfilled. We therefore chose to work with these 3 last cases (0.70 – 0.30, 0.90 – 0.10 and 0.95 – 0.05 for w_f and w_ϕ respectively) and to evaluate their results (Figure 23). In Figure 23 there are some marks (models with specific values for calibration parameters) named as "minimum values to analyze". These models will be reviewed in the next section.

a)

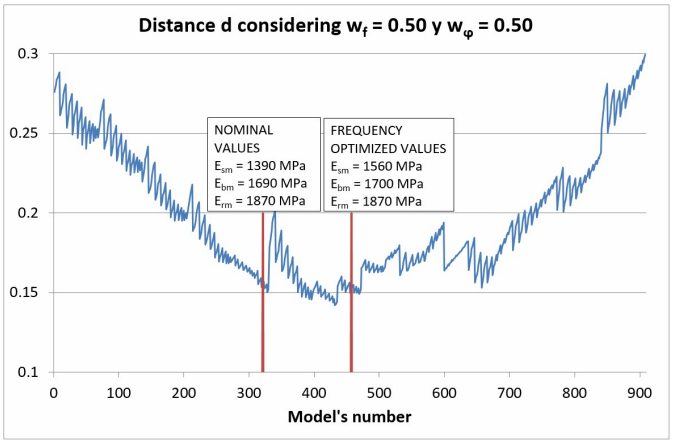

b)

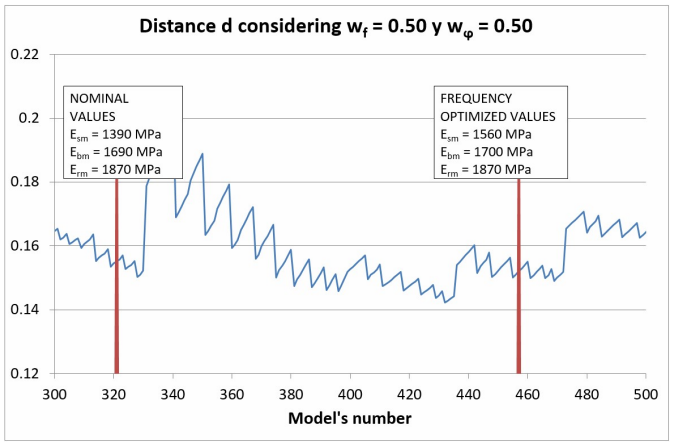

Figure 21. Distance between analytical model and experimental model with the same participation for frequency and modal shape term, a) Distance for all models, b) Zoom into area of interest for Young's modulus of stone masonry between 1320 and 1630 MPa.

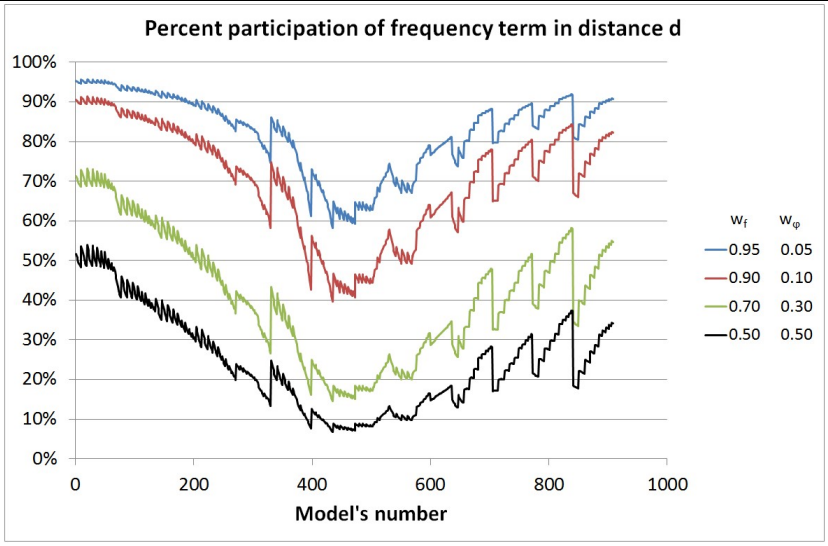

Figure 22. Participation of frequency term in the distance value of expression (1) for different couples of weighting factors.

a)

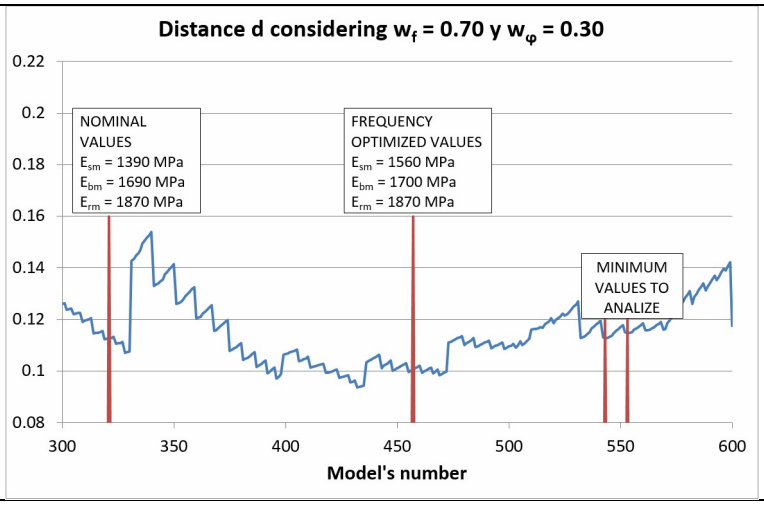

b)

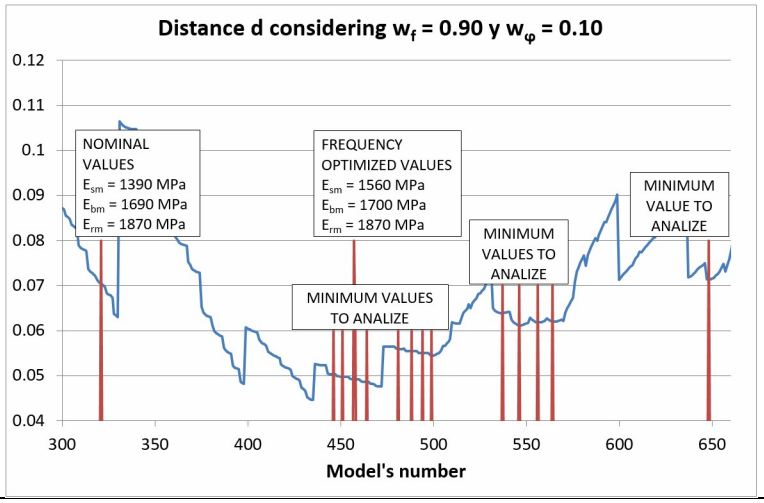

c)

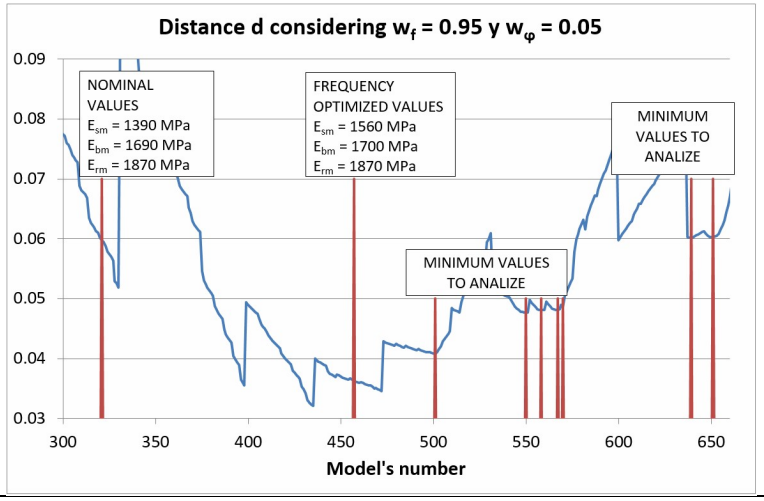

Figure 23. Distance between analytical and experimental model – for cases in which the factors w_f and w_ϕ vary. a) Case 1. Zoom in area of interest for Young's modulus of stone masonry between 1400 and 1720 MPa. b) Case 2. Zoom into area of interest for Young's modulus of stone masonry between 1320 and 1870 MPa. c) Case 3. Zoom in area of interest for Young's modulus of stone masonry between 1320 and 1870 MPa.

2.5. RESULTS of MODEL UPDATING

Two reference values were defined to continue evaluating the appropriate values for calibration parameters, (Table 8): errors between frequencies and the MAC, both

between the experimental and the analytical model. The analytical model was performed based on frequency optimized values (Table 6).

Table 8. Reference values for frequencies and modal shapes.

	Mode 1	Mode 2	Mode 3	Mode 4
Experimental frequencies (Hz)	1.96	2.38	2.95	3.18
Analytical frequencies for frequency optimized values (Hz)	2.00	2.28	2.97	3.11
Percentage errors betweeen frecuencies	2.0%	4.2%	0.8%	2.4%
MAC	0.85	0.64	0.59	0.74

Table 9. Analysis of frequencies and modal shapes for models with valid minimum distances.

Weighting factors		Model's mumber	Values of calibration parameters			Analytical frequencies (Hz) with percentage errors					MAC with percentage changes				
w_f	w_φ		E_{sm} (MPa)	E_{bm} (MPa)	E_{rm} (MPa)	Mode 1	Mode 2	Mode 3	Mode 4	avg. error	Mode 1	Mode 2	Mode 3	Mode 4	avg. change
0.70	0.30	543	1716	1020	1122	2.06	2.26	2.97	3.05		0.85	0.15	0.55	0.77	
						5.0%	4.6%	0.6%	4.1%	3.6%	0.3%	-76.4%	-6.7%	4.3%	-19.6%
0.90	0.10	**446**	1555	1528	1960	2.00	2.27	2.95	3.08		0.85	0.61	0.58	0.74	
						1.8%	4.6%	0.0%	3.2%	2.4%	-0.1%	-4.3%	-1.1%	0.1%	-1.4%
		451	1555	1613	1867	2.00	2.27	2.96	3.09		0.85	0.63	0.59	0.74	
						1.9%	4.4%	0.4%	2.8%	2.4%	0.0%	-1.7%	-0.3%	0.4%	-0.4%
		458	1555	1698	1961	2.00	2.28	2.97	3.11		0.85	0.63	0.59	0.74	
						2.1%	4.2%	0.8%	2.3%	2.3%	0.0%	-1.2%	0.0%	-0.1%	-0.3%
		464	1555	1783	2054	2.01	2.28	2.98	3.13		0.85	0.64	0.59	0.74	
						2.2%	4.0%	1.2%	1.7%	2.3%	-0.1%	-0.8%	0.3%	-0.7%	-0.3%
		481	1632	1528	1774	2.04	2.29	3.01	3.13		0.85	0.48	0.59	0.75	
						4.1%	3.6%	1.9%	1.7%	2.8%	0.0%	-25.7%	-0.4%	1.1%	-6.2%
0.95	0.05	501	1632	1783	2054	2.05	2.30	3.04	3.18		0.85	0.50	0.59	0.74	
						4.6%	3.0%	3.1%	0.0%	2.7%	-0.1%	-22.5%	0.7%	-0.3%	-5.6%

Table 9 shows the average error frequency and mean change for MAC in each model. The difference between the experimental and analytical frequency should be as low as possible; for the modal shape, MAC change between the analytical model with frequency optimized values and the experimental model should be positive. Thus, the analytical models 446, 451, 458 and 464 (in bold and gray background) are closest to the experimental model in the case $w_f = 0.90$ and $w_\phi = 0.10$.

A new variation range for the calibration parameters was therefore defined for the new area of interest (Table 10), where the steps of variation were 3%. The additional number of models generated for this last step is 147. The order for arranging these models based on changing parameters follows the same logic as the 910 previously analysed models. The calculated distance for this group of models can be seen in Figure 24.

Table 10. Range of calibration parameters in interest zone (147 models)

Calibration parameter	Min. value	Central value	Max. value
Young's modulus of stone masonry E_{sm} (MPa).	1510	1550	1600
Young's modulus of brick masonry E_{bm} (MPa).	1540	1700	1850
Young's modulus of the reinforced masonry E_{rm} (MPa).	1780	1960	2140

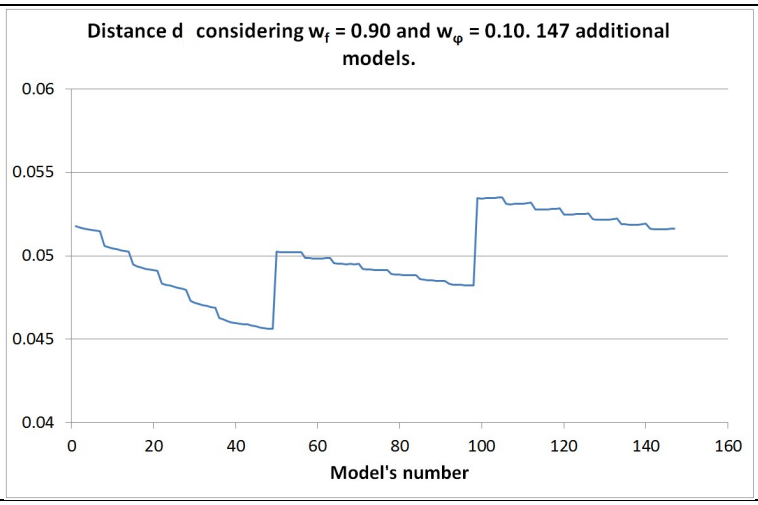

Figure 24. Distance between analytical and experimental model – Second stage.

Given the short difference between the experimental and analytical models (between 0.045 and 0.055) for this new group (see Figure 24), they will no longer be analyzed based on whether or not they have a strict minimum value, but rather by evaluating directly the error between experimental and analytical frequencies, and the MAC variation between the analytical and experimental modal shapes in the corresponding mode.

The error regarding the experimental frequency of each mode is represented in Figure 25. The analytical model is appropriate when the frequency error is below the segmented lines; these lines indicate the reference limits generated by the analytical frequency error, based on the analytical model with frequency optimized values.

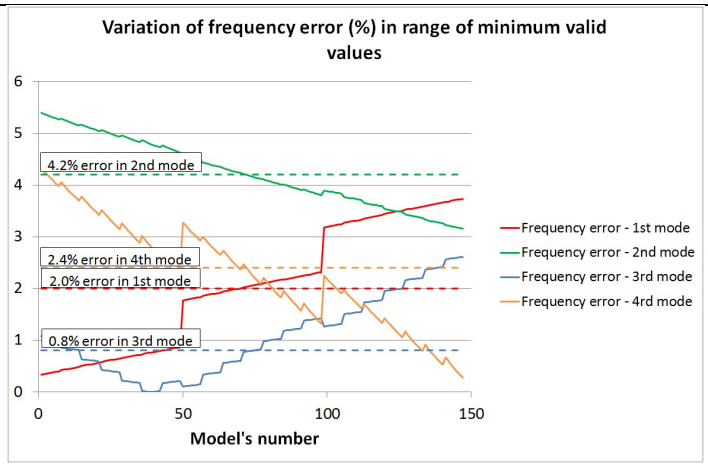

Figure 25. Frequency error for each mode.

Figure 26 uses the MAC analysis between each pair of analytical and experimental modal shapes. The MAC value in this figure is plotted and compared with the MAC for the analytical model with frequency optimized values (segmented lines) as a reference. The analytical model is appropriate when the MAC values are above the segmented lines.

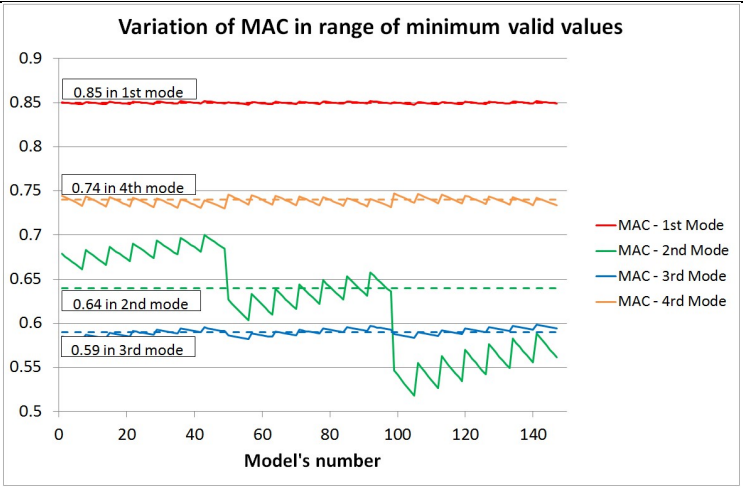

Figure 26. MAC for each mode.

Analyzing Figures 25 and 26, the first two sections of the elasticity modulus variation for stone masonry is an appropriate range when the MAC is adequate; however, this conclusion would only be true for the frequency error for the first and third mode. As the frequency error variation is not large, the sections mentioned in the elasticity modulus for stone can be said to be adequate; the other two modules can vary within the full range defined in this new variation of the 147 models (Table 10). Therefore, adequate ranges of calibration parameters can be established that get an analytical model similar to experimental one, based on in situ measurements. These ranges are shown in Table 11.

Table 11. Valid ranges of calibration parameters.

Calibration parameter	Min. value	Max. value
Young's modulus of stone masonry E_{sm} (MPa).	1510	1550
Young's modulus of brick masonry E_{bm} (MPa).	1540	1850
Young's modulus of the reinforced masonry E_{rm} (MPa).	1780	2140

Figure 27 graphically indicates the closeness of experimental frequencies and modal shapes with analytical frequencies. This graphs are similar to FMAC (Frequency-scaled MAC) (Ewins, 2000), and concentrate all the information on error frequencies and MAC between experimental and analytical modes in one picture. These graphs show FMAC for comparing calibration parameters that were assumed as frequency optimized values, and the results of second stage. These cases correspond to analytical models with minimum and maximum values indicated in Table 11. The size of the circles shown relates to the MAC in the analytical and experimental modes. It should be noted that the optimal ranges obtained for the calibration parameters produce adequate results in both frequencies and mode shapes through MAC.

2.1. BRIEF DISCUSSION AND SUGGESTIONS

The structure's natural frequencies concentrate to a narrow band; there are 4 experimental frequencies considered to the model updating in the 1.90 to 2.97 Hz range, and all these considered modes correspond to the out-of-plane flexure of the longitudinal walls. The first stage of the model updating process obtained similar results to the second one. Despite this, the latter takes into account the comparison between modal shapes by calculating the MAC between experimental and analytical modes.

As mentioned before, the selection of the calibration parameters involved in model updating depends on the importance of the variable in the model and the uncertainty that exists in its determination. In the first stage, the elastic moduli of the materials and the stiffness factors of the interaction conditions of the adjacent structures were defined as calibration parameters, only the modulus of elasticity was varied for the second stage since each new parameter increases by an order of magnitude the number of models to analyse.

a)

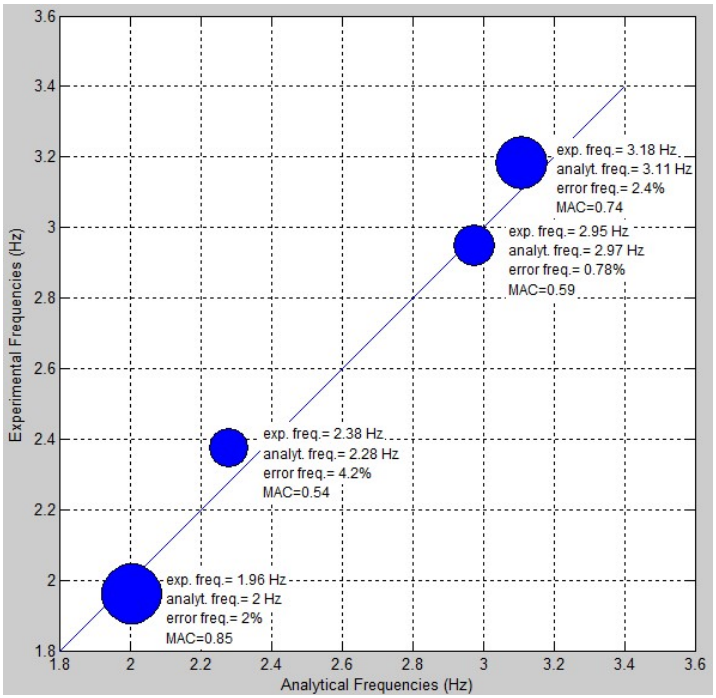
exp. freq.= 3.18 Hz
analyt. freq.= 3.11 Hz
error freq.= 2.4%
MAC=0.74
exp. freq.= 2.95 Hz
analyt. freq.= 2.97 Hz
error freq.= 0.78%
MAC=0.59
exp. freq.= 2.38 Hz
analyt. freq.= 2.28 Hz
error freq.= 4.2%
MAC=0.54
exp. freq.= 1.96 Hz
analyt. freq.= 2 Hz
error freq.= 2%
MAC=0.85
Experimental Frequencies (Hz)
Analytical Frequencies (Hz)
1.8
2
2.2
2.4
2.6
2.8
3
3.2
3.4
3.6

b)

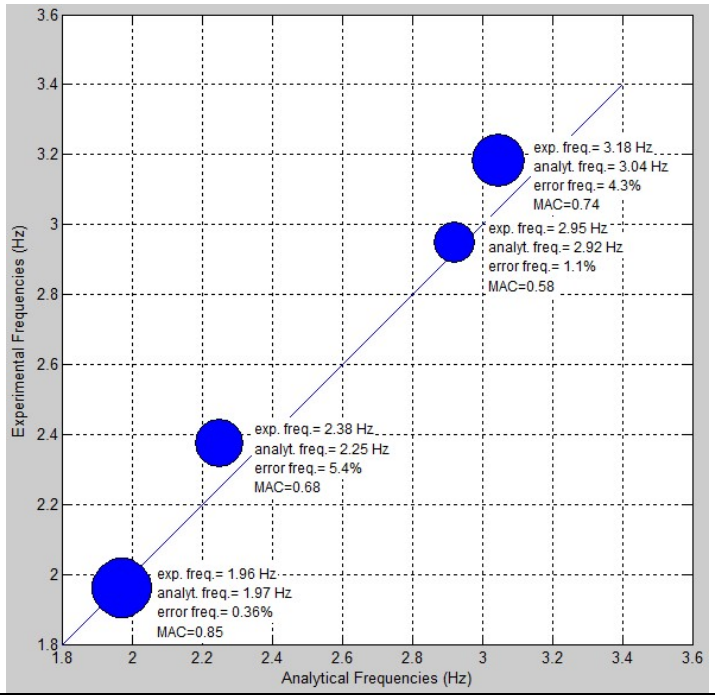
exp. freq.= 3.18 Hz
analyt. freq.= 3.04 Hz
error freq.= 4.3%
MAC=0.74
exp. freq.= 2.95 Hz
analyt. freq.= 2.92 Hz
error freq.= 1.1%
MAC=0.58
exp. freq.= 2.38 Hz
analyt. freq.= 2.25 Hz
error freq.= 5.4%
MAC=0.68
exp. freq.= 1.96 Hz
analyt. freq.= 1.97 Hz
error freq.= 0.36%
MAC=0.85
Experimental Frequencies (Hz)
Analytical Frequencies (Hz)
1.8
2
2.2
2.4
2.6
2.8
3
3.2
3.4
3.6

c)

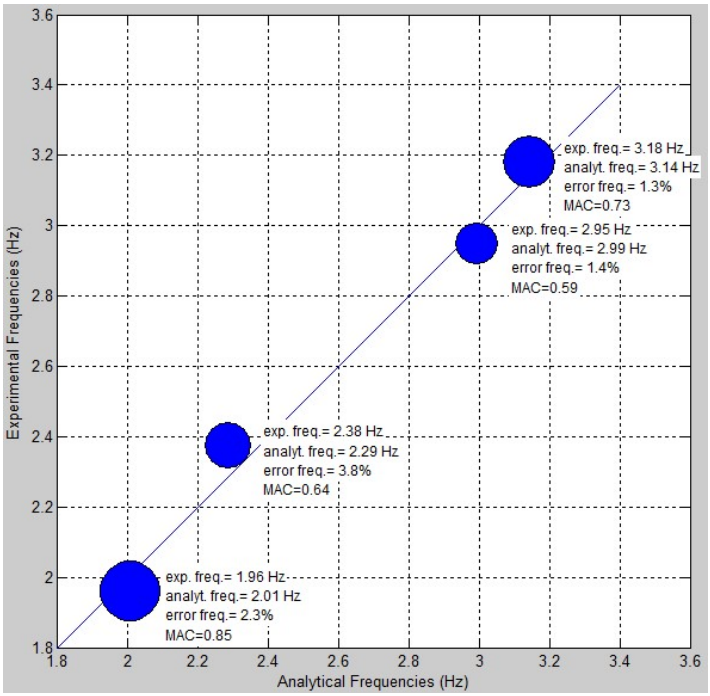

Figure 27. Graphical comparison between analytical and experimental frequencies for many cases: a) Frequency optimized values of calibration parameters, b) Minimum values in calibration parameters of final ranges, c) Maximum values in calibration parameters of final ranges.

The model updating stages determine single values (first stage) or physically possible ranges for calibration parameters (second stage). This processes contain uncertainties related with: the modeling of the structure, uniformity of mechanical properties in materials, noise present in measuring structure response to ambient vibration, the interaction between plane resistant components of the structure, among others. These uncertainties, although not explicitly considered in the model updating, are responsible for additional changes in the final obtained ranges of calibration parameters. The second stage of model updating process has shown that the range of values for each calibration parameter is best suited to representing the current behavior of the Metropolitan

Cathedral of Santiago Chile in future research. The final frequency errors show for both stages that the presented results are adequate, because the major error was not more than 5%, and the MAC values were maintained at approximately the same value between the both stages.

The Young's modulus of stone masonry is the most important value for the model updating. All graphs that show the distance between experimental and analytical models have stronger changes in the variation of this calibration parameter. Future research can be developed by considering the fact that the Cathedral is made up of single material (stone masonry) and assessing how different the results could be with this new consideration. This option is very important because if the number of calibration parameters is reduced, the workload will decrease, and other parameters can be considered, like stiffness factors in all support conditions.

Based on the experience gained during the research, some suggestions can be done in order to help future studies or engineering projects:

- The referential sensors must be located in places of the structure where movement is important for most modes. For that, a numerical model should be developed before the experimental campaign. The other sensors should be successively distributed based on the modes the user wants to capture. Other factors to consider in the experimental campaign are: measurement time, synchronizing the sensors and their precision.
- It is important to validate the records after each measurement. For that, the synchronization of sensors must be check in each setup. This can be done based on the graph of phase angle for transfer functions between measurements of the same setup.
- Evaluate the tool for identifying the system to be used. This tool can be generated by the user, or can be a commercial software built for this purpose. Similarly, the user should plan the tool for model updating. All these tools should be validated to ensure good performance in the study.

- If one of the calibration parameters is more important than the others in the final results, this fact should be properly evaluated, because the model updating could solely focus on this parameter. The model updating based on the second stage proposed in this study could be developed more quickly, with fewer calibration parameters, or it can neglect certain parameters to take others into account.
- The researcher experience is very important, because there are many decisions that are based on good judgment. All definitions in the process should be supported with alternative methods or literature related to the subject.
- In the case of study of model updating of structure based on local modes, it is important to note the process to follow in the experimental campaign. Firstly, the analytical model must be developed for defining the structure sensor locations. Secondly, the experimental campaign should be done, if the system identification process suggests the presence of local modes, it is important to update the analytical model so that these modes can be observed in the model. Finally, new setups must be planned to obtain information about these experimental local modes, which will be the basis for the final model updating.

3. FRAGILITY ANALYSIS OF THE NAVE MACRO-ELEMENT OF THE CATHEDRAL OF SANTIAGO, CHILE.

Wilson Torres[a], José Luis Almazán[a], Cristián Sandoval[a,b], Fernando Peña[c]

[a] *Department of Structural and Geotechnical Engineering, Pontificia Universidad Católica de Chile. Casilla 306, Correo 22. Santiago, Chile.*

[b] *School of Architecture, Pontificia Universidad Católica de Chile. Casilla 306, Correo 22. Santiago, Chile.*

[c] *Instituto de Ingeniería, Universidad Nacional Autónoma de México, Edificio 2–401, Circuito Escolar, Ciudad Universitaria, 04510 Mexico city, Mexico*

NOMENCLATURE:

Ao:	Effective acceleration for the site.
b_x :	Distance between the axial and shear springs in a vertical interface.
b_y :	Distance between the axial and shear springs in an horizontal interface.
C :	Random variable representing the limit state of the structure.
d_Y :	Yielding displacement.
d_U :	Ultimate displacement.
Ebm:	Young's modulus of brick masonry.
Erm:	Young's modulus of reinforced brick masonry.
Esm:	Young's modulus of stone masonry.
E^0 :	Elastic Young's modulus of axial stress in the interface.
E* :	Non elastic Young's modulus for loading and unloading of axial stress in the interface.
G^0 :	Elastic shear modulus in the interface.
G* :	Non elastic shear modulus for loading and unloading in the interface.
i_k :	Stiffness degradation index.

i_{k2} : Stiffness degradation index based on change of frequency of modes.

k^{A} : Spring stiffness values for compression loading.

k^{A*} : Spring stiffness values compression unloading.

k_h^{Q} : Stiffness of shear springs in horizontal direction.

k_v^{Q} : Stiffness of shear springs in vertical direction.

k_x^{A} : Stiffness of axial spring in X direction.

k_y^{A} : Stiffness of axial spring in Y direction.

mp_i : Modal mass participation of the i^{th} mode.

p : Value for generation of Chilean spectrum.

Pc : Probability of event C that has full compliance given a PGA value of x.

Q : Variable related to the level of seismic intensity expressed in terms of PGA.

Ti : Periods for generation of Chilean spectrum. Where, i could be a, b, c, or d.

w_f : Weighting factor based on natural frequency error.

w_i : Weighting factor for each mode.

w_ϕ : Weighting factor based on modal shape error.

x : PGA for which the cumulative probability is calculated.

Z : Factor of seismic zonification.

α_{JJ} : Factors for generation of Chilean spectrum. Where, J could be A, V, or D.

β : PGA logarithmic standard deviation for compliance with the limit state C.

ε^{Ac} : Strain at peak compression strength.

ε^{Ar} : Strain at the start of the residual stage in tension.

ε^{At} : Strain at peak tension strength.

ε^{Q*} : Maximum strain reached by the shear spring.

ε^{Qc} : Strain at peak shear strength.

$\varphi[]$: Normal cumulative distribution.

ΔV_b : Change in the base shear for each cycle.

$\Delta\delta$: Displacement of control point for each cycle.

μ : PGA for which the structure reaches 50% of the cumulative probability.

σ^{Ac} : Peak compression strength.

σ^{Ar} : Strength at the start of the residual stage in tension.

σ^{At} : Peak tension strength.

ω_{io} : Frequency of the i^{th} mode before the earthquake.

ω_{if} : Frequency of the i^{th} mode after the earthquake.

DM: Damage measure.

EDP: Engineering demand parameter.

MAC: Modal Assurance Criterion.

RBSM: Rigid body spring model.

3.1. INTRODUCTION

Recent earthquakes worldwide, such as the earthquakes of L'Aquila in Italy (2009), Maule in Chile (2010), Christchurch in New Zealand (2011), and Puebla in Mexico (2017), have caused severe structural damage, including partial and total collapse, in ancient masonry churches. The seismic assessment of complex structural systems, such as these structures, continues to be a difficult and challenging task. However, at present, this problem can be faced following some international guidelines mainly oriented to the study of existing constructions (ISCARSAH, 2003a). In this field, it is highly recommended that these studies be conducted following a multidisciplinary approach integrating different activities such as historical research, in-situ and laboratory tests, monitoring, and structural analysis.

Typically, ancient masonry churches are massive structures that were built without provisions for earthquake resistance. Due to this, complex and varied failure mechanisms are usually observed in this type of constructions after an earthquake. However, several and different post-earthquake surveys have shown that damage

observed in masonry churches can be grouped in accordance with their different architectonic elements, named macro-elements (Cattari & Lagomarsino, 2014; Da Porto et al. 2012; Doglioni et al. 1994; Lagomarsino & Podesta, 2004; Petrini et al. 1999). A macro-element corresponds to a portion of the structure generally related to an architectural part of the whole (façade, nave, apse, transept, dome, bell tower, etc.), and whose seismic response can be analysed independently from the rest of the structure. Therefore, the subdivision of the complete structure of a church into macro-elements is a way to face their seismic assessment.

Several researchers have investigated the structural behavior of historic masonry churches in terms of their macro-elements (Diaferio & Foti, 2017; Lourenço et al. 2012; Roca et al. 2013, among others). In this type of studies, different analysis methods according to the level of accuracy and simplicity desired have been employed. However, complex non-linear analyses, which demand a high computational cost, are commonly used. Therefore, it is desirable to explore more simplified analytical processes to achieve shorter processing times for this type of evaluations. On the other hand, another key aspect related to the study of ancient churches made of unreinforced masonry is the low tensile strength of the material. This fact produces a highly nonlinear behaviour in the structure. The modelling of this material in structures such as churches, castles, bridges, aqueducts, etc. remains a challenge although nowadays, powerful computational tools are available. One of these strategies is the Rigid Body Spring Model (RBSM) (Casolo, 2004, 2009; Casolo & Peña, 2007), which has certain advantages since it was specifically designed to undertake the non-linear dynamic analysis of this type of structures. Based on RBSM, Peña & Casolo (2012) have developed a specific numerical tool, RIGID software, which has been successfully applied to the analysis of existing masonry structures such as castles (Casolo & Sanjust, 2009), towers (Casolo et al. 2013), and churches (Casolo & Sanjust, 2009; Peña & García, 2016).

Recently, Lagomarsino and Cattari (2015) have proposed an exhaustive and detailed procedure to assess cultural heritage masonry structures. In this proposal, a performance-based assessment is promoted, where the performance levels are related to five damage states (Grünthal, 2009): slight, moderate, heavy, very heavy and collapsed; and four levels of performance: no damage, damage limitation, significant damage, and near collapse. Additionally, the study of Lagomarsino and Cattari (2015) suggests that the seismic assessment of heritage masonry structures can be carried out by two methods. The first method is based on nonlinear static (pushover) analysis combined with the capacity spectrum method, while the second one involves nonlinear dynamic analysis based on an adequate number of appropriate records and scaled to develop an incremental dynamic analysis (Vamvatsikos & Cornell, 2002). On the other hand, several fragility studies on masonry structures have confirmed the importance of performing analyses for a range of seismic intensities according to the location of the building (Abo-el-ezz et al. 2013; Negulescu et al. 2014; Rota et al. 2010; Simoes et al., 2015). In addition, it is well known that a vulnerability analysis requires the estimation of the damage level of structure or macro-element under study when is subjected to earthquakes of different intensities. In these studies, the seismic damage can be described through a qualitative way (Augusti et al. 2001; Lagomarsino & Podesta, 2004; Oliveira, 2003) or by means of a quantitative measure (Asteris et al. 2014; Mandal et al. 2016). In any case, it should be noted that there are several methodologies to carry out fragility analyses, each of one depends on the degree of accuracy desired (Lagomarsino, 2006; Mandal et al. 2013).

As is well known, fragility curves show the probability of exceeding a damage state of a structure, or a portion of it, as a function of a seismic intensity given by force, acceleration, deformation, or any other engineering demand parameter (EDP) (Porter et al. 2007). In addition, as already mentioned, the damage state can be quantified based on some damage measure (DM) in the structure. A damage index frequently used in fragility studies is the maximum inter-storey drift (e.g. Mandal et al. 2016) while, for

the case of masonry structures, Asteris et al. (2014) have recently proposed a DM based on the percentage of the damaged area of the structure relatively to the total area of the structure. For the specific case of heritage masonry structures, Casarin (2006) introduced as response parameter the structural stiffness where the ratio between the base shear and the displacement of a given control point is the base to assess the damage in the structure. This latter index, understood as a stiffness index, has not been previously used as a damage measure for fragility analysis of masonry structures, and therefore, has been adopted in the present research.

In Chile, the seismic action is the most important load in the performance of heritage structures throughout their useful life period. Due to this seismic condition, the set of masonry heritage buildings is relatively scarce in the country. In fact, recent earthquakes have caused significant damage, including partial or total collapse, in several historic and traditional masonry constructions (e.g. see D'Ayala & Benzoni 2012). For this reason, significant efforts have been devoted to preserve some of the most important Chilean heritage buildings. For example, Rendel et al. (2014) have presented a retrofit project of a 150 year-old masonry church that considers to introduce seismic insulators between the superstructure and a new underground level. Jorquera et al. (2017) have investigated structural characterization and seismic performance of San Francisco church, the most ancient masonry church in Santiago city. Meanwhile, Sandoval et al. (2017) have carried out other recent study about seismic analysis of an unreinforced masonry mansion built in 1872 and whose current state of damage is mainly due to the occurrence of two large earthquakes (the earthquakes of March 3, 1985 (Mw 8.0), and February 27, 2010 (Mw 8.8)). It is important to note that these recent investigations about Chilean historic constructions have permitted to characterize some relevant mechanical properties of ancient masonries by means of in-situ and laboratory tests.

If integrity of a heritage building is to be preserved, it is essential to study the behaviour of these structures given the different possible seismic intensities on the sites where they

are located. Santiago de Chile, the capital of one of the most seismic countries in the world, is an interesting location for this type of studies. The Metropolitan Cathedral of Santiago is undoubtedly one of the most important heritage buildings of the city because of its age, history and high architectural value. In view of its importance, some studies on archaeological (Prado & Barrientos, 2011), architectural (Pérez et al., 2009), and structural aspects (Torres et al. 2016, 2017) have been recently carried out. This neoclassical building, constructed about 250 years ago, is selected as a case study in this research.

In this framework, the present article focuses on the fragility analysis of a macro-element of the Cathedral taking into consideration the existing seismic risk in Santiago city, Chile. To achieve this aim, the following methodology are proposed: (1) to establish a suitable set of records for assessing the macro-element; (2) to define a damage indicator that properly represents the state of the structure subject to seismic action intensities; and (3) to characterize the behaviour of the macro-element given different scaled seismic intensities based on the seismic risk of the area. This methodology could be adopted for future studies on the fragility of others macro-elements, as well as of the whole Metropolitan Cathedral of Santiago, Chile.

3.2. THE METROPOLITAN CATHEDRAL OF SANTIAGO DE CHILE

3.2.1. General Description

The Metropolitan Cathedral of Santiago (Figure 1) is oriented in an east-west direction and is located in the northern centre of Santiago city. Figure 1a shows the main façade while the north façade is shown in Figure 1b. As can be observed, its main façade presents two towers housing belfries and a dome located above the main altar of the Cathedral. Its construction dates back to 1746 and its architectural style is neoclassical. The Cathedral presents in plan a length of 105 m, a width of 31.5 m, and it includes three longitudinal naves, as can be observed in Figure 1c. The south side of the

Cathedral is laterally supported by three adjacent structures: sacristy, tabernacle and chapel. Regarding the roof structure, the south nave presents a system of light roof supported by steel trusses, while the north and the central naves have wooden trusses.

Figure 1d shows the typical transversal section of a nave macro-element of the Cathedral, while a view from the interior is shown in Figure 1e. The structure of the Cathedral is mainly composed by stone masonry walls up a height of 11 m, and from there to a height of 17 m, is composed by brickwork walls. The thicknesses of the lime mortar joints is about 2-5 mm in the stone masonry and about 25-30 mm in the brickwork masonry. The structural walls presents an average thickness 1.1 m in the south façade and of 1.9 m in the north façade, and stand on foundations made up of stone continuous footing. It should be noted that during the period 2013-2015, the northern façade of the Cathedral was part of a strengthening project that considered steel bars injected vertically into the brickwork walls together with stainless steel cable system to avoid the out-of-plane failure of parapets. Due to these changes, brick masonry of this zone have been considered as an improved brick masonry (as a kind of reinforced masonry). Figure 2 shows all types of masonry encountered in the Cathedral structure.

a) 

b) 

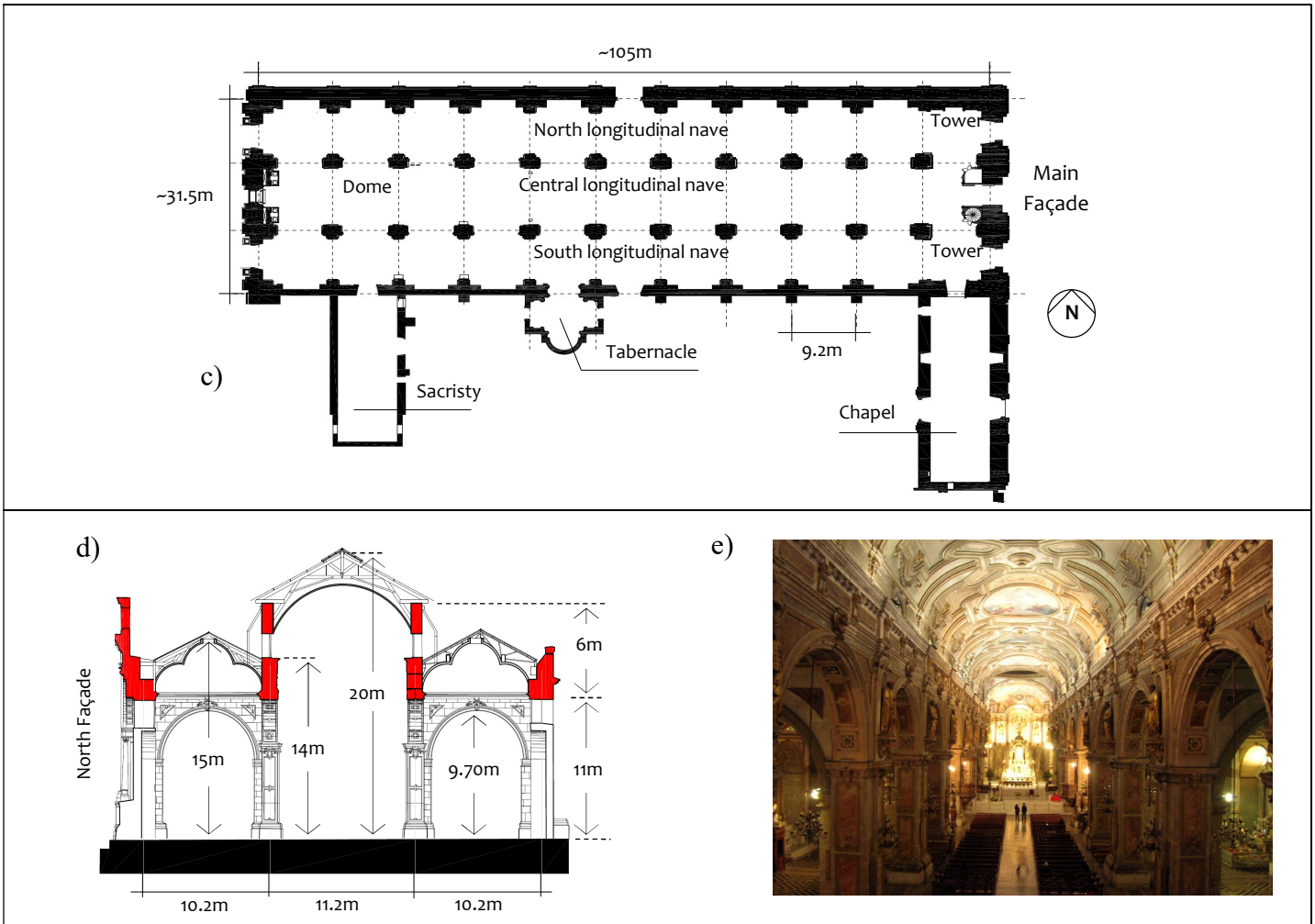

Figure 1. Metropolitan Cathedral of Santiago, Chile: (a) main façade; (b) north façade; (c) general plan view; (d) transversal section of a typical nave (brickwork walls in red colour); (e) view from the interior.

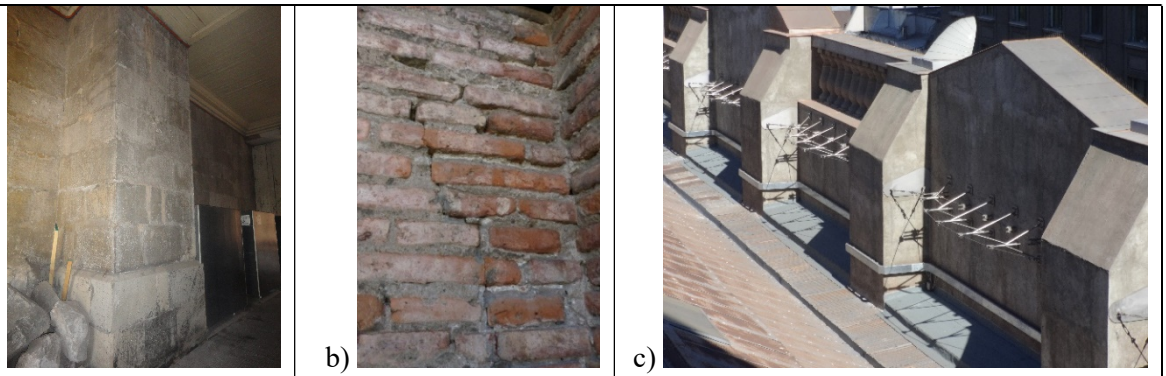

Figure 2. Types of masonry encountered in the Cathedral structure: (a) stone masonry, (b) brickwork masonry, (c) reinforced masonry.

3.2.2. Observed damage and historical seismic behaviour

Prior to the Cathedral that exists today, the original church was a structure oriented from south to north that was designed and built between 1544 and 1570. However, earthquakes and fire destroyed the first Cathedral church and a new one began to be built in 1748. The Metropolitan Cathedral of Santiago was declared National Historic Monument in 1951. A detailed description of the history of the Cathedral can be found in IDIEM (2011).

The current state of damage of the Metropolitan Cathedral is due to the occurrence of numerous earthquakes that have affected the structure over its lifetime. For example, the 1985 Valparaiso earthquake (Mw 8.0) affected both the structure and the lining of the Cathedral. As a result, in 1999 a process of repair of the most significant structural damage took place (Pérez et al. 2009). Following the 2010 Maule earthquake (Mw 8.8), serious, but eventually repairable, damage was observed in the Cathedral. The strengthening project developed during the period 2013-2015, mentioned in the previous section, was precisely carried out to repair and upgrade the resistance capacity of the north façade. However, this rehabilitation project was limited only to the north façade, and therefore, other areas of the Cathedral still show structural damage caused by the earthquake of February 27, 2010. Figure 3 summarizes some of the main

damages identified in the structure. A more detail description of the current state of damage of the Cathedral can be found in Torres et al. (2017). In any case, the current condition of the building does not compromise its overall stability but it could affect the local stability of certain elements (IDIEM 2011, Torres et al. 2017).

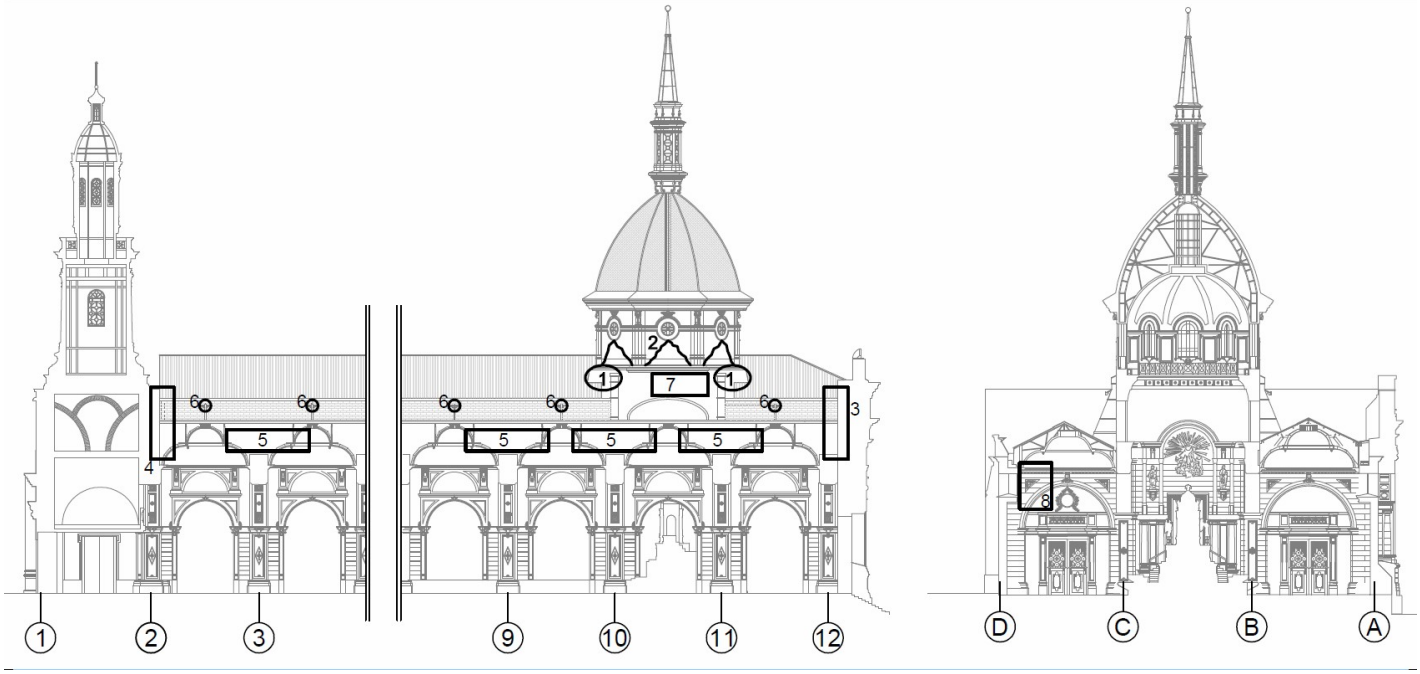

Figure 3. Current state of damage in Metropolitan Cathedral of Santiago, Chile: 1. Cracking at the base of the dome. 2. Cracking at the dome. 3. Cracking at the junction between the central longitudinal axis and the western façade. 4. Cracking at the junction between the central longitudinal axis and the tower base. 5. Cracking at the junction of brick masonry and stone masonry. 6. Steel shoring punching on the masonry. 7. Window of B axis between axes 11 and 12. 8. Cracks in the internal transversal arches.

3.3. Nave MACRO-ELEMENT

3.3.1. Calibrated model

In a previous research project (Torres et al., 2016; 2017) a complete 3D finite element model of the Cathedral structure was prepared (Figure 4a). The model, developed in the

DIANA software (TNO DIANA, 2015), was calibrated through an arduous and complex updating process that required a high computational effort. The model updating process was done by comparing the modal parameters obtained experimentally (via OMA test) with those calculated by FE model. For this purpose, the model was updated by adjusting the Young's modulus of the three masonries making up the structure as well as the lateral stiffness associated to the presence of adjacent structures (chapel, tabernacle, and sacristy). A more detailed description of the updating process and of the experimental campaign designed and implemented to estimate the modal properties of the Cathedral can be found in Torres et al. (2017).

The fragility analysis of a complex structure like the Cathedral requires simple computational models but sufficiently validated. As already commented, the subdivision of the complete structure of a church into macro-elements is a way to face this task. Figure 4b shows the portion of the whole model corresponding to the nave macro-element. Such macro-element has been considered as the most representative for the purpose of investigating the seismic fragility of the Cathedral. In addition, it is important to note that the main mode shapes of the Cathedral, both experimental and those obtained from the model, are precisely related with their transversal section (Torres et al. 2017).

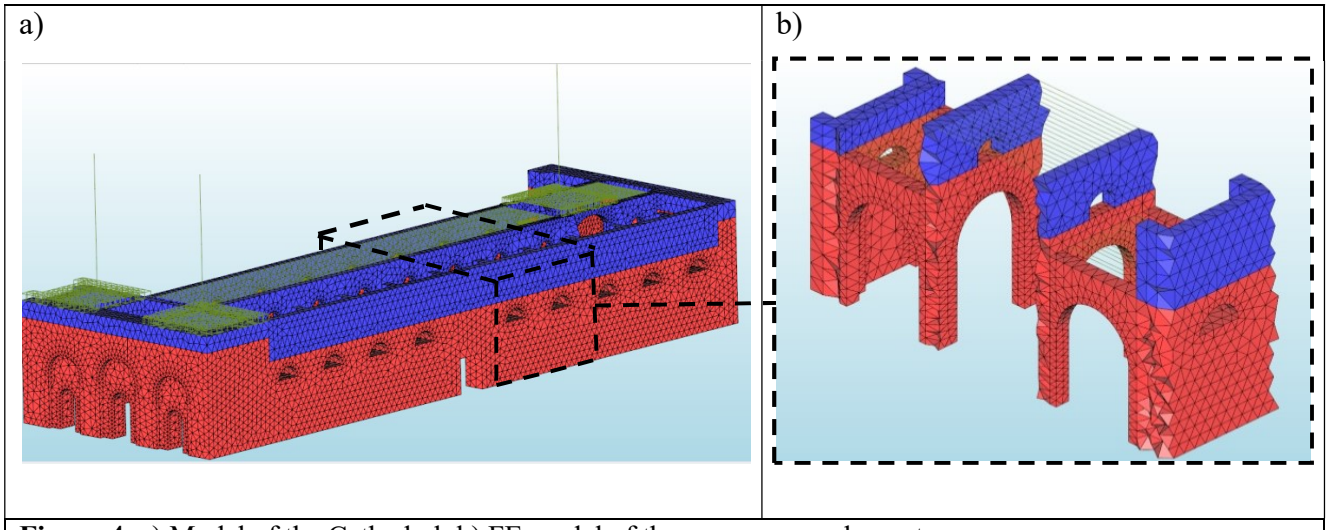

Figure 4. a) Model of the Cathedral, b) FE model of the nave macro-element.

3.3.2. Mechanical Properties

As commented, Torres et al. (2016; 2017) have defined the mechanical properties of the materials composing the Cathedral by means of an identification process of the structural system and of model updating of the whole structure. In this previous work, the process of model updating, i.e. the calibration of some mechanical properties such as the Young's moduli of the three materials that compose the Cathedral was performed through a minimization process of the error between experimental and analytical frequencies and modal shapes. Figure 5 shows the results of the minimization process which is expressed in terms of the distance between the experimental model and each of the analytical models. The final values of the Young's moduli after identification process are listed in Table 1. It is important to note that the final value obtained for the modulus of elasticity of brick masonry is quite similar to the values obtained in others heritage structures located in Santiago de Chile (Rendel et al., 2014; Sandoval et al., 2017).

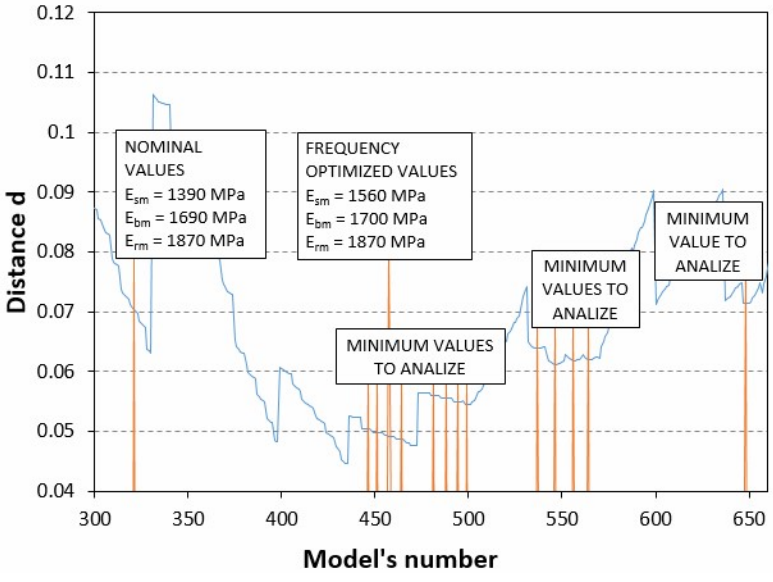

Figure 5. Distance between analytical and experimental model – for showed values of w_f (weighting factor based on natural frequency error) and w_ϕ (weighting factor based on modal shape error) (from Torres et al. 2017).

On the other hand, the compressive strength of brick masonry was defined based on a contemporary structure that is located close to Cathedral: Palacio Pereira building (Valledor et al. 2015). The compression strength of stone masonry was based on the expression E= α fc, with α=200 (Tomazevic, 1999). Moreover, all tensile strengths were assumed as 10% of compression strength (Angelillo et al. 2014; Meli, 1998). The cohesion was assumed as the same value of tensile strength (García & Meli, 2009). The residual tensile strength was assumed as the half of tensile strength based on the fracture energy and the ductility index (Angelillo et al., 2014). Table 1 summarizes all mechanical properties required for nonlinear analyses.

3.3.3. The Rigid Body Spring Model

For this study, the RBSM approach was selected as a simple method to analyse the nave macro-element. This is a simplified numerical method for masonry structures, which models the masonry as a set of rigid elements connected to each other through springs concentring the nonlinear behaviour (Figure 6). Each interface of the elements has incorporated three non-linear springs, i.e. two axial ones located near the edges of the interface and one central shear spring. The RBSM model is considered as in-plane model.

Table 1. Mechanical properties required for non-linear analysis of the macro-element.

	Stone masonry	Brick masonry	Reinforced masonry
Young's modulus (MPa)	1560	1700	1870
Compressive strength (MPa)	7.80	3.25	3.58
Tensile strength (MPa)	0.78	0.33	0.36
Residual Tensile strength (MPa)	0.39	0.18	0.22
Cohesion (MPa)	0.78	0.33	0.36
Friction angle (degrees)	30	35	35

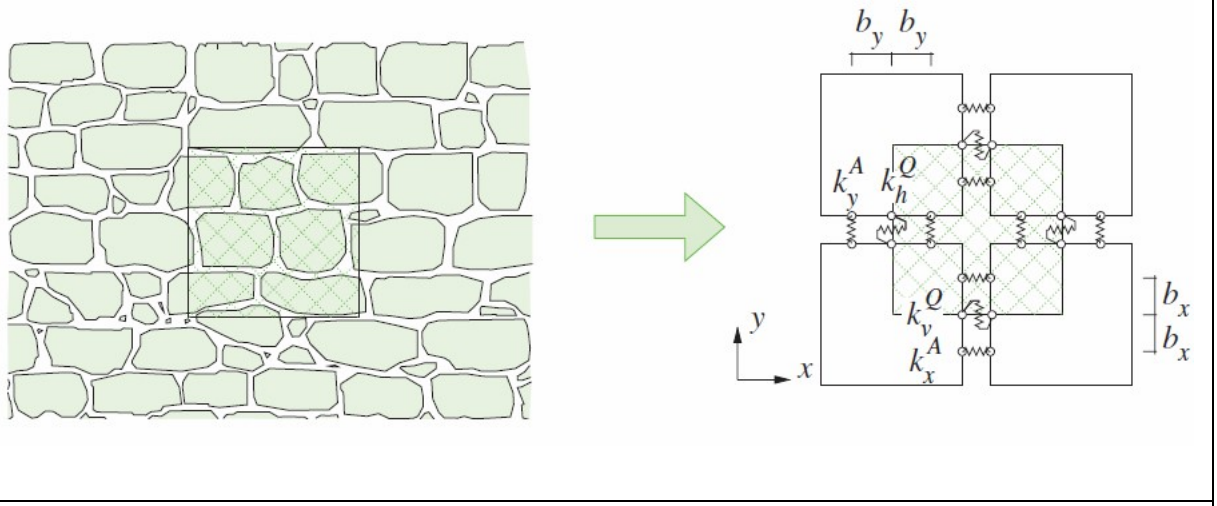

Figure 6. Scheme of an irregular masonry and the equivalent group of rigid elements (from Casolo & Peña 2007).

Figure 7 shows the constitutive laws of the springs in the RBSM model. In this figure, k_x^A and k_y^A are the stiffness of axial springs in X and Y direction, respectively; k_v^Q and k_h^Q are the stiffness of shear springs in vertical and horizontal direction, respectively; and b_x and b_y are the distances between the axial and shear springs in a vertical and horizontal interface, respectively. In the model encoded in the RIGID software (Peña & Casolo, 2012), it is assumed that each of the springs of the interface follows a hysteretic constitutive law. The lateral springs work axially (traction and compression), while the central spring that works in shear follows a Mohr Coulomb type law, where shear strength and normal stress are coupled.

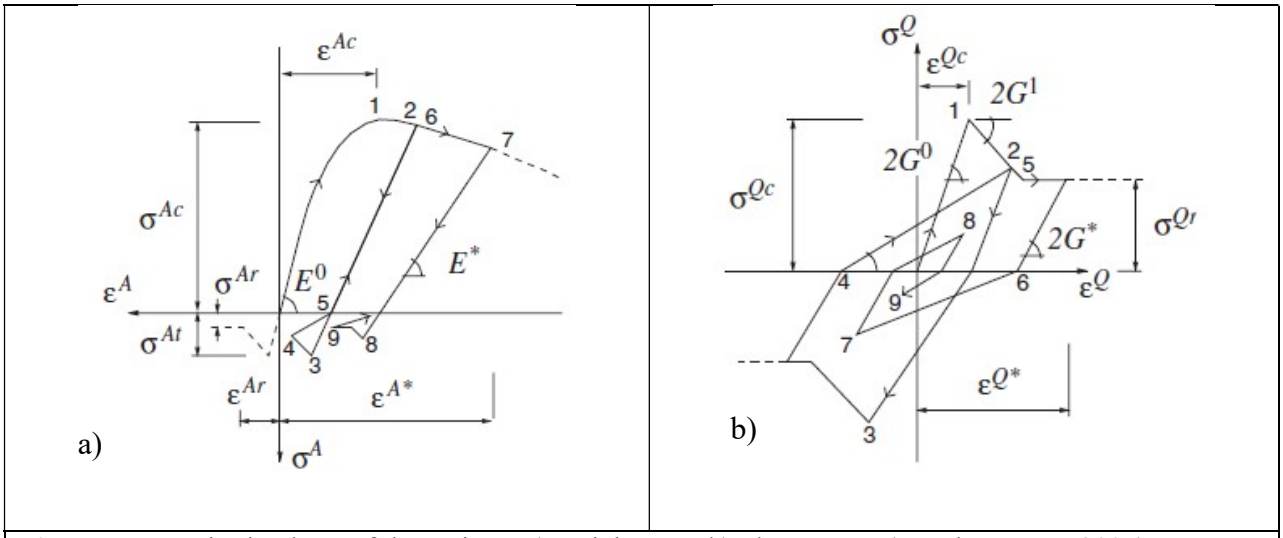

Figure 7. Constitutive laws of the springs: a) Axial stress, b) Shear stress (Casolo & Peña 2007)

For axial springs, ε^{Ac} is the strain that corresponds to the peak compression strength σ^{Ac}; in the same way, (σ^{At}, ε^{At}) is the point that defines the peak tensile strength, finally (σ^{Ar}, ε^{Ar}) defines the start of the residual stage in tension.

The spring stiffness values for compression loading k^{A} and for compression unloading k^{A*} are:

$$k^{A} = E^{0}\left(1 - \frac{\varepsilon^{A}}{\varepsilon^{Ac}}\right)e^{-\frac{\varepsilon^{A}}{\varepsilon^{Ac}}} \tag{1}$$

$$k^{A*} = E^{0}; if\left|\varepsilon^{A*}\right| \le \left|\varepsilon^{Ac}\right| \tag{2}$$

$$k^{A*} = E^{0}\left(1 - \frac{\varepsilon^{A}}{\varepsilon^{Ac}}\right)e^{-\frac{\varepsilon^{A}}{\varepsilon^{Ac}}}; if\left|\varepsilon^{A*}\right| > \left|\varepsilon^{Ac}\right| \tag{3}$$

For the shear spring, the behaviour is based on the Takeda hysteretic model (Takeda et al. 1970), where the unloading elastic modulus degrades as follows:

$$k^{Q*} = 2G^0; if \left|\varepsilon^{Q*}\right| \leq \left|\varepsilon^{Qc}\right| \quad (4)$$

$$k^{Q*} = 2G^* = 2G^0 \left|\frac{\varepsilon^{Qc}}{\varepsilon^{Q*}}\right|^{\beta}; if \left|\varepsilon^{Q*}\right| > \left|\varepsilon^{Qc}\right| \quad (5)$$

where ε^{Q*} is the maximum strain reached by the shear spring, and ε^{Qc} represents the strain at peak shear strength.

The macro-element also includes materials that do not correspond to masonry, such as the roof structure of the north and south naves, the vault of the central nave and the steel shoring of the highest part of the central walls. The properties of these materials are shown in Table 2 (IDIEM, 2011). The structural components before mentioned were modelled as linear-elastic, since the damage survey reports only damage in the masonry.

Table 2. Mechanical properties for non-masonry materials of macro-element.

	Wood structure roofing	Steel structure roofing and Steel shorings
Young´s moduli (MPa)	13,800	200,000
Compressive strength	Elastic	
Tensile strength	Elastic	
Cohesion	Elastic	

These structural components are not within the category of masonry, and represent in the model not only the mass and weight, but the additional stiffness and support that these offer to the whole structure. The vault and roof in the central nave load to the structure with their weight. Additionally, they play an important structural role since they connect the top of longitudinal central walls. In the case of northern and southern

trusses, they offer a support at the bottom of the central walls of the structure. In the same way, the steel shorings are supports to the top of central walls.

3.3.4. Nave macro-element: RBSM approach

The nave macro-element has been modelled using the software package RIGID (Peña & Casolo, 2012). The model is composed of 386 undeformable elements, i.e. there are 1158 dof in this model, a very small number compared with approximately 60,000 dof of the DIANA equivalent model. There are many sections in the macro-element, each one of those has a specific thickness because the model represents a three-dimensional part of the whole structure in a two-dimensional model. The base interfaces are fixed as they represent the support of the ground to the structure. Figure 8 shows the model of the macro-element.

The discrete model considers that each element concentrates mass, while the kinematics of the structure is based on the three degree of freedom of each two-dimensional rigid element (two translations and twisting). The nodes of the model only have a geometric meaning, since they help to start the graph of the model and to define the size of each element.

3.3.5. Validation of the nave macro-element

Based on research by Irizarry et al. (2003) and by (Lagomarsino & Cattari, 2015) the dynamic behavior of a macro-element is very similar irrespective of whether analyzed separately or as part of a complete structure. This is because the macro-element shows a sufficiently autonomous seismic response in respect to the rest of the structure. Thus, the natural frequencies and the mode shapes determined from the macro-element model of the naves can be directly compared with those obtained from the full model. This can be seen in form of a visual comparison in Figure 9.

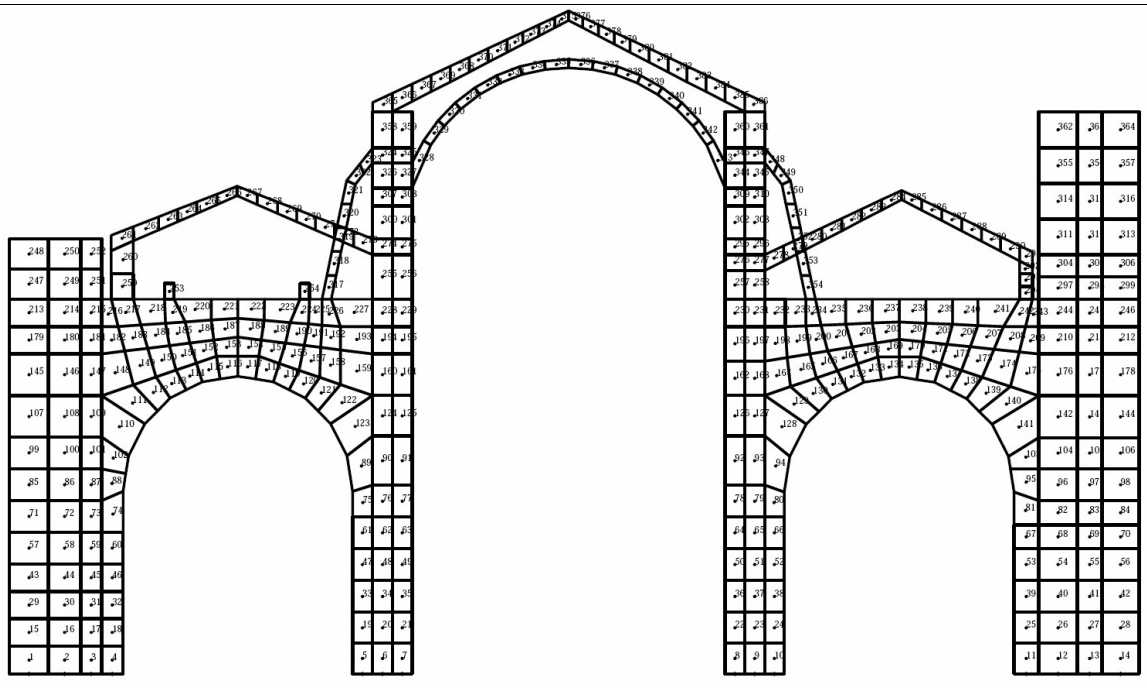

Figure 8. Macro-element model generated in RIGID software package.

Table 3. Comparison of two modes of the respective portion of the full model with model of the nave macro-element.

	First similar mode	Second similar mode
Frequency of complete model (Hz)	2.00	2.28
Frequency of isolated nave macro-element model (Hz)	2.01	2.14
Error between frequencies based on frequency of complete model (%)	0.50	6.14
MAC	0.84	0.77

In addition, this comparison was supported by calculating the MAC (Modal Assurance Criterion) (Allemang & Brown, 1982) between the model calibrated in DIANA and the model generated in RIGID. The MAC values and the errors between the natural frequencies are shown in Table 3. Based on the values displayed in this table, the

behaviour of an isolated macro-element is equivalent to the corresponding portion in the full model.

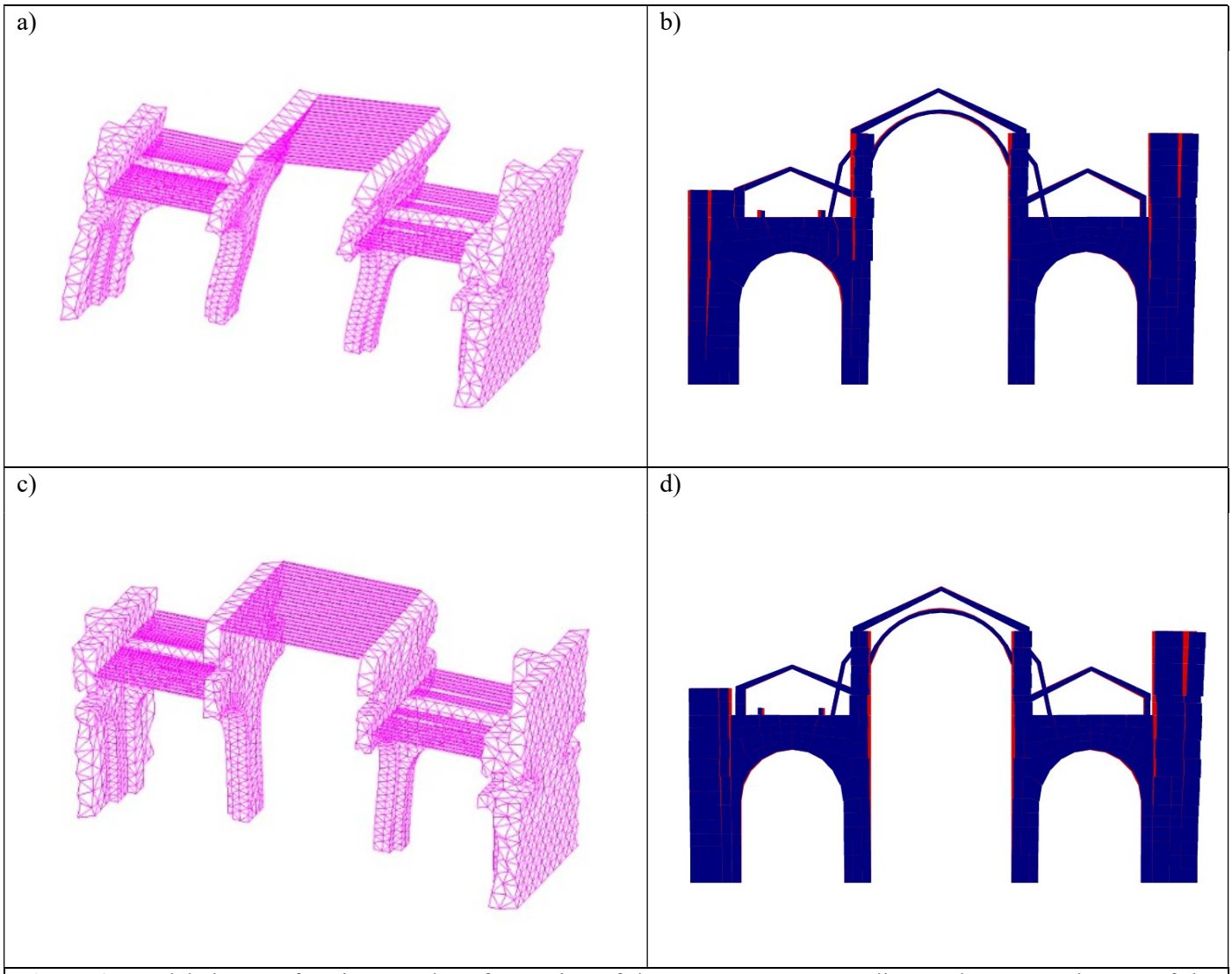

Figure 9. Modal shapes of various modes of a portion of the structure corresponding to the macro-element of the naves: a) fifth mode (DIANA model), b) first mode (RIGID model), c) seventh mode (DIANA model), and d) second mode (RIGID model).

Therefore, the study of the macro-element separately is representative of the corresponding section of the Cathedral. The simplicity of the model, the low

computational cost and the adequate results on validation of the model based on its natural frequencies, define to the RIGID model of the structure as appropriate to deal with fragility analysis of this part of the Cathedral.

3.4. FRAGILITY ANALYSIS OF THE MACRO-ELEMENT

Once validated, the RIGID model of the nave macro-element is used to study it under different seismic intensities. Then the probability of exceedance of each performance level based on PGA is evaluated. For this purpose, firstly we are going to define the base records to scale them to each seismic intensity. Secondly, a damage measure will be defined to calculate the probability curves of fragility. Finally, the fragility curves for the macro-element will be obtained.

3.4.1. Earthquake records

Eleven real seismic records were selected for the fragility analysis based on giving a greater statistical confiability to the mean response of structures (Haselton et al., 2014). This recommendation comes from comparison between Chapter 16 of proposed ASCE/SEI 7-16 standard and the existing one (ASCE, 2010). These events have been important in the recent history of seismic instrumentation in Santiago de Chile. Table 4 shows some of the main characteristics of these records.

The records mentioned in Table 4 have been selected based on the epicentral distance to the station location, but taking account that the station is located near to Santiago, Chile. The type of soil will be considered in the Chilean spectrum mentioned later.

Fifteen response spectrum-matching were generated using the 11 real records as a seed ground motions (Clough & Penzien, 2003). It is important to generate these synthetic accelerograms because the real records define an objective spectrum different to the spectrum of Chile earthquake standard; therefore, it is important to scale the record in the frequency domain. Figure 10 shows the spectrum from the Chilean seismic code (INN, 2009) considering the parameters described in Table 5. In this research, this spectrum was taken as the objective spectrum.

The records for the various intensities required in the fragility analysis were scaled according to 15 spectra related to the probability of exceedance in 50 years. Previous research using fragility analysis has been carried out based on the seismic risk in the area (Aguirre & Almazán, 2015; Colombo & Almazán, 2015) related with different seismic levels i.e. different probability of exceedance in a period of time. Table 6 shows the probabilities of exceedance in 50 years and the corresponding return periods. The variation of intensities was based on the design earthquake of the Chilean seismic design code (475 years of return period) and the hazard curve of Santiago de Chile (Fischer et al. 2002).

Table 4. Features of the 11 accelerograms of various events in different locations. This records were obtained from databases of COSMOS (University of California Santa Barbara, 2012) and RENADIC (Ingeniería Civil - Facultad de Ciencias Físicas y Matemáticas Universidad de Chile, 2010).

Seismic event	Moment magnitude (M_W)	Station	Maximum acceleration (m/s^2)	Duration (s)
Valparaíso, 1985	8.0	Melipilla	5.21	79.36
		Santiago Endesa	1.24	96.33
Punitaqui, 1997	7.1	Santiago Centro	0.19	106.00
Maule, 2010	8.8	Santiago Centro	2.11	205.00
		Maipú	5.50	167.01
		La Florida	1.40	208.00
		Peñalolén	2.60	171.01
		Puente Alto	2.60	147.01
Coquimbo, 2015	8.4	San Esteban	1.45	350.01
		Renca	1.08	355.01
		Talagante	0.53	358.01

Table 5. Parameters in the spectrum of the Chilean code NCh433 (INN 2009), Decree 177, Zone 2, and soil type II.

Parameter	Value
A_o (g)	0.30
Z	0.75
Ta (s)	0.00
Tb (s)	0.20
Tc (s)	0.32
Td (s)	2.02
α_{AA}	1099
α_{VV}	88
α_{DD}	37.5
P	0.60

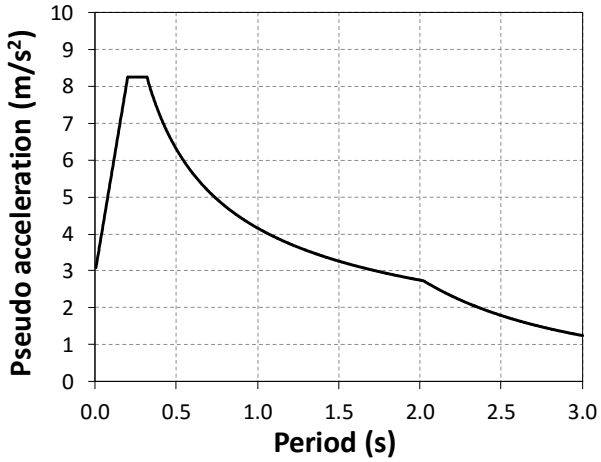

Figure 10. Pseudo acceleration spectrum according to the Chilean code NCh433D117.

Table 6. Variation of seismic intensities based on exceedance probability in 50 years.

Exceedance probability (%)	Return period (years)
2	2,475
3.5	1,403
5	975
7.5	641
10	475 (seismic design code)
15	308
20	224
25	174
30	140
40	98
50	72
60	55
70	42
80	31
90	22

3.4.2. Damage evaluation using pushover analysis

Based on related research on fragility analysis performed on masonry and concrete structures, four levels of performance are defined using as damage parameter the drift of the structure (Lagomarsino & Giovinazzi, 2006). Table 7 shows these four performance levels.

Table 7. Damage parameter for each performance level (d_Y = yielding displacement and d_U = ultimate displacement)

Performance level	Drift
1. No damage	$0.70*d_Y$
2. Damage limitation	$1.5*d_Y$
3. Significant damage	$0.5*(d_Y+d_U)$
4. Near collapse	d_U

For the case under study, the macro-element of the naves does not correspond to a regular body of masonry as it also contains two bodies of arches with roof systems of wood or metal, which are connected by a wooden roof and vault. Therefore, the damage parameter proposed in this study is the damage index based on stiffness degradation (i_k), which is defined as the ratio between the base shear and the displacement of a control point (Equation 6) (Casarin, 2006). The control point has been defined as a virtual point that represents the average displacement of points located on the head of the central longitudinal walls. The degradation is expressed based on the final stiffness index as a fraction of the initial stiffness index. The final stiffness index (i_k) is measured after the structure has been loaded by the earthquake, as follows:

$$i_k = \frac{\Delta V_b}{\Delta \delta}, \quad (6)$$

where ΔV_b is the change in the base shear and $\Delta\delta$ is the displacement, for each cycle.

All the damage levels of the structure based on stiffness degradation were established based on the two extremes of performance (performance levels 1 and 4), and intermediates were determined by comparison of the stiffness degradation index with the drifts given in Table 7. This comparison was carried out based on two static non-linear (pushover) analyses proportional to the mass (Caselles et al. 2011), one in the

positive direction and the other in the negative direction. Despite the structure is not symmetrical, the relation between drift and stiffness degradation presents the same result in this second damage parameter. Performance levels according to the stiffness degradation index are shown in Table 8.

The pushover analysis carried out not only served to calibrate performance levels between the drift and the stiffness index, but also to demonstrate that the mechanism of collapse generated in the structure is replicated while the damage is increasing. Figure 11 shows the state of damage in the macro-element for each level described in Table 8. Figure 12 shows the deformed structure at the end of pushover analysis. As shown in Figure 11d, the collapse mechanism of the macro-element consists in the development of plastic hinges on the extrados of the arches and on the bases of the columns.

Table 8. Damage parameter for each performance level based on the degradation of stiffness index.

Performance level	i_k (%)
1. No damage	90
2. Damage limitation	70
3. Significant damage	35
4. Near collapse	20

The performance levels defined in Table 8 generates five performance damage states: Slight damage state for a stiffness degradation index more than 90%, Moderate damage state if the stiffness degradation index between 70 and 90%, Heavy damage state for a stiffness degradation value between 35 and 70%, Very heavy damage state for a stiffness degradation value between 20 and 35%, and Collapse damage state for stiffness degradation values less than 20%.

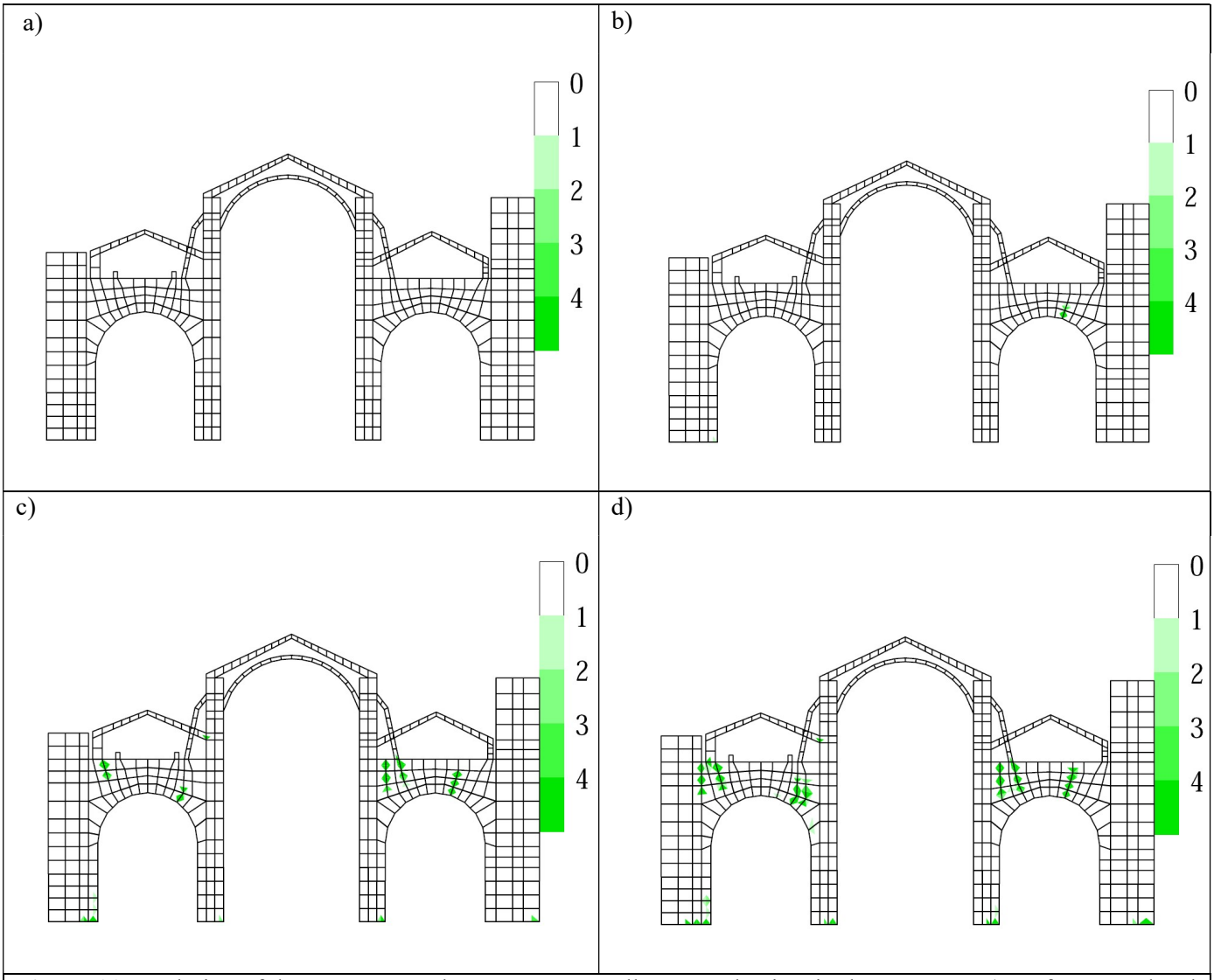

Figure 11. Evolution of damage pattern that generates a collapse mechanism in the structure: a) Performance level 1, b) Performance level 2, c) Performance level 3 and d) Performance level 4.

The values of base shear and displacement of the control point were obtained from numerical models for each accelerogram, an example of these values can be seen on Figure 13. In particular, this graph represents the relationship between the base shear and displacement of control point for the model seismically loaded with the fifth intensity (475 years of recurrence) of Maule 2010 – Santiago Centro station record seed.

With this information, the number of cycles was determined. A cycle is defined as the portion of information with a positive slope between the extreme values, i.e. the changes in base shear and displacement of the extreme values are either positive or negative. In Figure 14, there are many cycles of the complete curve seen in Figure 13, the stiffness index is calculated from the extreme points of each cycle.

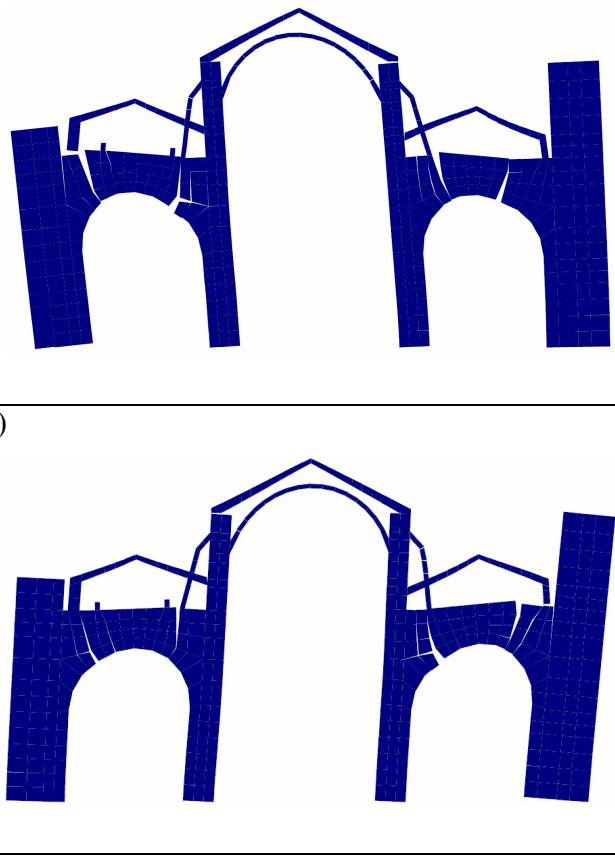

Figure 12. Deformed structure at the ending of pushover analysis: a) Negative direction. b) Positive direction.

For each record, the data (base shear and displacement of control point) was processed. First, the force-displacement time histories were filtered based on a band-pass filter with cut frequencies: 0.3 and 4.0 Hz. Second, the stiffness index was calculated for each

cycle. Considering that the seismic load is very fluctuating, the response of the structure is erratic, therefore the resultant stiffness index does not decrease always monotonically. Finally, to facilitate the interpretation and to improve the visualization of results, the stiffness index value was processed by a mobile media with a window of 8 values of width.

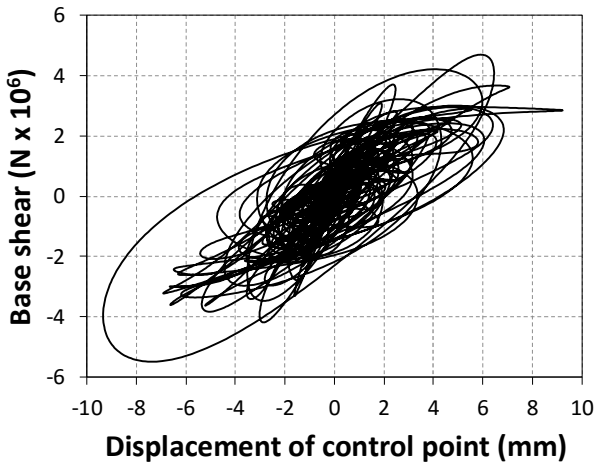

Figure 13. Complete curve of base shear vs. displacement of control point for the record Maule 2010 in Santiago Centro station, scaled to 10% of exceedance probability.

In Figure 15, graphs depict the stiffness degradation index versus the number of cycles for some of the seismic intensities (2%, 5%, 10%, 30%, 60% and 90% probability of exceedance in 50 years) of the Maule (2010) earthquake at the Santiago Centro station (see Table 4). As the seismic intensity increases, the residual stiffness degradation index decreases. The continuous curve is an approximation of the segmented curve based on the least square method.

To establish a value of comparison with the calculated damage index, it is proposed to use the natural frequencies of the macro-element. These frequencies can be obtained from the RIGID model at the beginning and at the end of the analysis. Therefore, the

change in the value of the squares of the natural frequencies can be determined; this value is directly related to the stiffness of the structure.

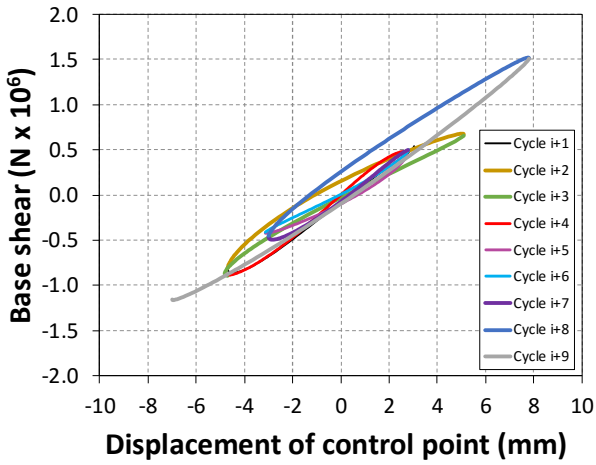

Figure 14. Many cycles in which were calculated stiffness index. Values from complete curve showed in Figure 13.

Since every natural frequency corresponds to a particular mode, it is proposed to work with the first three modes, weighting each mode according to its modal mass participation. Therefore, we can propose a new stiffness degradation index (i_{k2}) based on the change in the frequencies of the first three modes. This is shown in the expressions (7) and (8).

$$i_{k2} = \sum_i w_i \left(\frac{\omega_{if}}{\omega_{io}} \right)^2 \tag{7}$$

$$w_i = \frac{mp_i}{\sum_i mp_i} \tag{8}$$

where ω_{io} and ω_{if}, are the frequencies of the i^{th} mode before and after the earthquake, w_i is the weighting factor for each mode, which depends on the modal mass participation in the horizontal direction, and mp_i is the modal mass participation in the i^{th} mode. Since only the first three modes of the macro-element were considered, the values of the modal mass participation had to be readjusted according to only the modes that had been taken into account.

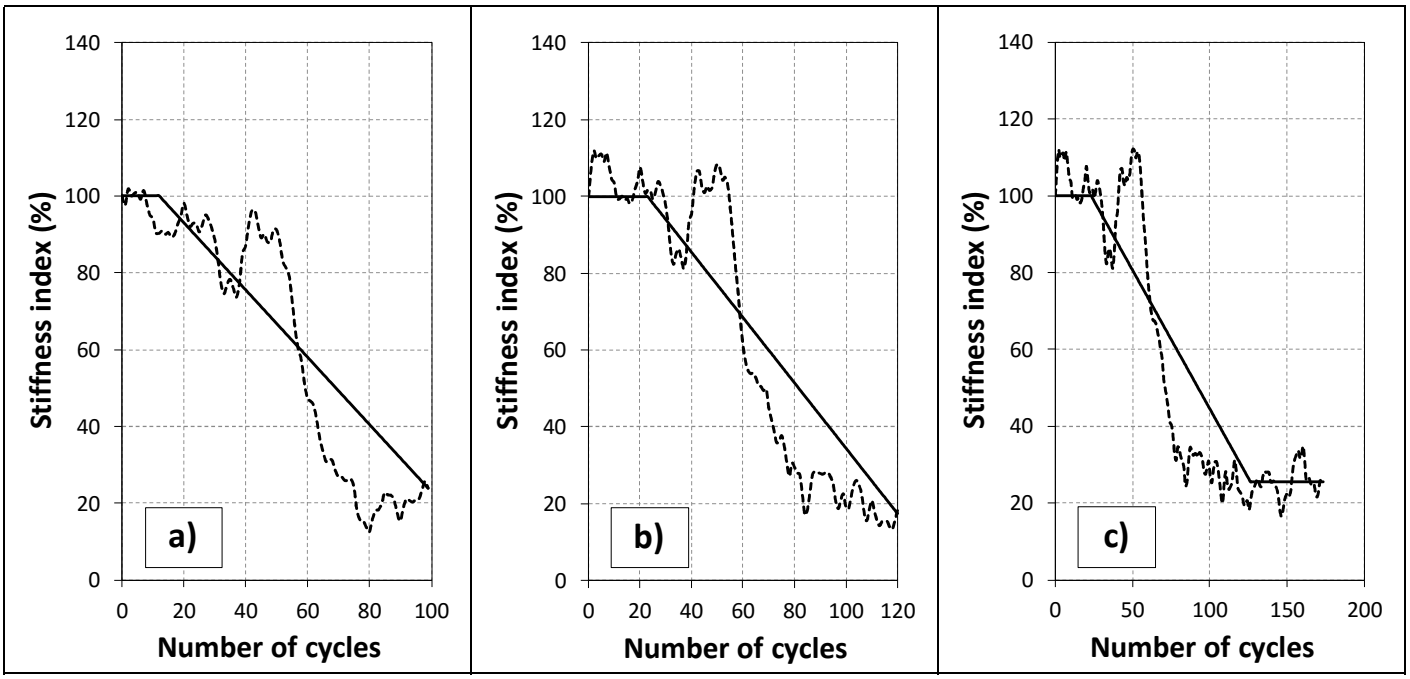

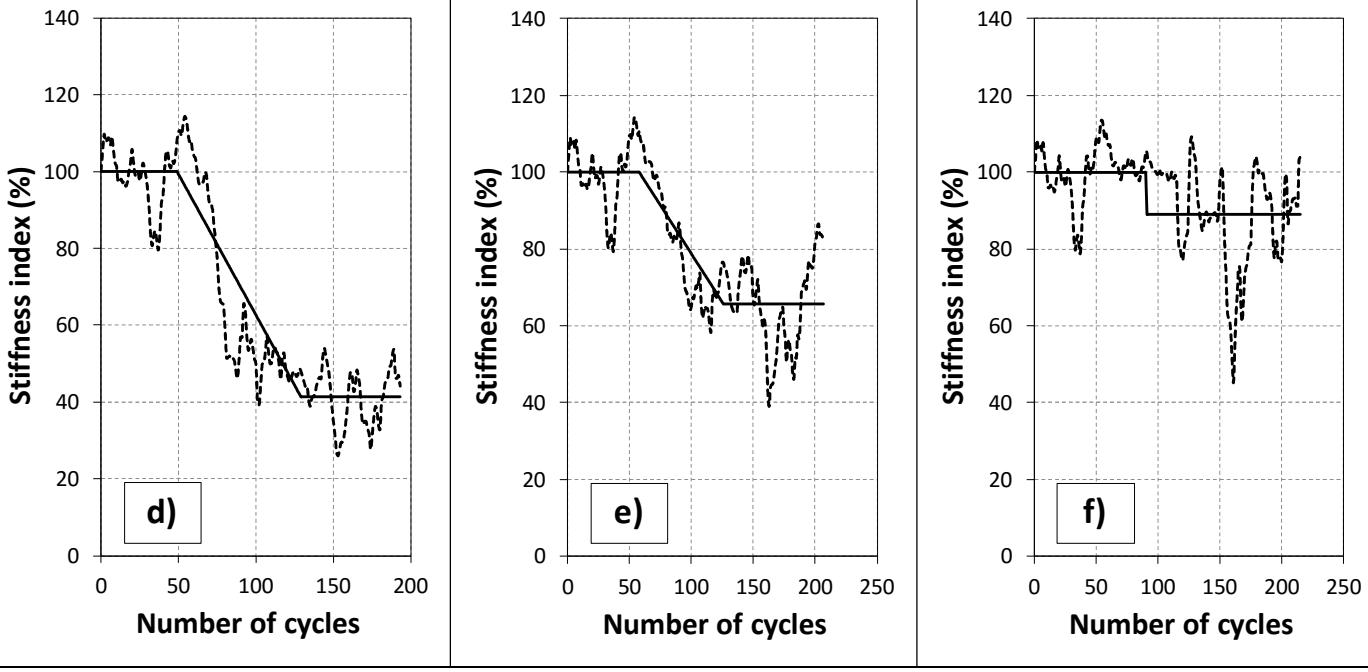

Figure 15. Evolution of stiffness degradation for the 2010 Maule earthquake (Santiago Centro station) with some dependent intensities of the probability of exceedance in 50 years: a) 2%; b) 5%; c) 10%; d) 30%; e) 60%; f) 90%.

The changes of the natural frequencies of the first three modes of the macro-element were calculated based on the 15 proposed seismic intensities; then for each seismic intensity the results of the 11 records were averaged and compared with the corresponding value of the stiffness degradation index, calculated initially. This comparison can be seen in Figure 16. This figure shows that the trend for the two stiffness degradation indices is similar. This comparison confirms that the stiffness degradation index initially proposed satisfactorily describes the damage of the structure.

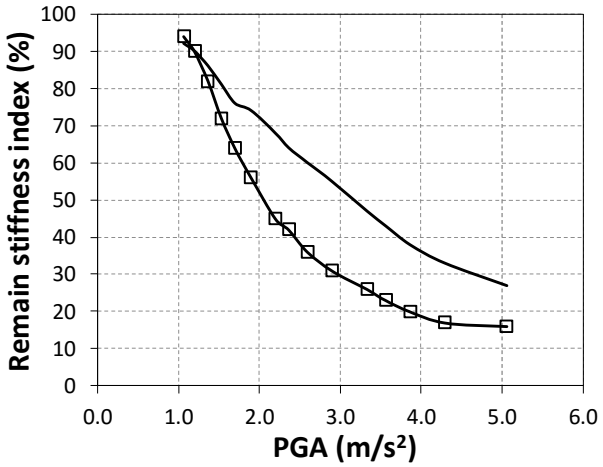

Figure 16. Comparison of the stiffness degradation indices for the 15 levels of seismic intensity represented by average Peak Ground Acceleration.

3.5. FRAGILITY CURVES FOR THE NAVE MACRO-ELEMENT

3.5.1. Generation of Fragility curves

For the definition of fragility curve, the engineering parameter adopted was the Peak Ground Acceleration (PGA). This parameter was calculated using the average of the PGA of synthetically generated records for each intensity defined in Table 6.

The distribution of the conditional probability of failure was assessed by numbering the cases where the remaining stiffness degradation index was located within each of the ranges given before (slight damage, moderate damage, heavy damage, very heavy damage and collapse damage). This was done for a given intensity and can be expressed by the expression (9),

$$Pc = P\left[C = 1 \mid Q = x\right] \tag{9}$$

where C is the random variable representing the limit state of the structure and Q is related to the level of seismic intensity expressed in terms of PGA. Therefore, Pc is the probability of event C that has full compliance given a PGA value of x (Colombo &

Almazán, 2015). After all the analyses were completed, the number of models whose performance exceeded or reached the damage states shown in Table 8 were counted, and the results are presented in Table 9.

Table 9. Case count for each state of damage in the 15 seismic intensities defined.

Damage state	I1	I2	I3	I4	I5	I6	I7	I8	I9	I10	I11	I12	I13	I14	I15
Moderate	11	11	11	11	11	11	11	11	11	11	11	11	10	5	4
Heavy	11	11	11	11	11	11	11	11	11	10	9	4	1	0	0
Very heavy	11	11	11	11	11	9	5	2	0	0	0	0	0	0	0
Collapse	11	9	5	1	0	0	0	0	0	0	0	0	0	0	0

The fragility curve (see expression 10) has the same form as the cumulative probability lognormal function described in Vargas et al. (2013) and is as follows:

$$Pc(x) = \phi\left[\frac{1}{\beta}\ln\left(\frac{x}{\mu}\right)\right] \qquad (10)$$

where φ[] is the normal cumulative distribution, x is the PGA for which the cumulative probability is calculated, μ is the value of PGA for which the structure reaches 50% of the cumulative probability, and β is the PGA logarithmic standard deviation for compliance with the limit state C. With the information shown in Table 9 and adjustment of the parameters μ and β of expression (10) the fragility curves showed in the next Section were obtained.

3.5.2. Fragility analysis

The collapse mechanism defined based on pushover analysis is given by the development of plastic hinges on the arches and in the base of the columns. In a previous research (Torres et al., 2017), one of damage found in the structure (many arches of northern longitudinal nave) given by its seismic history shows the coherence between the finding of this study and the current state of the Cathedral (Figure 17).

Although the macro-element is non-symmetric, the positive direction pushover and the negative one get the same collapse mechanism in the structure, i.e. the development of hinges on the arches. This is a valuable finding for the study carried out, because the performance of the structure for the seismic (cyclic) load is independent of its direction, therefore the weakening of the structure is only dependant of the seismic intensity.

Table 10. Setting the parameters for the fragility curves.

Damage state	Logarithmic standard deviation (β)	Median (μ)
Moderate	0.1582	1.1638
Heavy	0.0979	1.5736
Very heavy	0.1048	2.6262
Collapse	0.0853	3.9317

Based on the process described in the previous section and the curve fitting of expression (10), the values of the parameters β and μ for each damage state were determined. These values are shown in Table 10.

The fragility curves for the four damage states can be seen in Figure 18. It is important to note that the median values for each damage state correspond to the graphs displayed in Figure 18, but the logarithmic standard deviations cannot be compared between each other. These latter values are related to the slope of the straight middle part of the fragility curve i.e. if the value is high the slope is slight and vice versa. In this case, the fragility curve that describes the exceedance probability of the moderate damage state should have the smallest slope, and the curve of collapse should have the greatest slope of the 4 curves. However, this latter principle does not correspond with the graphs, because the median has a different value for each case.

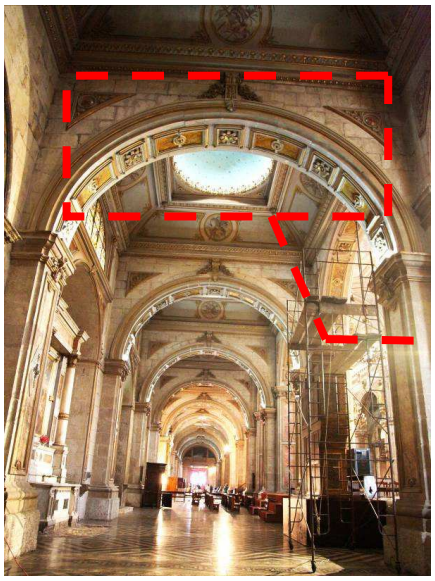

Figure 17. Evidence of opening in a transversal arch of Cathedral. a) Complete view of arch, b) Zooming the cracking of the arch.

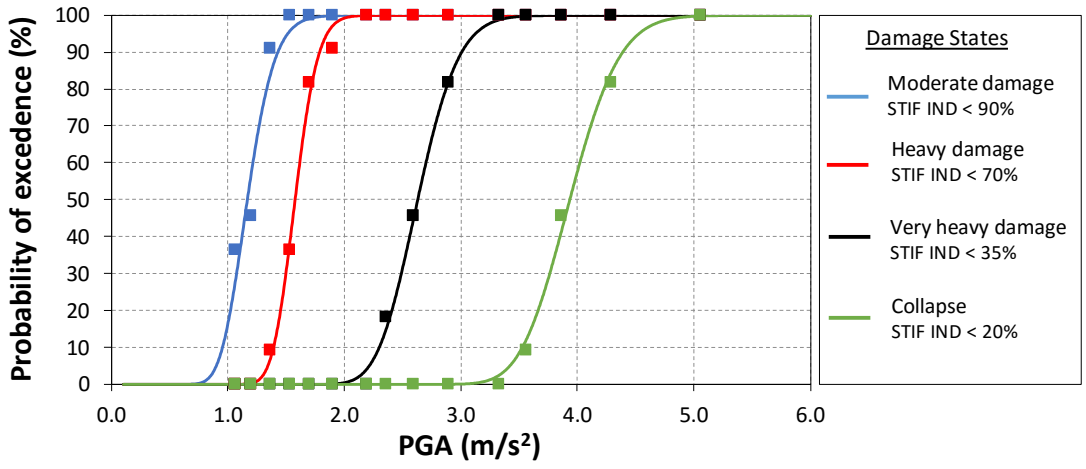

Figure 18. Fragility curves for Nave macro-element.

4. SEISMIC ASSESSMENT OF A MASONRY MACRO-ELEMENT THROUGH A NONLINEAR FRAMED MODEL. A CASE STUDY.

Wilson Torres[a], José Luis Almazán[a], Cristián Sandoval[a,b], Rubén Boroschek[c]

[a] *Department of Structural and Geotechnical Engineering, Pontificia Universidad Católica de Chile, Vicuña Mackenna 4860, Santiago de Chile, Chile.*

[b] *School of Architecture, Pontificia Universidad Católica de Chile, Casilla 306, Correo 22. Santiago de Chile, Chile.*

[c] *Department of Civil Engineering, University of Chile, Beauchef 850, Santiago de Chile, Chile.*

4.1. INTRODUCTION

The need to protect the heritage structures in places with high seismic activity remains a challenging task for the engineering community. A proper analysis of these structures requires that its structural assessment must be treated with accurate and reliable tools. The study of this type of structures can be done through various methodologies and tools developed for this purpose (Roca et al. 2010). Among them, nonlinear approaches based on Finite Element Method (FEM) are widely used in the seismic assessment of masonry constructions Generally, in this type of modelling strategy (also (e.g. Mallardo et al. 2008; Peña et al. 2010; Sandoval et al. 2017; among others)referred to as *macro-modelling*), the masonry is treated as a fictitious homogeneous continuum while the structure can be described by means of 2D or 3D finite elements. The use of this type of models in the seismic assessment of large structural members or full masonry structures often requires high computational effort because of the structure geometry generation and the complexity of model resolution.

Masonry structures can also be analyzed by means of others numerical strategies, such as the Equivalent Frame Method (EFM) (Lagomarsino et al., 2013). The structures studied using this method correspond to buildings where the following conditions must be satisfied: (i) the openings (doors and windows) of the walls must be regularly distributed, and based on this, the decomposition of resistant planes and facades in piers and spandrels is possible (Clementi et al., 2016); (ii) the horizontal displacement is coupled at the floor levels by the presence of horizontal diaphragms (Lagomarsino et al., 2013); and (iii) mass is concentrated at the story levels (Magenes, 2000). The EFM method, which essentially discretizes the masonry elements by means of column-beam elements, has been employed in several investigations with interesting results (Addessi et al., 2014; Belmouden & Lestuzzi, 2009; Chen et al., 2008; Magenes & Della Fontana, 1998; Roca et al., 2005). However, due to the aforementioned conditions of use, masonry structures with irregular geometry, without intermediate floors where mass could be concentrated, and with roofs without the adequate stiffness to unify the displacements of the wall tops, often they cannot be modeled with this type of approach. The models based on bar-type elements have less degrees of freedom compared with the FEM models with bi or tridimensional elements. For this reason, this modelling way constitutes a valuable solution to the problem of processing times. Additionally, there are several analysis programs —such as OpenSees (McKenna, 2014), SAP2000 (Computers and Structures, 2009), or Perform-3D (Computers and Structures, 2016)— that have very interesting tools for evaluating structures subjected to seismic loading considering bar-type elements with nonlinear constitutive laws. Some studies in which these programs have been used to evaluate masonry structures based on models with bars have shown interesting results and conclusions (Raka et al. 2015; Razzaghi & Javidnia, 2015; Vanin et al. 2017).

On the other hand, the Rigid Body Spring Model (RBSM) approach (Casolo, 2004, 2009; Casolo & Peña, 2007) has proven to be a reliable and accurate tool to investigate the in-plane seismic behavior of masonry structures. The RIGID software (Peña &

Casolo, 2012), based on the RBSM approach, has been successfully used in the study of several components of complex masonry structures. These components are called macro-elements and represent a way to decompose a structure to analyze it more easily. As mentioned before, while the models generated with this tool must be plane, there is no restriction regarding the geometry that can be obtained e.g. in the architecture of the churches: arches, flying buttresses, abutments, etc. Based on this, there are many cases in which certain macro-elements of heritage churches or castles have been modeled with the RIGID software, and the results show good agreement with the current state of those structures (Casolo & Sanjust, 2009; Peña & García, 2016; Torres et al. 2017).

The Metropolitan Cathedral of Santiago de Chile is perhaps the most important heritage building in the city of the same name. This structure has already been studied in order to estimate the mechanical properties of its materials based on system identification theory (Torres et al., 2016; 2017). In addition, a fragility analysis of its most recurrent macro-element (longitudinal naves) has been carried out using the RIGID software (Torres et al. 2017).

Based on the facts described regarding EFM method and the model developed in RBSM, there is a need to develop a simplified method that allows for optimization of time in the generation of structure geometry and reduction of processing times for finite element models, without neglecting the precision and reliability that the results must achieve. The aforementioned characteristics, which should be fulfilled by buildings in the EFM, do not correspond to the reality of churches. Thus, a new Nonlinear Framed Model (NLFM) is proposed to solve, with appropriate reliability, the problems related to the optimization of resources in the modelling of these heritage structures.

This simplified model will help to carry out a complete fragility analysis of the Cathedral in a future research, taking into account seismic behavior in the two main directions in the plant of the building. The first step in this process is the focus of this

article, i.e. it is to carry out research to establish equivalence between the model developed from rigid elements based on RBSM (Torres et al. 2017), and a proposed model of bars (NLFM). These bars will work in axial-bending stresses, and the masses in the proposed model must be properly lumped (location and intensity), such that both static and dynamic properties are calibrated to achieve similar behavior between the two models.

To address the seismic evaluation of the entire Cathedral, or part of it, using a three-dimensional model, the research being developed would thus follow a path that it is important to describe. First, an experimental campaign was carried out, in which mechanical properties were defined for the model by identifying its modal properties (Torres et al. 2017). Second, the definition of the macro-elements of the Cathedral, and the fragility analysis for one of these components was carried out (Torres et al. 2017). Third, the generation of a new model is proposed, which is composed of axial-bending bars with masses concentrated in singular points of the model. This article deals with this third stage of the process. Finally, a three-dimensional model with several resistant planes could be generated, this simplified model will help to carry out a complete fragility analysis of the Cathedral, taking into account seismic behavior in the two main directions of the building.

The process for proposing the NLFM model can be described as follows: i) a brief description of the first nave macro-element model developed in the Metropolitan Cathedral of Santiago de Chile using RBSM methodology; ii) a detailed description of the proposed NLFM model and calibration process based on comparison with the first model generated using the RBSM method; iii) performance comparison between the NLFM model and the RBSM method based on static and dynamic analyses; iv) conclusions, and v) future research.

4.2. CASE STUDY: METROPOLITAN CATHEDRAL OF SANTIAGO DE CHILE

The Metropolitan Cathedral of Santiago is located in the northern centre of Santiago city. Its construction dates back to 1746 and its architectural style is neoclassical. The structure of the Cathedral is mainly composed by stone masonry walls up a height of 11 m, and from there to a height of 17 m, is composed by brickwork walls. The thicknesses of the lime mortar joints is about 2-5 mm in the stone masonry and about 25-30 mm in the brickwork masonry. It should be noted that during the period 2013-2015, the northern façade of the Cathedral was part of a strengthening project. Due to these changes, brick masonry of this zone have been considered as an improved brick masonry (as a kind of reinforced brick masonry).

A complete model of Metropolitan Cathedral of Santiago de Chile was built to calculate its dynamic properties and the model's mechanical properties were then updated (Torres et al. 2017). The detailed process and results of this part can be seen in the second chapter. This study, which is part of a complete investigation of the Cathedral, aims to achieve a seismic evaluation of the entire structure; it is very difficult to carry out this out using the current methods, however (Roca et al. 2010).

One approach to modeling patrimonial buildings whose structure is complicated due to size and architecture is to divide them up into a series of components called macro-elements (Doglioni et al., 1994). Post-seismic study of some patrimonial structures has shown that the dynamic behavior and failure mechanisms of these macro-elements can be treated independently of the complete structure (Cattari & Lagomarsino, 2014; Irizarry et al., 2003), and thus they constitute an adequate means of study for complex patrimonial structure.

The nave macro-element of the Metropolitan Cathedral of Santiago was defined, validated and analyzed for many seismic intensities (fragility analysis) in the previous

chapter (Torres et al. 2017). The results obtained in this research show coherence with the current state of damage in the Cathedral. This model will therefore be used as a guide for matching with the proposed NLFM model based on bars.

This section is in regard to the RBSM model of nave macro-element: the model features, and the damage pattern of the structure loaded with a cyclic pushover.

4.2.1. Model Developed in RBSM (Rigid Body Spring Model).

The model generated for the nave macro-element in the RIGID program consists of 386 rigid quadrilateral elements, each of which has 3 DOF concentrated in its geometric center: a horizontal displacement, a vertical displacement, and a turn in the perpendicular direction to its plane (possible movements of a rigid plane body). The non-linear behavior of the model is based on two axial springs and one shear spring in each of the interfaces between the rigid elements. This behavior is based, respectively, on the constitutive axial and shear laws of the material making up the structure. The model can be seen in Figure 1.

One of the results that can be obtained from the RIGID program is the damage pattern occurring in the structure after the dynamic analysis has been carried out. This damage pattern shows the areas yielded in the model (Figure 2a).

4.2.2. Damage Pattern of RBSM Model.

As mentioned before, Figure 2a shows the damage pattern of nave macro-element based on cyclic pushover obtained from RBSM model. It can be noted the yielding in: the base of columns and the support zones of the arches. Based on these damaged zones and the zones without damage, the NLFM model will propose the location of the plastic hinges and rigid zones in the connection between bars, therefore, the rest of the model elements work only in the elastic range—this definition is established since the damage pattern defined in RIGID allows for it to be predicted that yielding will only occur in already-

established zones. It is important to note that the damage pattern is corresponding with the actual state of the structure, this can be seen on Figure 2b. In this figure, the cracks are located in the damage zone predicted by the model.

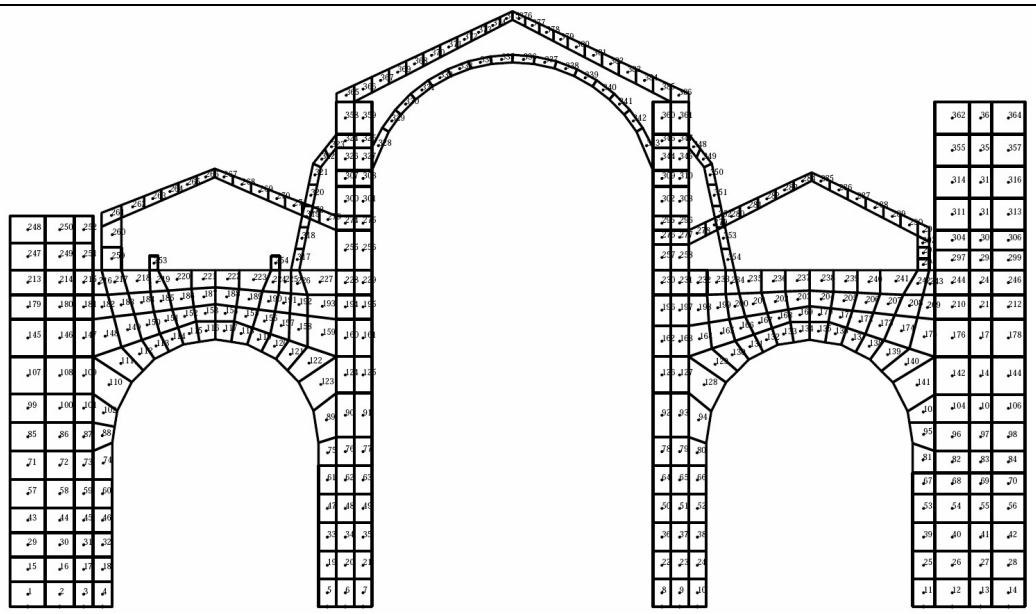

Figure 1. Macro-element model generated in RIGID software package. (Torres et al. 2017)

4.3. NONLINEAR FRAMED MODEL (NLFM) OF THE NAVE MACRO-ELEMENT

In this section, the methodology to built and validate the proposed Nonlinear Framed Model (NLFM) is presented in detail. This methodology has two steps. The first step is to propose an initial geometry based on interpreting the damage pattern obtained of the RBSM model (Figure 2a), i.e. recognizing the zones that remain essentially elastic without damage and the zones where the zones should be concentrated. The second step is the verification of the model by means of static and dynamic analyses.

a)

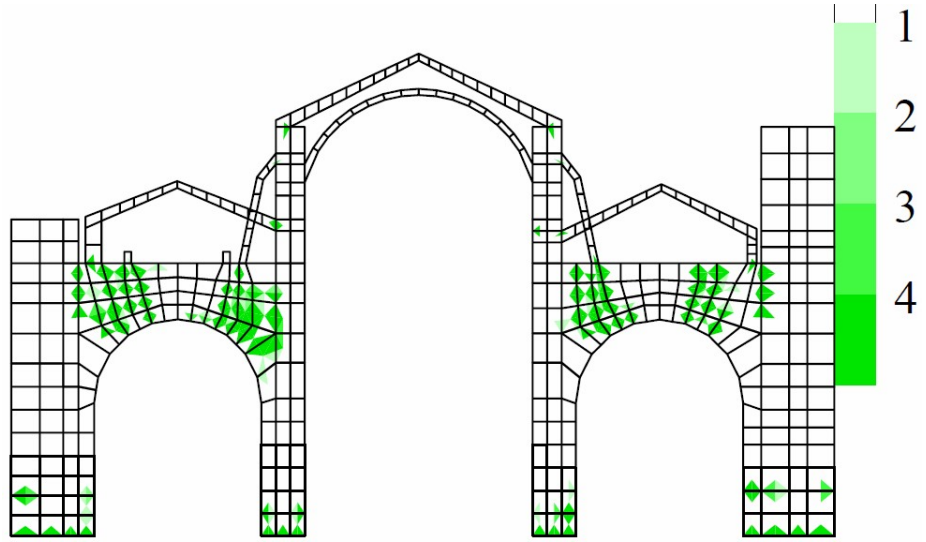

b)

Figure 2. Damage of the nave macro-element: a) Damage pattern of the nave macro-element for a cyclic pushover, obtained from RBSM model by means RIGID software (Torres et al. 2017), b) Actual damage encountered in the structure.

4.3.1. Geometry of the NLFM Model

Geometry (size and shape) play an important role in any structure, and further in heritage buildings. Various beam shape options were studied in the trial and error process. The last of these was the arch-shaped beam with rigid zones at the ends, length of potential hinges, and variable section height. This shape allows for the NLFM to have a geometry and bending behavior similar to the RBSM model.

The NLFM model generated by means of Opensees software (McKenna, 2014). Each of the bars for columns and beams in the arches is a *BeamwithHinges* element of Opensees software (Mazzoni et al., 2007). This element has a plastic hinge length at its ends (the length of yielding is defined by the user) and its intermediate zone remains elastic. Figure 3a shows the location of plastic hinges in the base of columns and portions of beams L1 and L2. The location of rigid zones should additionally be noted; i.e. the connection zone between piers and arches that are without damage, according to Figure 2. Aditionally, Figure 3b shows the distribution of all kind of masonry materials in the macro-element.

The cross sections of the NFLM elements correspond to the true dimensions of the structure, and based on this, the geometric properties for each of the elements were calculated. After several attempts to define the geometry of the arches in the structure, it was decided that straight sections of beams that define arch shape in the Cathedral's south and north naves would be used (Figure 3a). The section of the beams is not unique, as it changes based on the height of sections generated when defining a barycentric axis with respect to the top and bottom borders of the north and south arches (Figure 4). As previously mentioned, sections L1 and L2 are plastic hinge zones, and section C of the arch remains elastic in the analysis.

a)

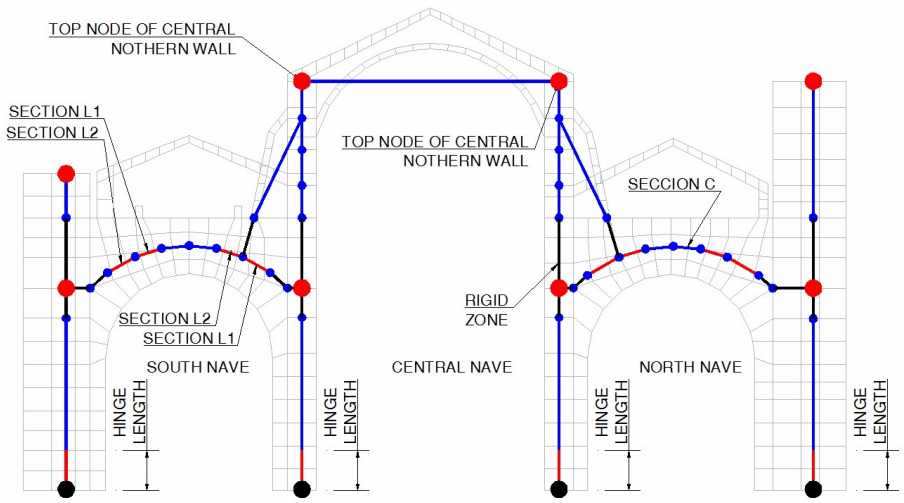

b)

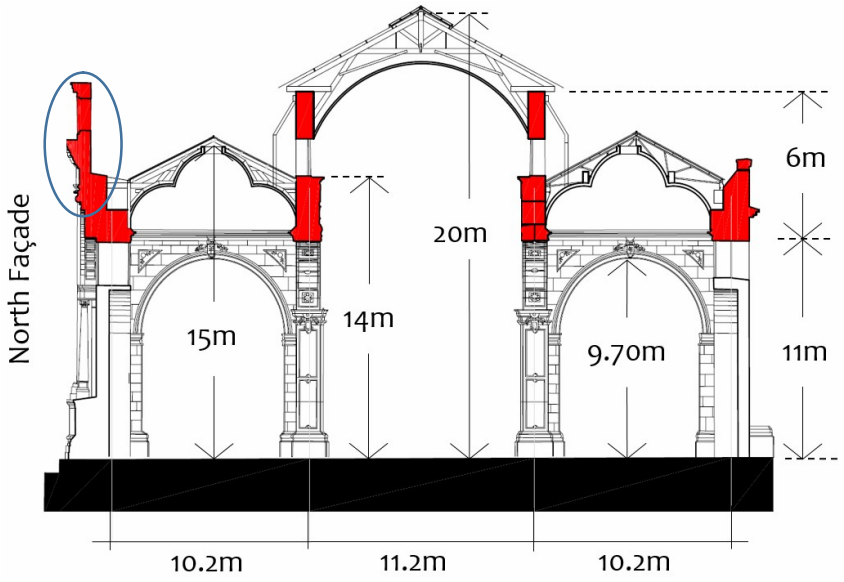

Figure 3. Opensees model of the nave macro-element: a) Location of hinges (red lines), rigid zones (black lines), zones that remains elastic (blue lines), structure nodes (blue filled circles), mass nodes (red filed circles), and fixed nodes (black filled circles), b) Materials that make up the nave macro-element: stone masonry at the base of structure, brickwork walls in red colour, and the highlighted top zone of north façade is made of reinforced brickwork, as was seen in the previous chapter (Torres et al. 2017).

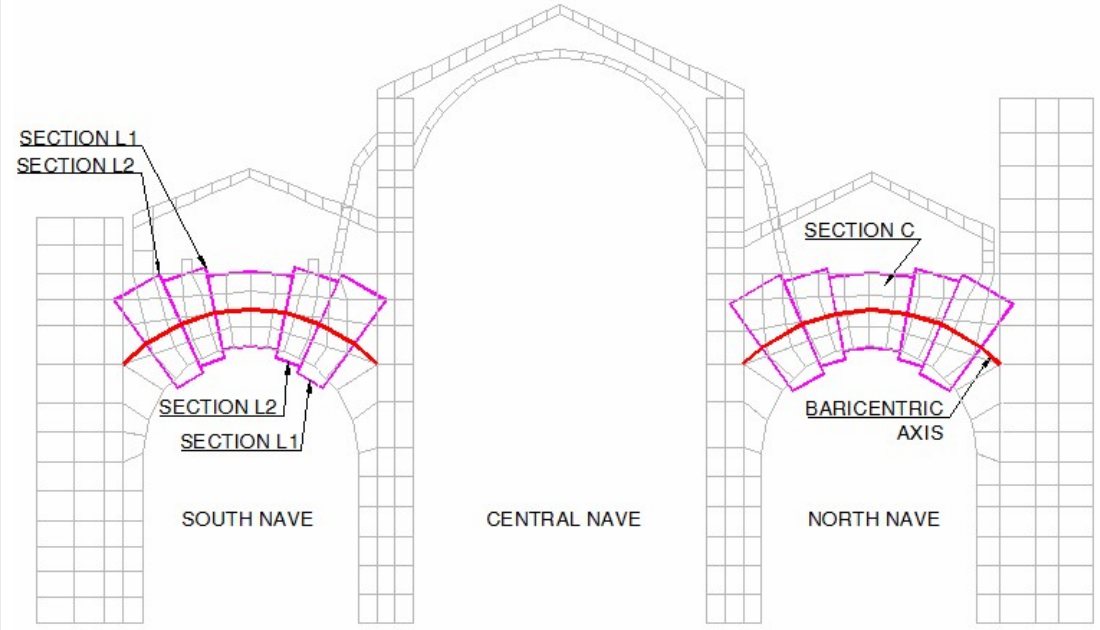

Figure 4. Variable sections of beams for the Cathedral's north and south arches.

The material used in Opensees software is *Concrete06* (Mazzoni et al., 2007) for the plastic hinge zones, since it is most similar to the constitutive axial law of RIGID software. This material has tensile strength, and its stiffness decreases both compression and tension when the material deteriorates. The behavior curve can be seen in Figure 5.

The equations that represent the axial constitutive law of *Concrete06* are:

$$\sigma_C = f_C' \frac{n\left(\frac{\varepsilon_C}{\varepsilon_0}\right)}{n-1+\left(\frac{\varepsilon_C}{\varepsilon_0}\right)^{nk}} \quad (1)$$

$$\sigma_C = \frac{f_T}{\varepsilon_T}\varepsilon_C \; ; if \; \varepsilon_T \leq \varepsilon_C < 0 \quad (2)$$

$$\sigma_C = f_T \left(\frac{\varepsilon_T}{\varepsilon_C}\right)^b \; ; if \; \varepsilon_C < \varepsilon_T \qquad (3)$$

Equation (1) is the calculated axial stress for the compression side; equation (2) is the calculated axial stress for the tension side from 0 to f_T; and equation (3) is the calculated axial stress for the tension side for stresses greater than f_T.

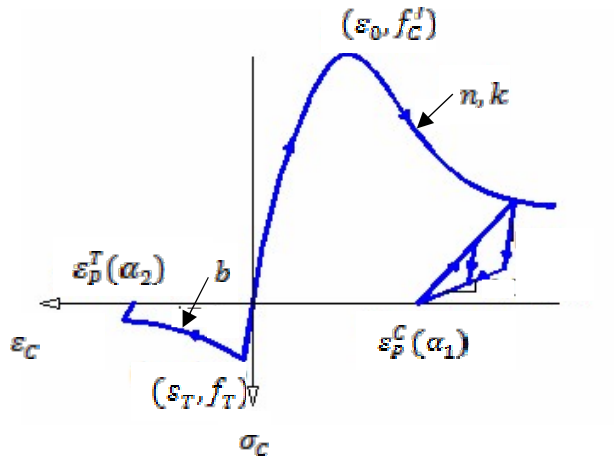

Figure 5. Axial constitutive law of the *Concrete06* material of Opensees software. Signs are negative for compression. (Masone, 2012).

In these expressions, σ_C is the calculated stress for each case of compression or tension; f'_C is the compressive strength; ε_C is the strain (independent variable in all constitutive law); ε_0 is the strain at compressive strength; n is the shape factor for the compression side of the curve; k is the post-peak compressive shape factor; f_T is the tensile strength; ε_T is the strain at tensile strength; b is the exponent in the tension side; ε_P^T is the tensile plastic strain; ε_P^C is the compressive plastic strain; α_1 is the parameter for compressive plastic strain definition; and α_2 is the parameter for tensile plastic strain definition. The values for α_1 and α_2 were defined as zero based on the shape of the behavior curve obtained in RIGID software.

Some research has been done on the coupling between axial and shear stress in masonry structures (Raka et al., 2015; Vanin et al., 2017). Since the damage registered in the structure is mainly due to tension yielding (Figure 2a), the axial constitutive law is most important. The influence of the shear stress on the structure, and its interaction with the axial stress within a frictional model, such as Mohr-Coulomb, has thus been neglected and left for future research.

4.3.2. Calibration Process of NLFM

An important factor to be taken into account in the comparison between the models is the difference between the lateral load pattern for the RBSM and the proposed NLFM. In the first model, lateral force is applied by low frequency acceleration in the base (quasi-static force), and thus the apparent force present is related to a distributed force over the entire length of the vertical elements. By the contrast, in the NFLM model the force is concentrated at certain nodes of the structure (Figure 3a). These nodes are points of mass concentration.

This difference was previously studied by Biggs (1964), who proposed an equivalent model for a single degree of freedom for a simple frame, and detected that certain equivalences could be established between the real model (with distributed mass) and that of a single degree of freedom (lumped mass). These equivalences are related to the concentrated amount of mass, lateral force at the beam level of the single frame, and additionally, the difference in reactions that should be expected between the real model and the equivalent single degree of freedom model. Other authors (Chopra, 2012; Clough & Penzien, 2003; Meirovitch, 2001) indirectly demonstrate this difference based on the Rayleigh quotient.

To exemplify this issue, a vertical bar model fully restricted at the bottom end and subject to a uniformly distributed load in its length was taken as basis. This model was

compared with the same bar, subject to a concentrated load of the free end node. If there is a condition in which the displacement in the free node is the same for both models, a relationship can be obtained between the reactions in the restricted node of the models (Figure 6). The adjustment factor between the two models is 8/3 = 2.67. Thus, if the first model should validate with respect to the second, based on the displacement of the free node, the force of the model with the concentrated load must be increased by this factor such that the two models are comparable. The displacement of the free node is taken as basis since it provides an idea of the element's deterioration within a non-linear analysis.

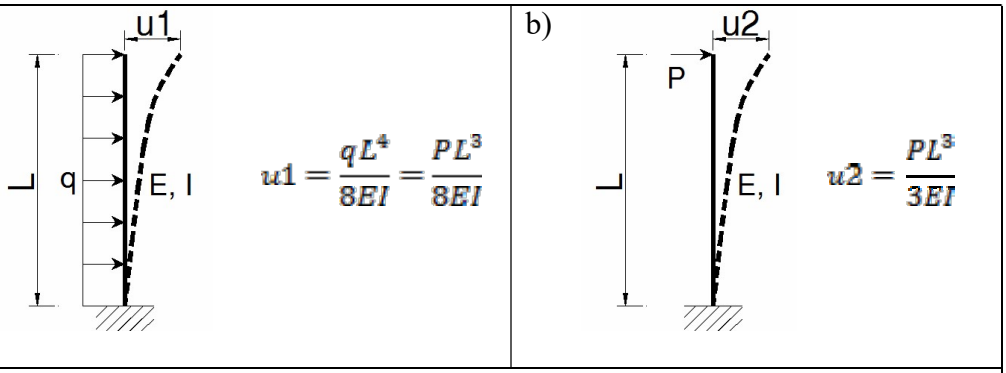

Figure 6. Comparison between models: a) Uniform distributed load on cantilever column, and b) Concentrated load on cantilever column.

Likewise, the RIGID model with distributed load should have an adjustment factor for comparison with the NLFM model. Unlike in the previous case, this factor is not easy to determine because there are many particularities in the macro-element model, such as the beam's stiffness compared with the stiffness of the piers, the non-uniform distribution of the load (based on mass distribution), etc. It is thus known that there is an adjustment factor, but its value cannot be easily determined.

To build the tandem of displacements that act in the pushover analysis for NLFM model, an elastic analysis of the macro-element was developed using the SAP2000 software package. The structure was loaded laterally by 10% of its weight, and the

equivalent forces and moments in the nodes were then obtained so as to reproduce the same lateral displacement at the column nodes (Figure 7).

The monotonic pushover analysis of the macro-element was generated based on the series of displacements of the control point obtained from the RIGID model of Torres et al. (2017). Two nodes were selected as control points: the top node of the southern center wall and the top node of the northern center wall (Figure 3a). The first control point is for the pushover from left to right, and the second for the pushover from right to left. These cases were analyzed as such because of the structure's non-symmetry.

4.3.3. Mass Distribution for Dynamic Loads.

Given that the process to calibrate static properties based on stiffness was developed in the previous section, it is now necessary to confirm that the dynamic behavior, fundamentally dependent on damping and mass, is similar between the two models. The critical damping ratio (for the Rayleigh case) assumed for this type of structures is 6% (Meli, 1998) based only on the structure's mass (Casolo & Pena, 2004). There is no problem in regard to this value because the two models have the same damping.

Considering that one of the proposed model's basic assumptions is to define lumped masses at the points of intersection with the rest of the possible transversal elements (for the case of three dimensional model in future research), the proposed mass distribution can be seen in Figure 3a. The mass of each vertical element is divided equally between its two extreme nodes; additionally, the mass of the arches is concentrated in the node that they reach in the columns. Based on this assumption of mass distribution, the first and second natural frequencies obtained from the NLFM model by means of the Opensees software were calculated and compared with those calculated from the RBSM model using the RIGID software (Table 1).

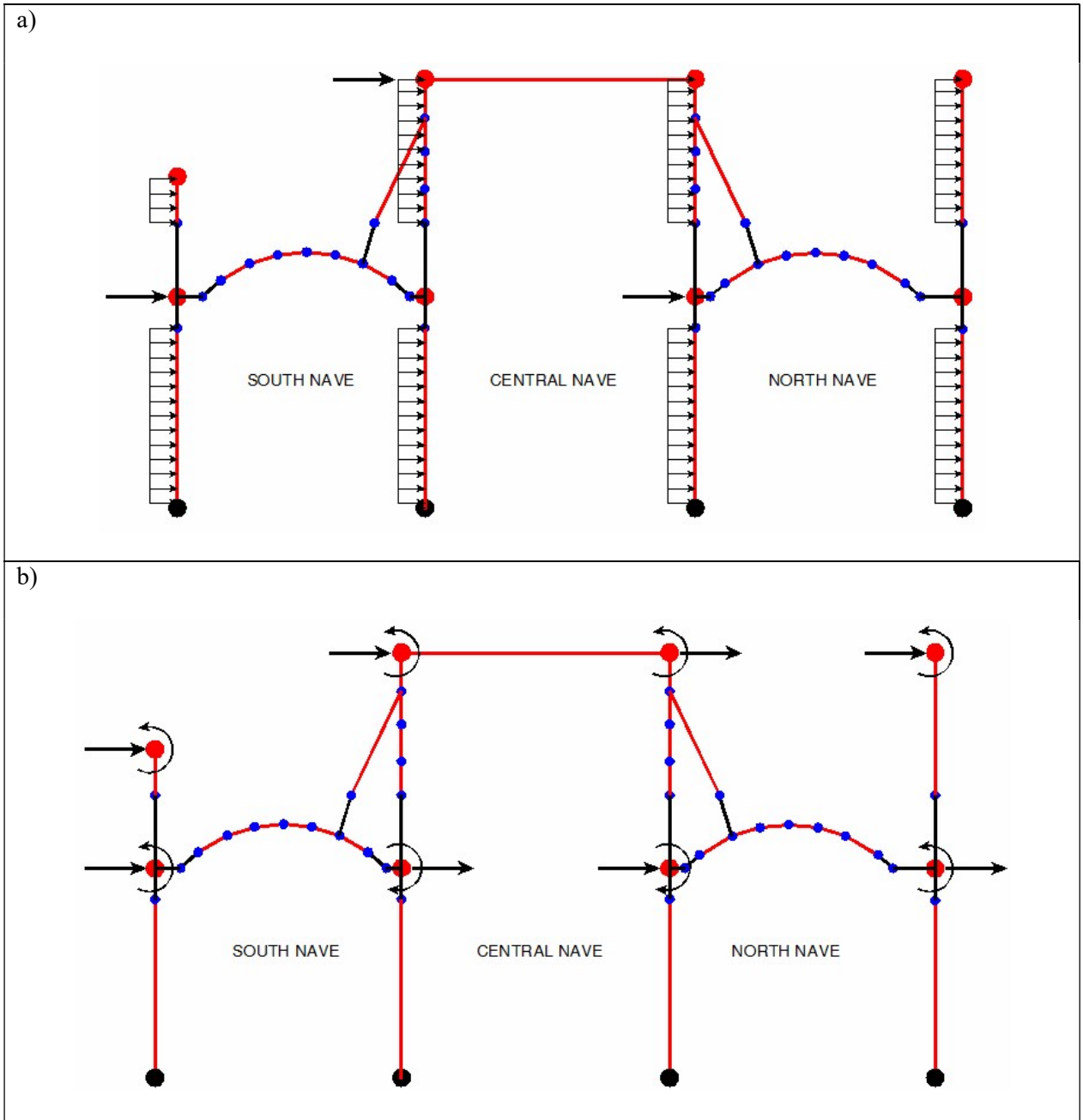

Figure 7. Elastic model in SAP2000 software: a) Macro-element model with load distributed over vertical elements and concentrated loads due to beam mass. b) Macro-element model with equivalent concentrated loads and moments to reproduce the same deformed configuration of the load described in a).

In this comparison it can be seen that there are differences between the frequencies of the models for the two modes; this is precisely due to the mass difference considered, since there is an amount of mass concentrated in the support nodes, which in reality does not occur.

Table 1. Comparison between the natural frequencies of the RBSM model and the NLFM model.

Mode	RIGID model frequency (Hz)	OpenSees model frequency (Hz)	Difference based on RIGID model frequency (%)
1	2.01	2.33	16%
2	2.14	2.38	11%

4.4. PERFORMANCE COMPARISON BETWEEN MODELS.

In this section, the analysis of results obtained previously with both models will be discussed. First, the static analysis based on the cyclic pushover to the RBSM model is compared with the monotonic pushover to the NLFM model. Second, a series of time history analyses for various seismic intensities is carried out, verifying the structural damage based on the change of stiffness index (Torres et al. 2017).

4.4.1. Analysis of Static Responses.

The static analysis of the two models was run, and the responses of the two models was compared. Figure 8 shows the response of each top node of the central walls.

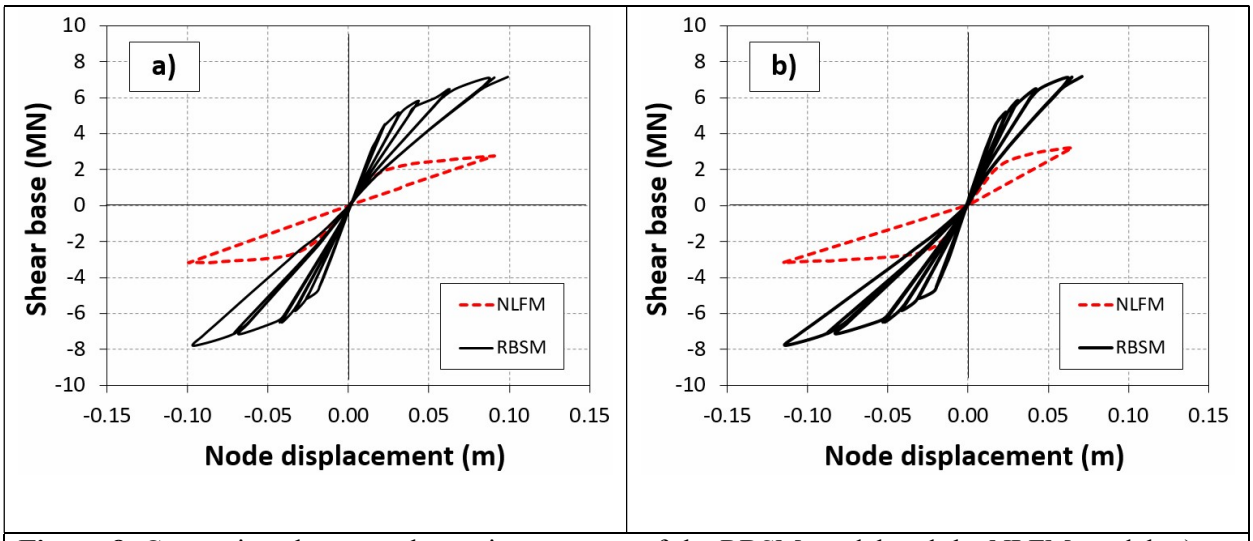

Figure 8. Comparison between the static responses of the RBSM model and the NLFM model: a) for the top node of the southern central wall, and b) for the top node of the northern central wall.

Because the analysis of the RBSM model corresponds with a cyclic pushover (pseudo-static analysis), and the analysis of NLFM model is a monotonic pushover, the response of the second model should be the envelope of the first. Therefore, if an adjustment factor is defined for the NLFM model to relate the two responses, it could be seen that the two models have a very close correspondence in shape and amplitude (Figure 9). The behavior and successive loss of stiffness can thus be shown to be logical between the two models. It should be noted that this adjustment factor ought to be validated in future analyses of other structural macro-elements.

4.4.2. Analysis of the Dynamic Responses.

For the dynamic verification, the fragility analysis carried out in the nave macro-element by means of the RIGID software in Torres et al. (2017) is taken as basis. In the aforementioned study, the measure of damage is the stiffness index, which is the relation between the change of the base shear and the change of the displacement of a control point of the structure. This stiffness index is also assumed as a measure of damage in this research.

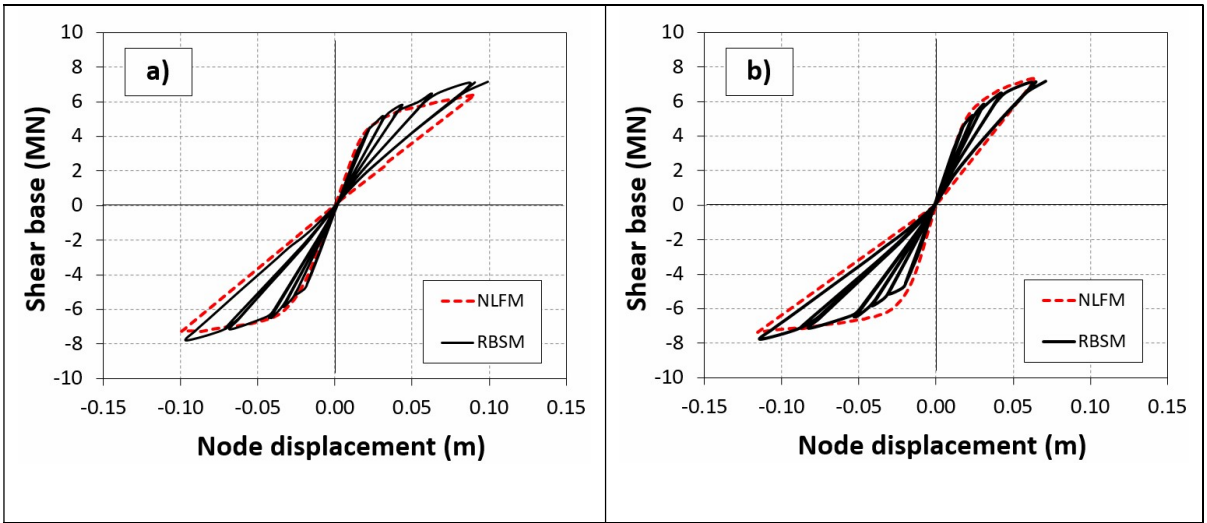

Figure 9. Comparison between the static responses of the RIGID model and bars model with adjustment factor: a) for the top node of the southern central wall, and b) for the top node of the northern central wall.

The model was tested based on 6 scaled seismic intensities (varying the exceedance probability of an event over a time period of 50 years) according to spectral matching methodology (Clough & Penzien, 2003), from a seed record of the 2010 Maule earthquake (Santiago Centro Station). The performance of both structure models can be seen in the graphs shown in Figure 10.

The Figure 10 graphs have two types of lines: the dashed line represents the evolution of a stiffness index processed by a mobile media with a window of 8 width values, and the continues line is an approximation of the segmented line based on the least square method. With the behavior graphs showing the loss of stiffness for each of the seismic intensities, it can be seen that the final results are very similar for the two models.

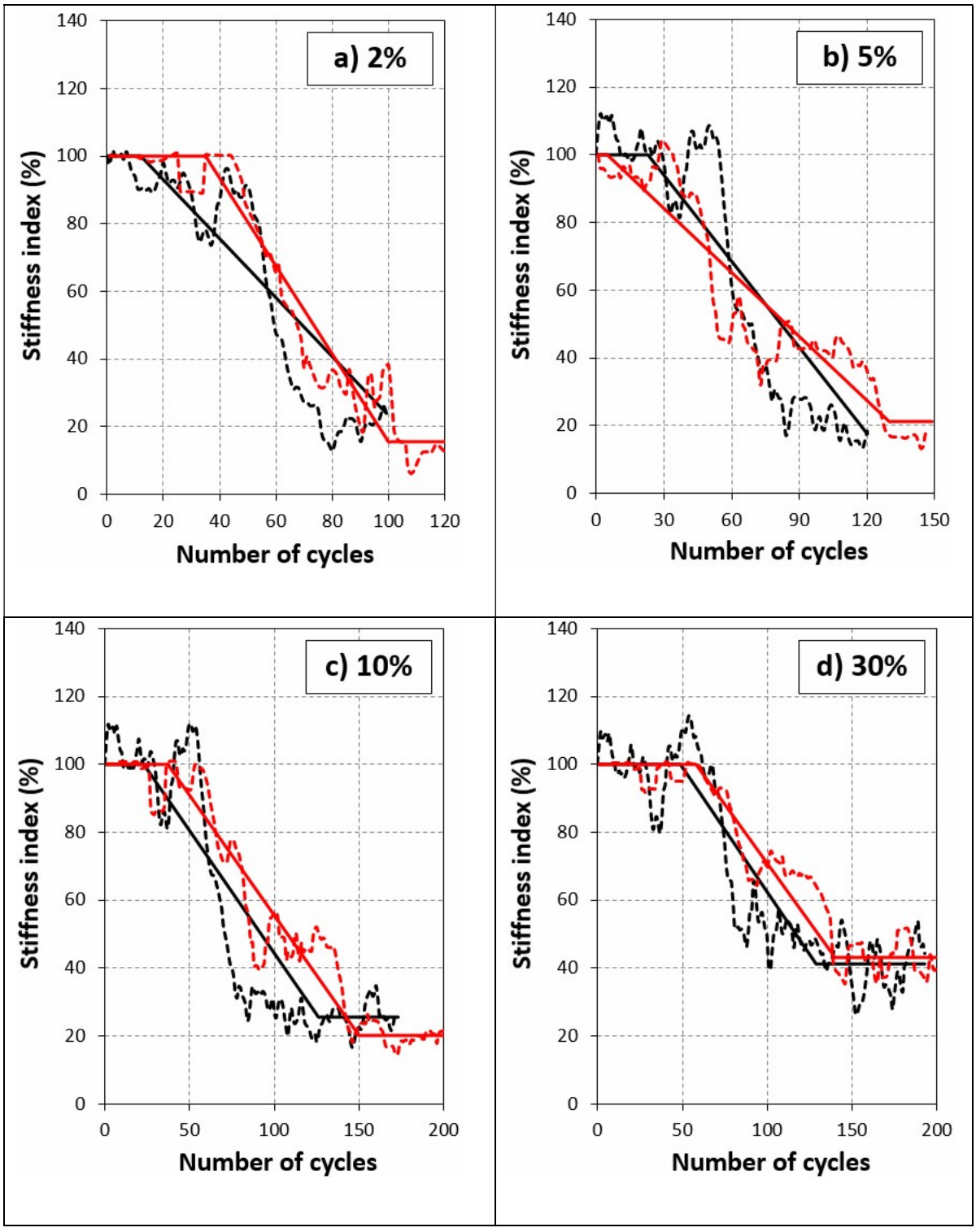
a) 2%
b) 5%
c) 10%
d) 30%
Stiffness index (%)
Number of cycles
0
20
40
60
80
100
120
140
30
50
90
150
200

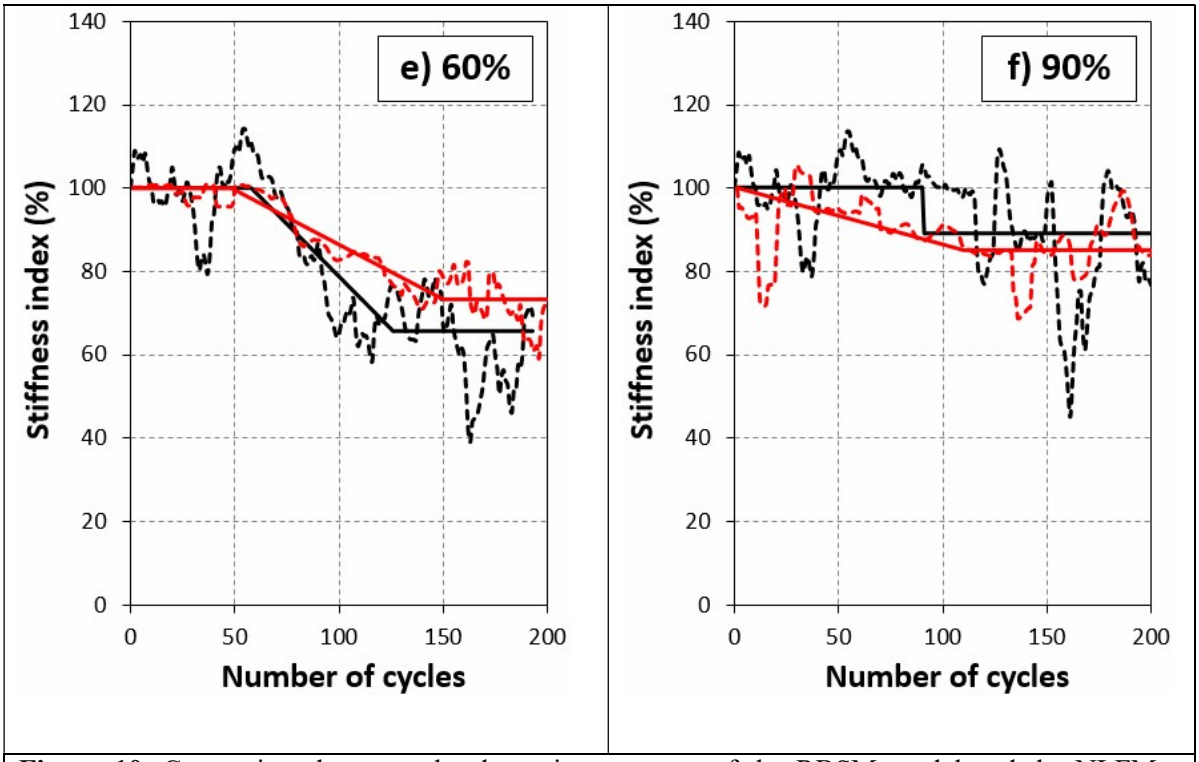

Figure 10. Comparison between the dynamic responses of the RBSM model and the NLFM model, for different seismic intensities based on exceedance probability in 50 years. In black the response obtained from RBSM model, and in red the response obtained from NLFM model.

5. CONCLUSIONS AND FUTURE RESEARCH.

This research presents the study of seismic behaviour of a part of the Cathedral of Santiago de Chile in three stages. The first stage consist in the structural system identification and the model updating of the church, based on these processes, the mechanical properties of different types of masonry that compose the Cathedral were estimated. Then, a methodology to establish the fragility curves of the nave macro-element of the Cathedral was presented. This macro-element is important because is the most repeated in the structure. The model of macro-element was developed with rigid elements based on RBSM methodology. The fragility analysis of macro-element is based on IDA and spectral matching methodologies. Finally, a simplified model, called Nonlinear Framed Model (NLFM), was developed to approximate the behavior of a resistant plane (nave macro-element) of the Cathedral, by means of axial-bending stressed bars and concentrated plasticity at the ends. The proposed model was validated by comparing it with the RBSM model, previously developed. All this process will aim to perform the fragility analysis of the complete model of the Cathedral or a tridimensional part of it. At the end of this research, the following conclusions can be drawn:

Related to the first stage – System Identification and Model Updating of the Cathedral:

1. The experimental campaign carried out through in-situ dynamic testing, allowed the estimation of the material properties of the structure. Additionally, OMA tests, with their non-invasive characteristics, allowed for the study of the structure without affectation and in service.
2. In the distance formulae for evaluating the similarity between experimental and analytical models, the term related to the modal shapes did not strongly change the analysed models; this is because the calibration parameters were only Young's modulus

of materials in the second stage; it probably would produce a better result if there were many more calibration parameters related to the structure support.

3. The determination range of the calibration parameters of any model depends on the weighting factors. The models show the presence of local minimum, as referenced in the graphs of the corresponding chapter, only when the weighting factors have certain values related (for example by means of MAC values) with the confidence of their determination.
4. The two stages of model updating produced similar results. The first stage obtains a single value for each calibration parameter, while the second allows to get ranges of values for each parameter. This latter can be more consistent with the structure's reality, because it is physically more logical to have a valid range for each calibration parameter, given the variability in structure properties. Additionally, in the second stage, the whole process is carried out based on logical steps given by the physics of the problem, while the first stage has a mathematical foundation that minimizes researcher judgment in solving the problem.
5. Although the results between stages are very close, it is important to note that the computational cost of the second stage is much greater; a practical decision would then be that the first stage is enough to get adequate results. However, although there is no greater difference between the results of these stages, there is a greater certainty in obtaining the results in the second stage because the interaction achieved by the user with the adjustment of the model is much greater.

Related to the second stage – Fragility Analysis of the nave macro-element of the Cathedral:

6. The state of damage predicted in the nave macro-element by pushover analyses is qualitatively consistent with the present state of damage of this portion of the Cathedral. Therefore, the RIGID model turned out to be a suitable approach to study the seismic response of the nave macro-element without excessive computational effort.

7. The use of the stiffness degradation index, defined as the change of the relation between the base shear and the displacement of a given control point, has proved to be a reliable damage index to carry out studies about fragility analysis of masonry structures. This behaviour was confirmed in this study by the natural frequencies of the first three modes of the macro-element. Therefore, it was found that the stiffness degradation index was the most appropriate way to assess the damage of the macro-element.
8. The results of the fragility analysis showed that only the record corresponding to the Santiago Centro station of the 2010 Maule earthquake had a high seismic load that affected the structure. The maximum acceleration of mentioned record was 2.11 m/s^2. The damage observed in the arches of the Cathedral after the 2010 earthquake coincides with the damage predicted by the RIGID model.
9. The results obtained also show that from a PGA value of 2.5 m/s^2 the state damage in the nave macro-element could be heavy. This is corresponding with the reality because all the near records used in this study have a maximum acceleration less than this value.

Related to the third stage – Equivalent Nonlinear framed model of the nave macroelement of the Cathedral:

10. The NLFM model requires a calibration process so that the results in the static analysis are similar to those obtained with a specialized tool for these structures (unreinforced masonry), such as the RIGID software. Verification with the time-history dynamic analysis then showed that the assumption of lumping mass is suitable. The potential of the generation of an equivalent model using software like Opensees lies in the versatility achieved in the analysis with a tool that allows for parallel processing of a structural model against different seismic intensities, and additionally, in the software's number of tools for non-linear analysis.
11. It should be noted that, despite having defined an adjustment factor for the static response of the NFLM model, this factor has no influence on the global dynamic response, and the behavior between the two models is similar. The only difference is based on the amount of mass not considered in the support nodes. This is because the stiffness index (simple rate between the change of base shear and the displacement of

the structure control point) separates the degradation behavior from the absolute value of the base shear which the model is capable of absorbing. The correspondence between the static and dynamic analysis shows that numerical yielding in the structure, as a signal of the deterioration, is similar and logically progressive between the RBSM model and the NLFM model.

12. The shape of the beams, i.e. the northern and southern arches in the nave macro-element, plays an important role in the analysis results. Various beam shape options were proposed in the process. The last of these was the arch-like beam with rigid zones at the ends, length of potential hinges, and variable section height. Other models had been tried at the beginning of this study: straight horizontal beams, and diagonal elements that could represent decomposition of the flexural moment into the two force components of tension and compression. The behavior of these failed attempts was not similar to the RBSM model, however, and the verification process allowed the suitable NLFM model to be achieved.
13. Validation of the NLFM model allows that the fragility analysis of the complete Cathedral can be discussed, in the future. If we start from the assumptions considered for generation of this model —concentration of mass only at points of intersection of macro-elements, resistance of the macro-elements only on their plane, and construction of the model by means of simple frame elements— then the evaluation of the seismic behavior of patrimonial structures with special architecture, such as churches, will be a feasible reality given adequate computational resources and processing times in order to obtain suitable results.

There are many ways to continue this research, the following proposals can be drawn:

1. In the first stage of System Identification process, the numerical model has been considered with all nodes rigidly joined; additionally, the experimental model, generated with the participation of all setups, has meant that global modes were used in the study of the structure. It is important to note that if the researcher wants to know the local modes, both the numerical and experimental model should be planned

accordingly. This is an opportunity for further study i.e. the model updating of the structure based on local modes.

2. In the NLFM model, the influence of the interaction between shear and axial load in the bottom areas of the structure is not addressed. The analysis carried out sought to define a simplified model that represents the behavior of the macro-element in its plane subjected to dynamic lateral loads through time-history analyses. In other words, the far-field seismic solicitation was the only source of loading for the model analyzed. Given that, the vertical component is more important in a near-field event, another pending issue that would provide continuity to this research is the study of the structure by means of the simplified NLFM model for this solicitation, taking into account the influence of the axial-shear interaction with the Mohr-Coulomb frictional model, as the RBSM model already treats it.
3. The basic assumptions in the formulation of NLFM model —the plane strength of the macro-element and the lumped mass in particular nodes, and the influence of only global modes in structural performance— apply only for the objective of analyzing the structure's global behavior. However, future research could study the performance of the proposed NLFM model, including out of plane behavior of macro-elements, distributed mass on elements, and the influence of local modes in the performance of each macro-element. A priori, there is no limitation regarding the use of the NLFM model with these features. This last assumption must be checked with the verification of additional macro-elements.

6. REFERENCES.

Abo-el-ezz, A., Nollet, M., & Nastev, M. (2013). Seismic fragility assessment of low-rise stone masonry buildings. *Earthquake Engineering and Engineering Vibration*, *12*(1), 87–97.

Addessi, D., Mastrandrea, A., & Sacco, E. (2014). An equilibrated macro-element for nonlinear analysis of masonry structures. *Engineering Structures*, *70*, 82–93. https://doi.org/10.1016/j.engstruct.2014.03.034

Aguilar, R., Marques, R., Sovero, K., Martel, C., Trujillano, F., & Boroschek, R. (2015). Investigations on the structural behaviour of archaeological heritagein Peru: From survey to seismic assessment. *Engineering Structures*, *95*, 94–111.

Aguirre, J., & Almazán, J. L. (2015). Damage potential reduction of optimally passive-controlled nonlinear structures. *Engineering Structures*, (89), 130–146.

Allemang, R. J., & Brown, D. L. (1982). A correlation coefficient for modal vector analysis. *First International Modal Analysis Conference*, 110–116.

Angelillo, M., Lourenco, P., & Milani, G. (2014). Masonry behaviour and modelling. In M. Angelillo (Ed.), *Mechanics of Masonry Structures* (First edit, pp. 1–26). International Centre for Mechanical Sciences.

Aras, F., Krstevska, L., Altay, G., & Tashkov, L. (2011). Experimental and numerical modal analyses of a historical masonry palace. *Construction and Building Materials*, *25*(1), 81–91. https://doi.org/10.1016/j.conbuildmat.2010.06.054

ASCE. (2010). *Minimum Design Loads for Buildings and Other Structures, ASCE/SEI 7-10*. Virginia.

Asteris, P. G., Chronopoulos, M. P., Chrysostomou, C. Z., Varum, H., Plevris, V., Kyriakides, N., & Silva, V. (2014). Seismic vulnerability assessment of historical masonry structural systems. *Engineering Structures*, *62–63*, 118–134. https://doi.org/10.1016/j.engstruct.2014.01.031

Augusti, G., Ciampoli, M., & Giovenale, P. (2001). Seismic vulnerability of monumental

buildings. *Structural Safety*, *23*(3), 253–274. https://doi.org/10.1016/S0167-4730(01)00018-2

Bayraktar, A., Altunişik, A. C., Sevim, B., Türker, T., Akköse, M., & Çoşkun, N. (2008). Modal Analysis, Experimental Validation, and Calibration of a Historical Masonry Minaret. *Journal of Testing and Evaluation*, *36*(6), 516–524. https://doi.org/10.1520/JTE101677

Belmouden, Y., & Lestuzzi, P. (2009). An equivalent frame model for seismic analysis of masonry and reinforced concrete buildings. *Construction and Building Materials*, *23*(1), 40–53. https://doi.org/10.1016/j.conbuildmat.2007.10.023

Biggs, J. (1964). *Introduction to Structural Dynamics* (1st ed.). Mc Graw Hill.

Binda, L., & Saisi, A. (2009). Knowledge of the building, on site investigation and connected problems. *Eurocode 8 Perspectives from the Italian Standpoint Workshop*, 213–224.

Brincker, R., Ventura, C. E., & Andersen, P. (2001). Damping Estimation by Frequency Domain Decomposition. In *19th International Seminar on Modal Analysis* (pp. 698–703).

Brincker, R., Zhang, L., & Andersen, P. (2000). Modal identification from ambient responses using Frequency Domain Decomposition. In *18th International Seminar on Modal Analysis*.

Cabboi, A., Magalhães, F., Gentile, C., & Cunha, Á. (2013). Automatic Operational Modal Analysis: Challenges and Practical Application to a Historical Bridge. *ECCOMAS Conference on Smart Structures and Materials*, (June), 24–26.

Carpinteri, A., Invernizzi, S., & Lacidogna, G. (2005). In situ damage assessment and nonlinear modelling of a historical masonry tower. *Engineering Structures*, *27*(3), 387–395. https://doi.org/10.1016/j.engstruct.2004.11.001

Casarin, F. (2006). *Structural Assessment and Seismic Vulnerability Analysis of a Complex Historical Building (Ph.D Thesis)*. University of Trento.

Caselles, J. O., Clapes, J., & Roca, P. (2011). Approach to Seismic Behavior of Mallorca Cathedral. In *15th World Conference on Earthquake Engineering*. Lisbon.

Caselles, O., Martínez, G., Clapes, J., Roca, P., & Pérez, M. (2013). Application of Particle

Motion Technique to Structural Modal Identification of Heritage Buildings. *International Journal of Architectural Heritage*, (9), 310–323. https://doi.org/10.1080/15583058.2013.784824

Casolo, S. (2004). Modelling in-plane micro-structure of masonry walls by rigid elements. *International Journal of Solids and Structures*, *41*(13), 3625–3641. https://doi.org/10.1016/j.ijsolstr.2004.02.002

Casolo, S. (2009). Macroscale modelling of microstructure damage evolution by a Rigid Body and Spring Model. *Journal of Mechanics of Materials and Structures*, *4*(3), 551–570.

Casolo, S., Milani, G., Uva, G., & Alessandri, C. (2013). Comparative seismic vulnerability analysis on ten masonry towers in the coastal Po Valley in Italy. *Engineering Structures*, *49*, 465–490. https://doi.org/10.1016/j.engstruct.2012.11.033

Casolo, S., & Pena, F. (2004). A Specific Rigid Element Approach for In-plane. *III Congreso Internacional Sobre Métodos Numéricos En Ingeniería Y Ciencias Aplicadas*.

Casolo, S., & Peña, F. (2007). Rigid element model for in-plane dynamics of masonry walls considering hysteretic behaviour and damage. *Earthquake Engineering and Structural Dynamics*, *36*, 1029–1048. https://doi.org/10.1002/eqe

Casolo, S., & Sanjust, C. A. (2009). Seismic analysis and strengthening design of a masonry monument by a rigid body spring model: The “Maniace Castle” of Syracuse. *Engineering Structures*, *31*(7), 1447–1459. https://doi.org/10.1016/j.engstruct.2009.02.030

Cattari, S., & Lagomarsino, S. (2014). Performance-Based Approach for the Seismic Assessment of Masonry Historical Buildings. *Second European Conference on Earthquake Engineering and Seismology*.

Chen, S. Y., Moon, F. L., & Yi, T. (2008). A macroelement for the nonlinear analysis of in-plane unreinforced masonry piers. *Engineering Structures*, *30*(8), 2242–2252. https://doi.org/10.1016/j.engstruct.2007.12.001

Chopra, A. (2012). *Dynamics of Structures Theory and Applications to Earthquake Engineering*. (Pearson Education, Ed.) (Fourth). Boston.

CIMNE. (2014). GiD. Retrieved from ftp://www.gidhome.com/pub/GiD_Documentation/Docs/GiD_Reference_Manual.pdf

Clementi, F., Gazzani, V., Poiani, M., & Lenci, S. (2016). Assessment of seismic behaviour of heritage masonry buildings using numerical modelling. *Journal of Building Engineering*, *8*(September), 29–47. https://doi.org/10.1016/j.jobe.2016.09.005

Clough, R., & Penzien, J. (2003). *Dynamics of Structures* (3rd editio). California: Computers & Structures, Inc.

Colombo, J., & Almazán, J. L. (2015). Seismic reliability of continuously supported steel wine storage tanks retrofitted with energy dissipation devices. *Engineering Structures*, *98*, 201–211.

Computers and Structures, I. (2009). SAP2000. California.

Computers and Structures, I. (2016). PERFORM-3D. California.

D'Ayala, D., & Benzoni, G. (2012). Historic and traditional structures during the 2010 Chile earthquake: Observations, codes, and conservation strategies. *Earthquake Spectra*, *28*(SUPPL.1), 425–451. https://doi.org/10.1193/1.4000030

Da Porto, F., Silva, B., Costa, C., & Modena, C. (2012). Macro-scale analysis of damage to churches after earthquake in Abruzzo (Italy) on April 6, 2009. *Journal of Earthquake Engineering*, *16*(6), 739–758. https://doi.org/10.1080/13632469.2012.685207

De Stefano, A., & Ceravolo, R. (2007). Assessing the Health State of Ancient Structures: The Role of Vibrational Tests. *Journal of Intelligent Material Systems and Structures*, *18*(8), 793–807. https://doi.org/10.1177/1045389X06074610

Diaferio, M., & Foti, D. (2017). Seismic risk assessment of Trani's Cathedral bell tower in Apulia, Italy. *International Journal of Advanced Structural Engineering*, *9*(3), 259–267. https://doi.org/10.1007/s40091-017-0162-0

Doebling, S., Farrar, C., & Prime, M. (1998). A Summary Review of Vibration-based Damage Identification Methods. *The Shock and Vibration Digest*, *30*, 91–105.

Doglioni, F., Moretti, A., & Petrini, V. (1994). Le chiese e il terremoto. In *Le chiese e il terremoto* (C.N.R. Edi). Trieste, Italy.

Douglas, B., & Reid, W. (1982). Dynamic Test and System Identification of Bridges.

Journal of the Structural Division, *108*, 2295–2312.

Elyamani, A., Caselles, O., Roca, P., & Clapes, J. (2016). Dynamic investigation of a large historical cathedral. *Structural Control and Helth Monitoring*. https://doi.org/10.1002/stc

Ewins, D. (2000). *MODAL TESTING theory, practice and application*. (John Wiley & Sons Ltd., Ed.) (Second edi). Research Studies Press Ltd.

Feenstrat, P., & De Borsts, R. (1996). A Composite Plasticity Model for Concrete. *International Journal of Solids and Structures*, *33*(5), 707–730.

Fischer, T., Alvarez, M., De la Llera, J. C., & Riddell, R. (2002). An integrated model for earthquake risk assessment of buildings. *Engineering Structures*, *24*, 979–998.

Foti, D., Diaferio, M., Giannoccaro, N. I., & Mongelli, M. (2012). Ambient vibration testing, dynamic identification and model updating of a historic tower. *NDT & E International*, *47*, 88–95. https://doi.org/10.1016/j.ndteint.2011.11.009

Friswell, M., & Mottershead, J. (1995). *Finite Element Model Updating in Structural Dynamics*. (G.M.L. GLADWELL, Ed.) (First edit). Springer-Science+Business Media, B.V.

García, N., & Meli, R. (2009). On Structural Bases for Building the Mexican Convent Churches From the Sixteenth Century. *International Journal of Architectural Heritage*, *3*, 24–51. Retrieved from http://www.tandfonline.com/doi/abs/10.1080/15583050701842344

Gentile, C., Saisi, A., & Cabboi, A. (2015). Structural Identification of a Masonry Tower Based on Operational Modal Analysis. *International Journal of Architectural Heritage*, *9*(2), 98–110. https://doi.org/10.1080/15583058.2014.951792

Gentile, C., & Saisi, a. (2007). Ambient vibration testing of historic masonry towers for structural identification and damage assessment. *Construction and Building Materials*, *21*(6), 1311–1321. https://doi.org/10.1016/j.conbuildmat.2006.01.007

Goodman, R. (1989). *Introduction to Rock Mechanics*. (John Wiley & Sons, Ed.) (Second edi).

Goursat, M., Dohler, M., Mevel, L., & Andersen, P. (2010). Crystal Clear SSI for

Operational Modal Analysis of Aerospace Vehicles. In *Proceedings of the 28th International Modal Analysis Conference (IMAC)*. Jacksonville, Florida.

Grünthal, G. (2009). Escala Macrosísmica Europea 1998. Luxemburgo: Comisión Sismológica Europea.

Haselton, C., Fry, A., Baker, J., Hamburger, R., Whittaker, A., Stewart, J., … Pekelnicky, R. (2014). Response-history analysis for the design of new buildings: A fully revised Chapter 16 methodology proposed for the 2015 NEHRP provisions and the ASCE/SEI 7-16 standar. In F. of E. Engineering (Ed.), *National Conference on Earthquake Engineering*. Alaska.

IDIEM, & Facultad de Ciencias Físicas y Matemáticas Universidad de Chile. (2011). *Estudio de ingeniería estructural edificio catedral metropolitana*. Santiago de Chile.

Ingeniería Civil - Facultad de Ciencias Físicas y Matemáticas Universidad de Chile. (2010). Red de cobertura de acelerógrafos. Retrieved from http://www.renadic.cl/

Instituto Nacional de Normalización INN - Chile. (2009). NCh 433. Of1996 Modificada en 2009, Diseño Sísmico de. Edificios.

Irizarry, J., Podestá, S., & Resemini, S. (2003). Curvas de Capacidad para Edificios Monumentales: La Iglesia de Santa María del Mar de Barcelona. In A. E. de I. Sísmica (Ed.), *2do Congreso Nacional de Ingeniería Sísmica* (pp. 541–555). Málaga.

ISCARSAH (International Scientific Committee for Analysis and Restoration of Structures of Architectural Heritage). (2003). *Recommendations for the analysis, conservation and structural restoration of Architectural Heritage*. *ICOMOS.*

Italian Code for Constructions NTC08. (2008). Norme tecniche per le costruzioni (NTC 2008) - Decreto 14 gennaio 2008.

Jorquera, N., Misseri, G., Palazzi, N., Rovero, L., & Tonietti, U. (2017). Structural Characterization and Seismic Performance of San Francisco Church, the Most Ancient Monument in Santiago, Chile. *International Journal of Architectural Heritage*. https://doi.org/10.1080/15583058.2017.1315620

Kim, G.-H., & Park, Y.-S. (2004). An improved updating parameter selection method and finite element model update using multiobjective optimisation technique. *Mechanical*

Systems and Signal Processing, *18*(1), 59–78. https://doi.org/10.1016/S0888-3270(03)00042-6

Lagomarsino, S. (2006). On the vulnerability assessment of monumental buildings. *Bulletin of Earthquake Engineering*, *4*(4), 445–463. https://doi.org/10.1007/s10518-006-9025-y

Lagomarsino, S., & Cattari, S. (2015). PERPETUATE guidelines for seismic performance-based assessment of cultural heritage masonry structures. *Bulletin of Earthquake Engineering*, (13), 13–47.

Lagomarsino, S., & Giovinazzi, S. (2006). Macroseismic and mechanical models for the vulnerability and damage assesment of current buildings. *Bulletin of Earthquake Engineering*, (4), 415–443.

Lagomarsino, S., Penna, A., Galasco, A., & Cattari, S. (2013). TREMURI program: An equivalent frame model for the nonlinear seismic analysis of masonry buildings. *Engineering Structures*, *56*, 1787–1799.

Lagomarsino, S., & Podesta`, S. (2004). Seismic Vulnerability of Ancient Churches: II. Statistical Analysis of Surveyed Data and Methods for Risk Analysis. *Earthquake Spectra*, *20*(2), 395–412. https://doi.org/10.1193/1.1737736

Leyton, F., Ruiz, S., & Sepúlveda, S. (2010). Reevaluación del peligro sísmico probabilístico en Chile central. *Andean Geology*, *37*(2), 455–472.

Lorenzoni, F., Casarin, F., Modena, C., Caldon, M., Islami, K., & da Porto, F. (2013). Structural health monitoring of the Roman Arena of Verona, Italy. *Journal of Civil Structural Health Monitoring*, *3*(4), 227–246. https://doi.org/10.1007/s13349-013-0065-0

Lourenço, P. (1996). *Computational strategies for masonry structures*. Universidade do Porto.

Lourenço, P. B., Krakowiak, K. J., Fernandes, F. M., & Ramos, L. F. (2007). Failure analysis of Monastery of Jerónimos, Lisbon: How to learn from sophisticated numerical models. *Engineering Failure Analysis*, *14*(2), 280–300. https://doi.org/10.1016/j.engfailanal.2006.02.002

Lourenço, P. B., Trujillo, A., Mendes, N., & Ramos, L. F. (2012). Seismic performance of

the St. George of the Latins church: Lessons learned from studying masonry ruins. *Engineering Structures*, *40*, 501–518. https://doi.org/10.1016/j.engstruct.2012.03.003

Magenes, G. (2000). A Method for Pushover Analysis in Seismic Assessment of Masonry Buildings. *12th World Conference on Earthquake Engineering*, 1–8.

Magenes, G., & Della Fontana, A. (1998). Simplified Non-linear Seismic Analysis of Masonry Buildings. *5th International Masonry Conference*, (January 1998), 190–195. https://doi.org/10.6092/UNINA/FEDOA/8417

Mallardo, V., Malvezzi, R., Milani, E., & Milani, G. (2008). Seismic vulnerability of historical masonry buildings: A case study in Ferrara. *Engineering Structures*, *30*(8), 2223–2241. https://doi.org/10.1016/j.engstruct.2007.11.006

Mandal, T. K., Ghosh, S., & Pujari, N. N. (2016). Seismic fragility analysis of a typical Indian PHWR containment: Comparison of fragility models. *Structural Safety*, *58*, 11–19. https://doi.org/10.1016/j.strusafe.2015.08.003

Mandal, T., Pujari, N., & Sidhhartha, G. (2013). A comparative study of seismic fragility estimates using different numerical methods. In M. Papadrakakis, N. Lagaros, & V. Plevris (Eds.), *Computational Methods in Structural Dynamics and Earthquake Engineering*. Kos Island.

Masciotta, M., Roque, J., Ramos, L., & Lourenço, P. (2016). A multidisciplinary approach to assess the health state of heritage structures: The case study of the Church of Monastery of Jerónimos in Lisbon. *Construction and Building Materials*, *116*, 169–187. https://doi.org/10.1016/j.conbuildmat.2016.04.146

Masjedian, M., & Keshmiri, M. (2009). A Review on Operational Modal Analysis Researches : Classification of Methods and Applications. In *IOMAC'09 - 3rd International Operational Modal Analysis Conference* (pp. 707–716).

Masone, L. (2012). OpenSeesWiki. Retrieved from http://opensees.berkeley.edu/wiki/index.php/Concrete06_Material

Mathworks. (2015). MATLAB.

Mazzoni, S., McKenna, F., Scott, M. H., & Fenves, G. L. (2007). OpenSees command language manual. University of California. Retrieved from

http://opensees.berkeley.edu/OpenSees/manuals/usermanual/OpenSeesCommandLanguageManual.pdf

McKenna, F. (2014). OpenSees. Retrieved from http://opensees.berkeley.edu/OpenSees/user/download.php

Meirovitch, L. (2001). *Fundamentals of vibrations*. (Mc Graw Hill, Ed.) (1st ed.). Singapore.

Meli, R. (1998). *Ingeniería Estructural de los Edificios Historicos*. (Fundación ICA. A.C., Ed.) (Primra edi). México D.F.

MICROMED. (2012). User's manual.

Negulescu, C., Ulrich, T., Baills, A., & Seyedi, D. (2014). Fragility curves for masonry structures submitted to permanent ground displacements and earthquakes. *Natural Hazards*, (74), 1461–1474.

Niedbal, N. (1984). ANALYTICAL DETERMINATION OF REAL NORMAL MODES FROM MEASURED COMPLEX RESPONSES. Paper presented at the Collection of Technical Papers - AIAA/ASME/ASCE/AHS/ASC Structures, Structural Dynamics and Materials Conference, (pt 2) 292-295. Retrieved from www.scop. *Collection of Technical Papers - AIAA/ASME/ASCE/AHS 25th Structures, Structural Dynamics & Materials Conference and AIAA Dynamics Specialists Conference*, (2), 292–295.

Oliveira, C. (2003). Seismic Vulnerability of Historical Constructions : A Contribution. *Bulletin of Earthquake Engineering*, *1*, 37–82.

Oliveira, D. (2002). *Experimental and numerical analysis of blocky masonry structures under cyclic loading análise experimental e numérica de estruturas de alvenaria de blocos sob acções cíclicas*. Universidade do Minho.

Page, A. (1978). Finite element model for brick masonry. *Journal of Structural Division ASCE*, *104*, 1267–1285.

Peña, F., & Casolo, S. (2012). RIGID - Programa de Elementos Rígidos para el Análisis dinámico no lineal de Estructuras de Mampostería - Manual de Usuario. México D.F.: Instituto de Ingeniería de la UNAM.

Peña, F., & García, N. (2016). Numerical evaluation of the seismic behavior of façades of Mexican colonial churches. *Engineering Failure Analysis*, *62*(February), 164–177.

https://doi.org/10.1016/j.engfailanal.2016.01.011

Peña, F., Lourenço, P. B., Mendes, N., & Oliveira, D. V. (2010). Numerical models for the seismic assessment of an old masonry tower. *Engineering Structures*, *32*(5), 1466–1478. https://doi.org/10.1016/j.engstruct.2010.01.027

Pérez, F., Beas, M., Leonard, D., Muzio, F., Pardo, J., & Prado, F. (2009). *El interior de la Catedral: antecedentes histórico morfológicos y bases para su conservación*. Santiago de Chile.

Petrini, V., Casolo, S., & Doglioni, F. (1999). Models for vulnerability analysis of monuments and strengthening criteria. In *Proceedings of the Eleventh European Conference on Earthquake Engineering* (pp. 179–198).

Porter, K., Kennedy, R., & Bachman, R. (2007). Creating Fragility Functions for Performance-Based Earthquake Engineering. *Earthquake Spectra*, *23*(2), 471–489. https://doi.org/10.1193/1.2720892

Prado, C., & Barrientos, M. (2011). Aporte de la arqueología al estudio urbano de la ciudad de Santiago de Chile. El caso de "la manzana de la catedral." *Canto Rodado*, *6*, 1–32.

Raka, E., Spacone, E., Sepe, V., & Camata, G. (2015). Advanced frame element for seismic analysis of masonry structures: model formulation and validation. *Earthquake Engineering & Structural Dynamics*, *44*, 2489–2506.

Ramos, L., Aguilar, R., Lourenço, P., & Moreira, S. (2013). Dynamic structural health monitoring of Saint Torcato church. *Mechanical Systems and Signal Processing*, *35*(1–2), 1–15. https://doi.org/10.1016/j.ymssp.2012.09.007

Ramos, L. F., Marques, L., Lourenço, P. B., De Roeck, G., Campos-Costa, a., & Roque, J. (2010). Monitoring historical masonry structures with operational modal analysis: Two case studies. *Mechanical Systems and Signal Processing*, *24*(5), 1291–1305. https://doi.org/10.1016/j.ymssp.2010.01.011

Razzaghi, M. S., & Javidnia, M. (2015). Evaluation of the effect of infill walls on seismic performance of RC dual frames. *International Journal of Advanced Structural Engineering*, *7*(1), 49–54. https://doi.org/10.1007/s40091-015-0081-x

Rendel, M., Lüders, C., Greer, M., Vial, I., & Westenenk, B. (2014). Retrofit, using seismic

isolation, of the heavily damaged Basílica del Salvador in Santiago, Chile. *New Zealand Society for Earthquake Engineering Inc.*

Roca, P., Cervera, M., Gariup, G., & Pela', L. (2010). Structural analysis of masonry historical constructions. Classical and advanced approaches. *Archives of Computational Methods in Engineering*, *17*(3), 299–325. https://doi.org/10.1007/s11831-010-9046-1

Roca, P., Cervera, M., Pelà, L., Clemente, R., & Chiumenti, M. (2013). Continuum FE models for the analysis of Mallorca Cathedral. *Engineering Structures*, *46*, 653–670. https://doi.org/10.1016/j.engstruct.2012.08.005

Roca, P., Molins, C., & Marí, A. R. (2005). Strength Capacity of Masonry Wall Structures by the Equivalent Frame Method. *Journal of Structural Engineering*, (October), 1601–1610.

Rodriguez, J. (2004). *Identificacao Modal Estocástica, Métodos de Análise e Aplicacoes em Estruturas de Engenharia Civil*. University of Porto.

Rota, M., Penna, a., & Magenes, G. (2010). A methodology for deriving analytical fragility curves for masonry buildings based on stochastic nonlinear analyses. *Engineering Structures*, *32*(5), 1312–1323. https://doi.org/10.1016/j.engstruct.2010.01.009

Sandoval, C., Valledor, R., & Lopez-Garcia, D. (2017). Numerical assessment of accumulated seismic damage in a historic masonry building. A case study. *International Journal of Architectural Heritage*, *3058*(September), 15583058.2017.1356945. https://doi.org/10.1080/15583058.2017.1356945

Simoes, A., Milosevic, J., Meireles, H., Bento, R., Cattari, S., & Lagomarsino, S. (2015). Fragility curves for old masonry building types in Lisbon. *Bulletin of Earthquake Engineering*, (13), 3083–3105.

Structural Vibration Solutions A / S. (2015). ARTeMIS.

Takeda, T., Sozen, M., & Nielson, N. (1970). Reinforced Concrete response to simulate earthquakes. *Journal of the Structural DivisionStructural Divi*, *96*(12), 2257–2573.

TNO DIANA. (2015). DIANA finite element analysis. Delft.

Tomazevic, M. (1999). *Earthquake-resistant design of masonry buildings* (First). London: Imperial College Press.

Torres, W., Almazán, J. L., Sandoval, C., & Boroschek, R. (2016). Determination of modal properties and FE model updating of the Metropolitan Cathedral of Santiago de Chile. *SAHC (Structural Analysis of Historical Constructions)*, 804–811.

Torres, W., Almazán, J. L., Sandoval, C., & Boroschek, R. (2017). Operational modal analysis and FE model updating of the Metropolitan Cathedral of Santiago , Chile. *Engineering Structures*, *143*, 169–188.

Torres, W., Almazán, J. L., Sandoval, C., & Peña, F. (2017). Fragility analysis of the nave macro-element of the Cathedral of Santiago, Chile. *Bulletin of Earthquake Engineering*, 1–26. https://doi.org/10.1007/s10518-017-0292-6

University of California Santa Barbara. (2012). Strong-Motion virtual data center (VDC). Retrieved from http://www.strongmotioncenter.org/vdc/scripts/about.plx

Valenzuela, G. (1978). *Suelo de Fundacion del Gran Santiago*.

Valledor, R., López-García, D., & Sandoval, C. (2015). Linearly elastic seismic evaluation of masonry historical buildings in Santiago , Chile : The case of the Pereira Palace. In *3rd International Conference on Mechanical Models in Structural Engineering*.

Vamvatsikos, D., & Cornell, C. A. (2002). Incremental dynamic analysis. *Earthquake Engineering & Structural Dynamics*, (31), 491–514. https://doi.org/10.1002/eqe.141

Van Overschee, P., & De Moor, B. (1996). *Subspace Identification for Linear Systems. Theory - Implementation - Applications*. (K. U. Leuven, Ed.) (First). Leuven: Kluwer Academic Publishers.

Vanin, F., Almeida, J. P., & Beyer, K. (2017). Force-Based Finite Element for Modelling the Cyclic Behaviour of Unreinforced Masonry Piers. In *16th World Conference on Earthquake Engineering, Santiago Chile*.

Vargas, Y., Pujades, L., Barbat, A., & Hurtado, J. (2013). Evaluación probabilista de la capacidad, fragilidad y daño sísmico de edificios de hormigón armado. *Revista Internacional de Métodos Numéricos Para Cálculo Y Diseño En Ingeniería*, *29*(2), 63–78.